

Gauss–Bonnet corrected string/black hole transition in large dimensions

Bum-Hoon Lee^{a,b,c} **Hocheol Lee**^d **Somyadip Thakur**^a

^a*Center for Quantum Spacetime, Sogang University, Seoul 04107, Republic of Korea*

^b*Department of Physics, Sogang University, Seoul 04107, Republic of Korea*

^c*Department of Physics, Shanghai University, 99 Shangda Road, Baoshan District, Shanghai 200444, China*

^d*Department of Physics, Dongguk University, Seoul 04620, Republic of Korea*

E-mail: bhl@sogang.ac.kr, insaying@dongguk.edu,
somyadip@sogang.ac.kr

ABSTRACT: We develop a unified analytic treatment of the Horowitz–Polchinski string/black hole correspondence that systematically incorporates higher-derivative corrections to gravity. Working in Euclidean signature—where the Euclidean black hole and the thermal scalar arise as competing saddles of the same finite-temperature ensemble—we include the Gauss–Bonnet term. The analysis is rendered tractable in this UV-sensitive regime by the large- D expansion, which sharply separates the geometry into a universal near-zone and an asymptotic far-zone. In the near-zone, the coupled large- D equations reduce the thermal-scalar sector to an exactly solvable Schrödinger problem, from which we extract the α' -corrected decay exponent and the corresponding shift of the Hagedorn temperature. In the far-zone, we construct closed-form Euclidean solutions of Einstein–Gauss–Bonnet theory at leading order in both $1/D$ and α' . Matching the two regions yields the complete corrected saddle—fixing its temperature, horizon data, and on-shell action—and permits a fully analytic comparison of free energies between the thermal-scalar and black hole phases. This provides a controlled derivation of the HP correspondence point with explicit higher-curvature corrections.

KEYWORDS: String model, Large- D black holes, Phase transition, Gauss–Bonnet correction

Contents

1	Introduction	1
2	Higher-Derivative Horowitz–Polchinski Model	5
2.1	Euclidean EGB–Dilaton–Thermal Scalar Action	6
2.2	Equations of Motion	7
2.2.1	Metric Equation of Motion	7
2.2.2	Dilaton Equation of Motion	7
2.2.3	Thermal Scalar Equation of Motion	8
3	Solutions in large number of dimensions	8
3.1	Large- D Expansion: Methodology and Structure	8
3.2	Static EGB black hole and basic notation	11
3.3	Leading-order fields in the large- D expansion	11
3.3.1	Geometry: Boulware–Deser background and large- D cigar	12
3.3.2	Dilaton: leading-order constant profile	14
3.3.3	Thermal scalar: leading-order mode at large- D	17
3.4	Next-to-leading order fields in the large- D expansion	21
3.4.1	NLO metric correction F_1	22
3.4.2	NLO dilaton profile in the probe regime	25
3.4.3	NLO thermal scalar profile	29
3.4.4	Exact LO+NLO free energy	32
3.5	Relation to FZZ duality and the quasi-tricritical regime	36
4	Numerical evaluation in finite dimensions	37
4.1	Numerical methodology	38
4.2	Numerical Implementation and results	39
5	Discussion	45
A	Quick recap of the existing methodology and introduction to known literature	47
B	Subsystem for the numerical analysis	54
B.1	Derivation of subsystem equations	54
B.2	Numerical results of subsystem	55
C	Details of the next-to-leading-order solution	58
C.1	Metric correction $F_1(\rho)$	58
C.1.1	Near-zone equation and source	58
C.1.2	Closed-form solution and asymptotics	59
C.2	Dilaton correction $\phi_1(\rho)$	60

C.2.1	Near-zone equation and integral representation	60
C.2.2	Far-zone behaviour	60
C.3	Thermal scalar correction $\chi_1(\rho)$	61
C.3.1	Linearised equation and source decomposition	61
C.3.2	Green’s function and integral basis	62
C.3.3	Structure of the solution and coefficients	62

1 Introduction

Black holes sit at the crossroads of classical geometry, thermodynamics, and quantum theory. Their equilibrium properties are elegantly captured by Euclidean gravity, yet their microscopic origin remains subtle and theory dependent. String theory offers a particularly concrete arena where both viewpoints coexist: at weak coupling, highly excited *long strings* provide a statistical description of entropy, while at larger masses gravitational backreaction produces black holes. A sharp formulation of this crossover is the Horowitz–Polchinski (HP) correspondence [1, 2], which asserts that a fundamental string transitions into a black hole when its self-gravity becomes comparable to the string scale. At the correspondence point, the entropies, free energies, and characteristic length scales of the two descriptions match parametrically, suggesting a continuous interpolation between string microstates and coarse-grained geometry.

The HP mechanism is most naturally framed in *Euclidean signature*, where thermal physics is encoded by compactifying time on a circle of period $\beta = 1/T$. In the Euclidean worldsheet description, strings can wind the thermal circle; the lightest winding excitation—the *thermal scalar*—governs the approach to the Hagedorn transition [3–5]. As the temperature is raised, the thermal scalar becomes light and can turn tachyonic, signaling the breakdown of the perturbative string gas. On the gravitational side, a Euclidean black hole is a smooth saddle of the thermal path integral, whose regularity at the horizon fixes the periodicity of the Euclidean time circle and reproduces the Hawking temperature [6, 7]. In this language, the HP crossover becomes a competition between Euclidean saddles in a common ensemble: a thermal long string phase and a Euclidean black hole phase, with the winding sector providing the order–parameter-like degree of freedom that distinguishes them.

Near the correspondence point the curvatures reach the string scale, so the low-energy effective action inevitably receives *stringy higher-derivative corrections*. In heterotic and type II theories, Gauss–Bonnet and more general curvature-squared terms appear at $\mathcal{O}(\alpha')$ [5, 8, 9]. These corrections modify both the Euclidean black hole geometry and the effective dynamics of the thermal scalar/winding sector, and therefore shift the location and nature of the HP crossover. A quantitative study of the transition thus demands a framework that **(i)** isolates the universal near-horizon physics responsible for winding

condensation and (ii) incorporates higher-derivative effects in a controlled, systematic expansion. Recent analyses of self-gravitating strings and near-Hagedorn dynamics [10] underscore the same need for precision.

Two additional developments sharpen the motivation for such a framework. First, the large- D expansion connects higher-dimensional Euclidean Schwarzschild black holes to an *exact* two-dimensional worldsheet background: in an appropriate near-horizon scaling limit, the geometry reduces to the $SL(2)_k/U(1)$ cigar, with the coset level k set by the black hole temperature/horizon scale [11]. In particular, one has $\beta/2\pi = 2r_0/(D-3)$ and $k = (2r_0/(D-3))^2$ (in $\alpha' = 1$ units), so that $\beta/2\pi = \sqrt{k}$ in this limit [11]. This provides a clean physical interpretation of “Large- k ” versus “small- k ” as a dial on the stringiness of the Euclidean cap: for large k the winding condensate is sharply localized near the tip, while decreasing k causes the stringy atmosphere to spread outward and, at a critical value, become non-normalizable and make a formally divergent contribution to the entropy [11]. Second, motivated by FZZ duality, it has been observed that the HP effective string equations admit a nontrivial *first-order* reformulation for the metric-dilaton-winding sector, and that in higher dimensions an analogous first-order structure persists in the cap/low-temperature regime; remarkably, at a critical winding amplitude the Euclidean cigar develops a puncture and the entropy carried by the winding condensate reproduces the Schwarzschild Bekenstein–Hawking entropy [12]. Together, these insights suggest that a universal, effectively two-dimensional cap dynamics controls the onset of the HP transition, while the exterior region primarily supplies boundary data and organizes corrections.

Black holes corrected by higher-derivative interactions often display a much richer thermodynamic landscape than their two-derivative counterparts. In particular, such corrections can generate novel critical behavior and thermodynamic phase structure—including first-order/second-order transitions and re-entrant phenomena—and may also trigger topological transitions, where the qualitative structure of the spacetime/Euclidean saddle (and the associated thermodynamic branch data) changes discontinuously. For recent discussions of these exotic features in concrete higher-derivative setups, see Refs. [13–15].

In this paper we develop a controlled implementation of this philosophy: we use the large- D near-/far-zone decomposition to isolate the universal cap physics governing the thermal scalar, while treating the far-zone within Einstein–Gauss–Bonnet gravity to systematically incorporate $\mathcal{O}(\alpha')$ effects. The large- D expansion therefore functions as an analytic microscope that disentangles the universal winding/thermal scalar dynamics from model-dependent asymptotics and higher-derivative corrections, enabling a sharper characterization of the Euclidean saddle competition underlying the HP correspondence.

Broader Physical Connections: Superconductivity, QCD, and Fuzzballs

The thermal scalar perspective also illuminates broader connections that extend beyond the HP correspondence. Its onset near the Hagedorn point behaves as an emergent order parameter undergoing a symmetry-breaking transition, evocative of condensate formation in superconductivity. In holographic settings, Euclidean scalar condensation near black holes generates an effective Ginzburg–Landau potential for a boundary order parameter [16, 17];

here, the thermal scalar provides a natural worldsheet origin for such Euclidean instabilities and suggests a stringy analogue of superconducting order.

There is also a long standing analogy with strong interaction physics. The long string/black hole crossover resembles the confinement/deconfinement transition in QCD and Large- N gauge theories, where chromoelectric flux tubes proliferate and become nearly tensionless at high temperature [18, 19]. The limiting Hagedorn temperature of hadronic spectra plays the same structural role as the string Hagedorn point, and the emergence of a black hole-like saddle mirrors the dominance of deconfined plasma phases in gauge theory.

A third connection arises with proposals for black hole microstructure, particularly the fuzzball paradigm. In fuzzball models, individual microstate geometries replace the classical horizon [20–22]. The HP framework instead provides a thermal interpolation in which a long string, once sufficiently self-gravitating, evolves into a Euclidean black hole. The large- D viewpoint sharpens this bridge by isolating the universal cap region where winding condensation and tip dynamics are controlled by an effectively two-dimensional system, thereby linking microscopic string structure to coarse-grained geometry in a particularly transparent way.

Large- D and Large- k Motivation

A powerful analytic tool for studying these issues is the large- D expansion. In the limit of large spacetime dimension, black holes exhibit a sharp separation between a thin *near-zone* of thickness r_h/D , where the gravitational field and light degrees of freedom localize, and a *far-zone* that rapidly approaches its asymptotic form. This structure, emphasized in [23–25], reduces the near-zone dynamics to a universal effectively one-dimensional problem, while the far-zone can be treated systematically (for us, within Einstein–Gauss–Bonnet gravity) [26, 27].

The large- D limit is especially well matched to the HP problem because it provides a controlled bridge between higher-dimensional Schwarzschild black holes and the exact two-dimensional cigar CFT. In the Euclidean near-horizon scaling limit, one obtains the $SL(2)_k/U(1)$ cigar with $\beta/2\pi = \sqrt{k}$ [11]. This turns “Large- k ” versus “small- k ” into a physical diagnostic of gravity-like versus stringy cap physics: for large k the winding condensate is tightly localized near the tip, while lowering k makes the stringy atmosphere extend farther outward and ultimately become non-normalizable at a critical level, signaling a qualitative change in the thermodynamics [11]. In parallel, recent work motivated by FZZ duality shows that the HP effective string equations admit a first-order reformulation for the metric–dilaton–winding sector even in higher dimensions, and that in the cap (low-temperature/Large- β) regime the higher-dimensional system reduces in a precise way to the 1 + 1 first-order HP equations; at a critical winding amplitude the cigar develops a puncture and the winding entropy reproduces the Schwarzschild entropy [12]. These results strongly suggest that the cap region captures the universal physics relevant for winding condensation and the onset of the HP crossover.

Although large- D methods are often presented through the dynamical membrane paradigm [28–34] the HP problem is static and Euclidean. Dynamical membrane degrees of freedom therefore trivialize, leaving precisely the static near-far-zone decomposition as the

relevant structure. This is the regime where the thermal scalar, stringy higher-derivative corrections, and Euclidean saddle competition can be analyzed with maximal clarity: the near-zone isolates the universal cap dynamics, while the far-zone organizes matching to asymptotic data and systematically controls corrections. In the large- D framework, including $1/D$ corrections can be viewed as incorporating finite- k effects in the Euclidean cap region. This is because the large- D near-horizon limit of a D -dimensional Schwarzschild black hole is described by an $SL(2)_k/U(1)$ cigar, with the effective level k fixed by the horizon scale (equivalently the inverse temperature), so varying D away from $D \rightarrow \infty$ translates into deviations away from the strict large- k cigar. Consequently, subleading terms in the $1/D$ expansion systematically refine the universal leading-order cap dynamics and capture the geometric/field-theoretic component of finite- k physics within the truncated metric–dilaton–thermal-scalar system. At the same time, finite k in the exact worldsheet theory can encode additional genuinely stringy effects (higher- α' corrections and contributions from modes beyond the thermal scalar), which are not automatically reproduced by the $1/D$ expansion unless they are included explicitly through higher-derivative terms and corrected effective thermal-scalar data.

In this work, we develop a unified large- D framework for analysing the HP transition with higher-derivative gravitational corrections. We derive the leading near-zone equations for the metric, dilaton, and thermal scalar in Einstein–Gauss–Bonnet gravity, solve the far-zone geometry analytically, and perform matching across the overlap region. This yields the thermal-scalar profile, its decay exponent, and the shift of the Hagedorn temperature induced by higher-derivative terms. The resulting picture is a refined, UV-controlled understanding of the HP correspondence point. The framework generalises straightforwardly to charged or rotating backgrounds, more general higher-curvature theories, and potentially to analyses of critical behaviour and microstructure in string-corrected black hole geometries. The paper is organized as follows:

- In 2, we introduce the Horowitz–Polchinski model and the higher derivative correction. We present the corresponding Euclidean effective action and derive the full set of coupled equations of motion for the metric, dilaton, and thermal scalar, which serve as the starting point for the subsequent analysis.
- In 3, we construct analytic solutions in the expansion of the large- D limit. The geometry naturally separates into a near-horizon region and an asymptotic region, each admitting a systematic expansion in $1/D$, which is then matched to obtain a global solution. At leading order, the background reduces to a universal large- D cigar geometry, with the dilaton remaining constant and the thermal scalar obeying a simplified radial equation. At next-to-leading order, the scalar backreacts on the metric and dilaton, generating corrections that remain perturbative in $1/D$, while modifying the global structure through matching conditions. We also present a detailed derivation of the free energy within this framework and extract the corresponding Landau coefficient from the effective action.
- In 4, we explicitly present the equations of motion in finite dimensions by adopting

a unit radial gauge. We then solve these equations numerically and illustrate the resulting solutions in the presence and absence of the cosmological constant Λ . In particular, we analyze how the numerical behavior changes for finite-dimensional cases and highlight the qualitative and quantitative behavior. And finally we conclude the paper with discussion and future directions in 5.

- We have also supplemented with Apps. A, B, and C explaining some of the solutions methodology and some quick reviews.

2 Higher-Derivative Horowitz–Polchinski Model

HP correspondence [1, 2] provides a controlled framework for analysing the transition between highly excited long strings and black holes. In the Euclidean thermal ensemble, obtained by compactifying time on a circle of circumference $\beta = 1/T$, the dominant degrees of freedom near the Hagedorn temperature arise from singly wound strings. Integrating out all non-winding oscillators yields an effective spacetime description in terms of the *thermal scalar* [3, 4, 35]. Its effective mass,

$$m_{\text{th}}^2 = \frac{\beta^2 g_{\tau\tau}}{4\pi^2 \alpha'^2} - \frac{4}{\alpha'} + \dots, \quad (2.1)$$

becomes tachyonic as $T \rightarrow T_H$, making the thermal scalar the natural order parameter for the HP transition. Because the Euclidean time circle shrinks near a black hole horizon, the thermal scalar localises in the near-tip region and is sensitive to the detailed structure of the Euclidean geometry.

Dilaton Contribution

String theory necessarily incorporates a dilaton field ϕ , which controls the local string coupling and appears in both the worldsheet sigma model and the low-energy effective action. A nontrivial dilaton background shifts the thermal scalar mass and influences the radial dynamics relevant for the HP transition. Since the correspondence point occurs in a regime where curvature and dilaton gradients are of order ℓ_s^{-1} , it is essential to retain ϕ in any effective description.

Higher-Derivative Corrections and the Gauss–Bonnet Term

The HP transition probes curvatures of order the string scale, where the two-derivative Einstein action is no longer sufficient. The leading α' corrections in heterotic and type II string theory include curvature-squared terms, most notably the Gauss–Bonnet (GB) combination [5, 8, 9],

$$R_{\text{GB}}^2 = R_{\mu\nu\rho\sigma} R^{\mu\nu\rho\sigma} - 4R_{\mu\nu} R^{\mu\nu} + R^2. \quad (2.2)$$

These corrections modify the Euclidean black hole metric, shift the Hawking temperature and entropy, and alter the Schrödinger potential that governs the thermal scalar. Thus, they play a direct role in determining the corrected correspondence point.

Gauss–Bonnet Coupling versus α'

In this work, we treat the Gauss–Bonnet coupling as an *independent EFT Wilson coefficient*, not fixed by string theory. This viewpoint is natural in the effective field theory of gravity, where all higher-derivative operators consistent with diffeomorphism invariance appear with arbitrary coefficients. However, in *string theory* the GB term arises at order $\mathcal{O}(\alpha')$ [5, 8], typically accompanied by dilaton-dependent prefactors. Thus, while our EFT operator matches the algebraic structure of the stringy correction, we do *not* impose the specific relation $\alpha \sim \alpha'$. This allows us to study universal features of curvature-squared corrections without committing to any particular UV completion, while still recognising the string-theoretic origin of such terms.

Large- D Motivation

The coupled Euclidean system involving the metric, dilaton, thermal scalar, and Gauss–Bonnet corrections is analytically intractable at fixed dimension. The large- D expansion [23–25] provides a powerful simplification: gravitational fields localise in a thin near-zone region of width r_h/D , the thermal scalar becomes effectively one-dimensional, and higher-derivative terms acquire controlled D -scaling. The far-zone is governed by Einstein–Gauss–Bonnet equations, while the near-zone reduces to a universal Schrödinger-type problem that determines the thermal scalar decay exponent. Although the dynamical membrane paradigm [29, 30] is extremely useful for real-time perturbations, the HP transition is *static* in Euclidean signature. Thus only the static near-/far-zone decomposition is required.

At this point, let us make a short statement clear: *Even though critical string theory is defined in a fixed target-space dimension ($D = 10$ for type II and $D = 26$ for the bosonic string), the large- D expansion can be used as a controlled analytic continuation in precisely the spirit of [36]. One may treat D as a parameter of the worldsheet CFT/effective equations, compute observables in a systematic $1/D$ expansion, only at the end set D to the physical value, with the reliability assessed by the size of subleading $1/D$ corrections. Moreover, there is an explicit Euclidean string-theoretic embedding of this logic: by considering a $(D+1)$ -dimensional string background with a timelike linear dilaton (whose central charge contribution can be tuned arbitrarily), the Euclidean D -dimensional Schwarzschild factor can be incorporated into a consistent worldsheet background, so that large- D becomes a legitimate analytic laboratory for string-scale black hole thermodynamics (albeit intrinsically Euclidean, without a standard Lorentzian continuation).*

2.1 Euclidean EGB–Dilaton–Thermal Scalar Action

A unified description of the HP correspondence in curved backgrounds must capture: **(i)** the Euclidean black hole geometry, **(ii)** the dilaton dynamics, **(iii)** the thermal scalar near the Hagedorn point, and **(iv)** the leading higher-derivative corrections expected from string theory. We therefore adopt the Euclidean action

$$I = - \int d^D x \sqrt{g} e^{-2\phi} \left[\frac{1}{2\kappa} (R - 2\Lambda + \alpha R_{\text{GB}}^2 + 4(\partial\phi)^2) - (\partial\chi)^2 - \frac{1}{4\pi^2 \alpha'^2} (\beta^2 g_{\tau\tau} - \beta_{\text{H}}^2) \chi^2 \right], \quad (2.3)$$

which encompasses all ingredients relevant to the corrected HP transition. The thermal scalar appears with the expected string-frame dilaton prefactor $e^{-2\phi}$, and the potential term correctly reproduces the mass shift responsible for the Hagedorn instability. The Gauss–Bonnet piece encodes the leading curvature-squared correction, treated here as an EFT deformation with structural similarity to the $\mathcal{O}(\alpha')$ term of string theory.

In the following sections we derive the large- D equations of motion from (2.3), analyse the near- and far-zone geometries, and determine the corrected condition for the string/black hole correspondence.

2.2 Equations of Motion

We now derive the equations of motion obtained by varying the Euclidean EGB–dilaton–thermal scalar action (2.3) with respect to the metric $g_{\mu\nu}$, the dilaton ϕ , and the thermal scalar χ . Throughout we keep the full string-frame prefactor $e^{-2\phi}$.

2.2.1 Metric Equation of Motion

Varying (2.3) with respect to $g_{\mu\nu}$ yields

$$\frac{1}{2\kappa} e^{-2\phi} \left[G_{\mu\nu} + \Lambda g_{\mu\nu} + \alpha H_{\mu\nu} + 2\nabla_\mu \nabla_\nu \phi - 2g_{\mu\nu} \nabla^2 \phi + 4\partial_\mu \phi \partial_\nu \phi - 4g_{\mu\nu} (\partial\phi)^2 \right] = T_{\mu\nu}^{(\chi)}, \quad (2.4)$$

where $G_{\mu\nu}$ is the Einstein tensor and $T_{\mu\nu}^{(\chi)}$ is the thermal scalar stress tensor,

$$T_{\mu\nu}^{(\chi)} = e^{-2\phi} \left[\partial_\mu \chi \partial_\nu \chi - \frac{1}{2} g_{\mu\nu} (\partial\chi)^2 - \frac{1}{2} g_{\mu\nu} m_{\text{th}}^2 \chi^2 + \frac{1}{2} \frac{\beta^2}{4\pi^2 \alpha'^2} \chi^2 \delta_{\mu\tau} \delta_{\nu\tau} \right], \quad (2.5)$$

with

$$m_{\text{th}}^2 = \frac{1}{4\pi^2 \alpha'^2} (\beta^2 g_{\tau\tau} - \beta_{\text{H}}^2). \quad (2.6)$$

The Gauss–Bonnet contribution $H_{\mu\nu}$ is

$$H_{\mu\nu} = 2RR_{\mu\nu} - 4R_{\mu\rho}R^\rho{}_\nu - 4R_{\mu\rho\nu\sigma}R^{\rho\sigma} + 2R_\mu{}^{\rho\sigma\lambda}R_{\nu\rho\sigma\lambda} - \frac{1}{2}g_{\mu\nu}R_{\text{GB}}^2. \quad (2.7)$$

Notice the explicit $e^{-2\phi}$ everywhere: we are in string frame, not Einstein frame.

2.2.2 Dilaton Equation of Motion

Variation with respect to ϕ gives

$$0 = \frac{1}{2\kappa} \left[4\nabla^2 \phi - 4(\partial\phi)^2 + R - 2\Lambda + \alpha R_{\text{GB}}^2 \right] - 2(\partial\chi)^2 - 2m_{\text{th}}^2 \chi^2. \quad (2.8)$$

This is the string-frame generalisation of the usual dilaton beta-function equation. Every term couples universally because of the global prefactor $e^{-2\phi}$ in the action.

2.2.3 Thermal Scalar Equation of Motion

Varying with respect to χ yields

$$\nabla_\mu \left(e^{-2\phi} \nabla^\mu \chi \right) - e^{-2\phi} m_{\text{th}}^2 \chi = 0. \quad (2.9)$$

Expanding the prefactor gives the explicitly dilaton-modified Schrödinger equation,

$$\nabla^2 \chi - 2 \partial_\mu \phi \nabla^\mu \chi - m_{\text{th}}^2 \chi = 0. \quad (2.10)$$

This is the equation that reduces, in the large- D near-zone, to the universal Schrödinger problem governing the HP instability.

The full set of equations is:

$$\boxed{\begin{aligned} G_{\mu\nu} + \Lambda g_{\mu\nu} + \alpha H_{\mu\nu} + 2\nabla_\mu \nabla_\nu \phi - 2g_{\mu\nu} \nabla^2 \phi + 4\partial_\mu \phi \partial_\nu \phi - 4g_{\mu\nu} (\partial\phi)^2 &= 2\kappa T_{\mu\nu}^{(\chi)}, \\ 4\nabla^2 \phi - 4(\partial\phi)^2 + R - 2\Lambda + \alpha R_{\text{GB}}^2 &= 4\kappa [(\partial\chi)^2 + m_{\text{th}}^2 \chi^2], \\ \nabla^2 \chi - 2 \partial_\mu \phi \nabla^\mu \chi - m_{\text{th}}^2 \chi &= 0. \end{aligned}} \quad (2.11)$$

These are the equations we will now reduce in the large- D expansion.

3 Solutions in large number of dimensions

In the previous section we have noted the equation of motion for the Einstein–Gauss–Bonnet dilaton system with the thermal scalar. In this section, we attempt to solve these equations explicitly in large- D expansion to leading order and subleading order in D .

3.1 Large- D Expansion: Methodology and Structure

We begin by giving a simple systematics of implementing the large- D expansion for the metric functions $F(r)$, $\chi(r)$, and the scalar field $\phi(r)$. The key idea is that, in the $D \rightarrow \infty$ limit, gravitational dynamics localise near the horizon within a radial layer of thickness $\mathcal{O}(1/D)$, allowing the geometry to be treated separately in two regions—the *near-zone* and the *far-zone*. A consistent global solution is then obtained by matching the two expansions in their common region of validity. Here we summarise the structure at leading and subleading orders, without solving any equations.

Near-Zone Coordinates and Leading-Order Fields Close to the horizon, radial gradients scale as D , making the rescaled coordinate

$$\rho = D(r - r_h) \quad (3.1)$$

the natural variable in the near-zone. The metric functions and scalar field admit the $1/D$ expansions

$$F(r) = F_0(\rho) + \frac{1}{D} F_1(\rho) + \dots, \quad \chi(r) = \chi_0(\rho) + \frac{1}{D} \chi_1(\rho) + \dots, \quad \phi(r) = \phi_0(\rho) + \frac{1}{D} \phi_1(\rho) + \dots. \quad (3.2)$$

At leading order (LO), the Einstein–scalar equations simplify considerably because only the highest radial derivatives survive. This produces a universal set of ordinary differential equations determining the dominant near-horizon behaviour:

- the horizon location and regularity,
- the exponential decay of $F_0(\rho)$ away from the horizon,
- the leading behaviour of $\chi_0(\rho)$,
- and the near-horizon profile of $\phi_0(\rho)$.

model-dependent corrections (Gauss–Bonnet terms, nonlinear $P(X)$, flux effects, *etc.*) do not contribute at this leading order.

Subleading Near-Zone Behaviour At subleading order, previously suppressed components of the Einstein and scalar-field equations contribute, giving linear ODEs for $F_1(\rho)$, $\chi_1(\rho)$, and $\phi_1(\rho)$ with sources determined entirely by the LO solution. These next-to-leading-order (NLO) equations contain several integration constants; regularity at the horizon fixes part of them, while the remaining constants are fixed by matching to the far-zone behaviour. This NLO sector captures all theory-dependent corrections.

Far-Zone Expansion and Background Asymptotics In the far-zone, where $r - r_h = \mathcal{O}(1)$, the fields vary slowly and admit the expansions

$$F(r) = \sum_{n=0}^{\infty} \frac{1}{D^n} \widehat{F}_n(r), \quad \chi(r) = \sum_{n=0}^{\infty} \frac{1}{D^n} \widehat{\chi}_n(r), \quad \phi(r) = \sum_{n=0}^{\infty} \frac{1}{D^n} \widehat{\phi}_n(r). \quad (3.3)$$

The leading-order far-zone equations describe the asymptotic background (*e.g.*, flat or AdS), where the gravitational field of the black hole is exponentially localised. The scalar field shows the characteristic large- D decay,

$$\phi(r) \sim r^{-(D-2)} \quad \text{or} \quad \phi(r) \sim e^{-Dr/L}, \quad (3.4)$$

depending on the asymptotic geometry. Subleading terms correct this tail and encode how the near-zone data affect the exterior fields.

Overlap Region and Matching Conditions The near-zone and far-zone expansions overlap in the regime

$$1 \ll \rho \ll D, \quad (3.5)$$

where both the large- ρ limit of the near-zone solution and the near-horizon limit of the far-zone solution are simultaneously valid. Matching requires that:

- the two expansions agree order by order in $1/D$,
- F , χ , and ϕ (and their first derivatives) are continuous in the overlap region,
- no spurious divergences arise when extrapolating either expansion.

These matching conditions uniquely determine the integration constants in the NLO near-zone solution and fix the normalisation of the far-zone tails, yielding a globally consistent large- D solution without the need to solve second-order equations across the entire radial domain.

We consider Euclidean Einstein–Gauss–Bonnet gravity with a dilaton ϕ and a complex thermal scalar χ . The Einstein equation takes the form

$$R_{\mu\nu} - \frac{1}{2}Rg_{\mu\nu} = \frac{(D-1)(D-2)}{2\ell^2}g_{\mu\nu} + \frac{\alpha}{2(D-4)(D-3)}(R_{\text{GB}}^2g_{\mu\nu} - 4\mathcal{G}_{\mu\nu}) + T_{\mu\nu}^{(\phi)} + T_{\mu\nu}^{(\chi)}, \quad (3.6)$$

where

$$R_{\text{GB}}^2 = R^2 - 4R_{\mu\nu}R^{\mu\nu} + R_{\mu\nu\rho\sigma}R^{\mu\nu\rho\sigma}, \quad (3.7)$$

and $\mathcal{G}_{\mu\nu}$ is the Gauss–Bonnet tensor. The cosmological constant is

$$\Lambda = -\frac{(D-1)(D-2)}{2\ell^2}. \quad (3.8)$$

The dilaton contribution is grouped as

$$T_{\mu\nu}^{(\phi)} = 2(\square\phi)g_{\mu\nu} - 2(\partial\phi)^2g_{\mu\nu} - 2\nabla_\mu\nabla_\nu\phi, \quad (3.9)$$

and the thermal scalar contribution as

$$T_{\mu\nu}^{(\chi)} = \kappa\left[\nabla_\mu\chi^*\nabla_\nu\chi + \nabla_\mu\chi\nabla_\nu\chi^* - |\partial\chi|^2g_{\mu\nu} - (\bar{\beta}^2g_{\tau\tau} - \bar{\beta}_{\text{H}}^2)|\chi|^2g_{\mu\nu} - 2\bar{\beta}^2|\chi|^2g_{\tau\mu}g_{\tau\nu}\right], \quad (3.10)$$

where $\bar{\beta} = \beta/(2\pi)$ is the physical inverse temperature and $\bar{\beta}_{\text{H}} = \beta_{\text{H}}/(2\pi)$ the local Hawking inverse temperature. The dilaton equation of motion is

$$0 = R - 2\Lambda + \alpha R_{\text{GB}}^2 + 4\square\phi - 4(\partial\phi)^2 - 2\kappa\left[|\partial\chi|^2 + (\bar{\beta}^2g_{\tau\tau} - \bar{\beta}_{\text{H}}^2)|\chi|^2\right]. \quad (3.11)$$

It is convenient to define the combination

$$C(x) \equiv R - 2\Lambda + \alpha R_{\text{GB}}^2 - 2\kappa\left[|\partial\chi|^2 + (\bar{\beta}^2g_{\tau\tau} - \bar{\beta}_{\text{H}}^2)|\chi|^2\right], \quad (3.12)$$

so that (3.11) becomes

$$C(x) + 4\square\phi - 4(\partial\phi)^2 = 0. \quad (3.13)$$

The thermal scalar satisfies

$$0 = \square\chi - 2\partial^\mu\chi\partial_\mu\phi - (\bar{\beta}^2g_{\tau\tau} - \bar{\beta}_{\text{H}}^2)\chi. \quad (3.14)$$

We consider the Euclidean metric ansatz

$$ds^2 = F(r)d\tau^2 + \frac{dr^2}{F(r)} + g(r)d\Omega_{D-2,k}^2, \quad \phi = \phi(r), \quad \chi = \chi(r), \quad (3.15)$$

where $k = 1, 0, -1$ labels spherical, planar, or hyperbolic symmetry. The function $g(r)$ is left arbitrary at this stage; later we will specialise to the areal gauge $g(r) = r^2$ when writing the explicit Boulware–Deser solution and computing simple expressions for the Laplacian.

Near-zone coordinate and leading-order expansion We define

$$n \equiv D - 3, \quad \rho \equiv n \ln \left(\frac{r}{r_h} \right), \quad (3.16)$$

where r_h is the horizon radius defined by $F(r_h) = 0$. In terms of ρ one has

$$r = r_h e^{\rho/n}, \quad \partial_r = \frac{n}{r} \partial_\rho. \quad (3.17)$$

We then expand the fields at fixed ρ as $n \rightarrow \infty$:

$$F(r) = F_0(r) + \mathcal{O}(1/n), \quad (3.18)$$

$$\phi(r) = \phi_0(r) + \mathcal{O}(1/n), \quad (3.19)$$

$$\chi(r) = \chi_0(r) + \mathcal{O}(1/n). \quad (3.20)$$

In the remainder of the paper, we focus on the case in which the background metric at LO is the standard Boulware–Deser solution in areal gauge, corresponding to the choice $g(\rho) = r(\rho)^2$.

3.2 Static EGB black hole and basic notation

Areal gauge and Boulware–Deser solution

In areal gauge the metric ansatz becomes

$$ds^2 = F(r) d\tau^2 + \frac{dr^2}{F(r)} + r^2 d\Omega_{D-2,k}^2, \quad g_{\tau\tau} = F(r), \quad (3.21)$$

with $k = 0, \pm 1$ and $D \geq 5$. The Euclidean metric is obtained by Wick rotation of the standard Lorentzian static ansatz. We write

$$D = n + 3, \quad n \gg 1, \quad (3.22)$$

and define the EGB coupling

$$\tilde{\alpha} \equiv \frac{\alpha}{(D-4)(D-3)}. \quad (3.23)$$

The vacuum EGB+ Λ equation for the ansatz (3.21) is solved exactly by the Boulware–Deser [37, 38] black hole

$$F(r) = k + \frac{r^2}{2\tilde{\alpha}} \left[1 - \sqrt{1 + 4\tilde{\alpha} \left(\frac{1}{\ell^2} + \frac{\mu}{r^{D-1}} \right)} \right], \quad (3.24)$$

where μ is an integration constant proportional to the mass. The horizon radius r_h is defined by $F(r_h) = 0$, and the square root branch is chosen such that the solution reduces continuously to the Einstein black hole as $\alpha \rightarrow 0$.

3.3 Leading-order fields in the large- D expansion

In this subsection we collect the leading-order large- D data for the Euclidean Einstein–Gauss–Bonnet (EGB) black hole, the dilaton, and the complex thermal scalar that propagates on the resulting cigar geometry. Throughout we work in the static ansatz (3.21), take $D = n + 3$ with $n \gg 1$, and employ the standard near- and far-zone coordinates adapted to the large- D limit.

3.3.1 Geometry: Boulware–Deser background and large- D cigar

Boulware–Deser background at large- D As reviewed in Section 3.2, the vacuum EGB+ Λ equation with the static ansatz

$$ds^2 = F(r) d\tau^2 + \frac{dr^2}{F(r)} + r^2 d\Omega_{D-2,k}^2, \quad k = 1, 0, -1, \quad (3.25)$$

admits the Boulware–Deser solution

$$F_0(r) = k + \frac{r^2}{2\tilde{\alpha}} \left[1 - \sqrt{1 + 4\tilde{\alpha} \left(\frac{1}{\ell^2} + \frac{\mu}{r^{D-1}} \right)} \right], \quad \tilde{\alpha} \equiv \frac{\alpha}{(D-4)(D-3)}, \quad (3.26)$$

where μ is an integration constant proportional to the mass and ℓ is the AdS radius. The horizon radius r_h is defined by

$$F(r_h) = 0. \quad (3.27)$$

At leading order in $1/D$ the geometry of interest is precisely (3.26); all matter fields enter only at subleading orders.

Near-zone coordinate and cigar profile We now zoom into the near-horizon region by introducing the standard large- D near-zone coordinate

$$D = n + 3, \quad n \gg 1, \quad \rho \equiv n \ln \frac{r}{r_h}, \quad r = r_h e^{\rho/n}, \quad \partial_r = \frac{n}{r} \partial_\rho. \quad (3.28)$$

The horizon is at $\rho = 0$, and the near-zone corresponds to $r - r_h = \mathcal{O}(r_h/n)$ at fixed $\rho = \mathcal{O}(1)$. Near the horizon we expand the BD blackening function as

$$F(r) = F(r_h) + F'(r_h)(r - r_h) + \mathcal{O}((r - r_h)^2) = F'(r_h)(r - r_h) + \dots, \quad (3.29)$$

using $F(r_h) = 0$ from (3.27). Inserting $r - r_h \simeq (r_h/n) \rho$ at fixed ρ gives

$$F(r) \simeq \frac{r_h}{n} F'(r_h) \rho, \quad (3.30)$$

so the leading near-zone behaviour is linear in ρ . It is convenient to define the dimensionless *cigar scale*

$$K \equiv \frac{r_h}{n} F'(r_h) \Big|_{\text{BD}} > 0, \quad (3.31)$$

which encodes all dependence on $(\tilde{\alpha}, \ell, k, \mu)$ through the BD derivative $F'(r_h)$. Solving the LO radial Einstein–Gauss–Bonnet equation in the scaling limit (3.28) with this near-horizon behaviour yields a universal first-order ODE for $F_0(\rho)$, whose solution is

$$F(r) = F_0(\rho) + \mathcal{O}\left(\frac{1}{n}\right), \quad F_0(\rho) = K(1 - e^{-\rho}). \quad (3.32)$$

By construction,

$$F_0(0) = 0, \quad F_0(\rho) \sim K\rho \quad (\rho \rightarrow 0), \quad F_0(\rho) \rightarrow K \quad (\rho \rightarrow +\infty), \quad (3.33)$$

so the Euclidean time circle closes smoothly at the tip ($\rho = 0$) and opens into a plateau of constant $F_0 = K$ deeper in the near-zone. The LO geometry in this region is therefore a standard “large- D cigar” with scale set by K .

Far-zone variable and matching plateau To describe the region away from the horizon it is convenient to use the standard large- D far-zone radial variable

$$R \equiv \left(\frac{r}{r_h}\right)^{D-2} = \left(\frac{r}{r_h}\right)^{n+1}, \quad r = r_h R^{1/(D-2)}. \quad (3.34)$$

In terms of R , the exact BD solution (3.26) interpolates between the near-horizon region and the asymptotic (A)dS $_D$ background. For the purposes of the leading-order matching to matter fields it is sufficient to note that, in the “matching far-zone” where

$$r - r_h = \mathcal{O}(r_h), \quad 1 \ll \rho \ll n, \quad 1 \ll R \ll e^n, \quad (3.35)$$

the blackening function has already climbed to its near-zone plateau value,

$$F(r) \simeq K, \quad (3.36)$$

up to corrections that are subleading in the $1/D$ expansion. This constant- F approximation will be used repeatedly in the analysis of the dilaton and thermal scalar equations.

Near-far matching for the geometry The near and far descriptions overlap in the window

$$1 \ll \rho \ll n, \quad 1 \ll R \ll e^n. \quad (3.37)$$

Using the definitions (3.28) and (3.34), one finds

$$\rho = n \ln \frac{r}{r_h}, \quad \ln R = (D-2) \ln \frac{r}{r_h} = \frac{n+1}{n} \rho = \rho + \mathcal{O}\left(\frac{\rho}{n}\right), \quad (3.38)$$

so in the overlap region we can identify

$$\ln R \simeq \rho \quad (1 \ll \rho \ll n). \quad (3.39)$$

In this regime the near-zone profile (3.32) has already reached its plateau

$$F_0(\rho) \rightarrow K, \quad (3.40)$$

while the exact BD solution (3.26) is also well-approximated by the constant value (3.36). Thus the LO geometry is globally described by the BD black hole, with the large- D near-zone captured by the universal cigar profile (3.32), and a matching plateau of height K smoothly connecting to the asymptotic (A)dS $_D$ region.

Boxed leading-order metric For later reference we summarise the LO geometry in compact form:

Background:	$ds^2 = F(r) d\tau^2 + \frac{dr^2}{F(r)} + r^2 d\Omega_{D-2,k}^2,$ $F(r) = k + \frac{r^2}{2\tilde{\alpha}} \left[1 - \sqrt{1 + 4\tilde{\alpha} \left(\frac{1}{\ell^2} + \frac{\mu}{r^{D-1}} \right)} \right],$ $\tilde{\alpha} = \frac{\alpha}{(D-4)(D-3)},$
Near-zone:	$\rho = n \ln \frac{r}{r_h}, \quad D = n + 3, \quad F(r) = F_0(\rho) + \mathcal{O}\left(\frac{1}{n}\right),$ $F_0(\rho) = K(1 - e^{-\rho}), \quad K \equiv \frac{r_h}{n} F'(r_h) \Big _{\text{BD}} > 0,$ $K = \frac{1}{n} \left[-2k + \frac{n+2}{1 + \frac{2\tilde{\alpha}k}{r_h^2}} \left(k + \frac{\tilde{\alpha}k^2}{r_h^2} - \frac{r_h^2}{\ell^2} \right) \right], \quad (n = D - 3)$
Matching far-zone (LO):	$R = \left(\frac{r}{r_h} \right)^{D-2}, \quad F_0(r) \simeq K \quad \text{for } 1 \ll \rho \ll n, \quad 1 \ll R \ll e^n.$

(3.41)

This LO geometric background will be used below as the fixed large- D cigar on which the dilaton and thermal scalar propagate.

3.3.2 Dilaton: leading-order constant profile

Dilaton equation and large- D scaling The dilaton equation following from the HP+GB action (2.3) can be written as

$$R - 2\Lambda + \alpha R_{\text{GB}}^2 + 4\Box\phi - 4(\partial\phi)^2 - 2\kappa \left(|\partial\chi|^2 + (\bar{\beta}^2 g_{\tau\tau} - \bar{\beta}_{\text{H}}^2) |\chi|^2 \right) = 0. \quad (3.42)$$

We now separate three ingredients:

- the purely geometric combination

$$\mathcal{G}_{\text{HP}} \equiv R - 2\Lambda + \alpha R_{\text{GB}}^2, \quad (3.43)$$

which is $\mathcal{O}(D^2)$ on a black hole background;

- the dilaton kinetic piece $4\Box\phi - 4(\partial\phi)^2$;
- the matter source

$$\mathcal{S}_{\chi} \equiv 2\kappa \left(|\partial\chi|^2 + (\bar{\beta}^2 g_{\tau\tau} - \bar{\beta}_{\text{H}}^2) |\chi|^2 \right). \quad (3.44)$$

We assume that the *background* geometry is a vacuum solution with thermal scalar switched off, $\chi = 0$. In that case the dilaton equation reduces to

$$\mathcal{G}_{\text{HP}} + 4\Box\phi_0 - 4(\partial\phi_0)^2 = 0. \quad (3.45)$$

We take the Boulware–Deser solution (3.26) on the branch such that $\mathcal{G}_{\text{HP}} = 0$ with a *constant* background dilaton $\phi_0 = \phi_\infty$. This is the standard HP construction: the EGB black hole with a constant string coupling $g_s = e^{\phi_\infty}$ solves the tree-level string equations with the thermal scalar turned off.

When the thermal scalar is turned on, we work in a probe approximation for χ :

$$\chi = \mathcal{O}(1), \quad \mathcal{S}_\chi = \mathcal{O}(1), \quad \mathcal{G}_{\text{HP}} = \mathcal{O}(D^2). \quad (3.46)$$

In the large- D counting, \mathcal{G}_{HP} is parametrically larger than \mathcal{S}_χ by a factor of D^2 . Thus,

- the Einstein equation is dominated by \mathcal{G}_{HP} and is solved by the BD metric at LO (as used in Sec. 3.3.1);
- the dilaton backreaction sourced by χ can be consistently postponed to subleading orders in $1/D$.

Concretely, we expand

$$\phi(x) = \phi_0 + \phi_1(x) + \dots, \quad \phi_0 = \phi_\infty, \quad \phi_1 = \mathcal{O}\left(\frac{1}{D^2}\right), \quad (3.47)$$

and keep only ϕ_0 at leading order. The non-trivial profile ϕ_1 is then determined at next-to-leading order by (3.42) on the fixed background and constitutes a small backreaction effect which we will not need for the LO analysis of the thermal scalar. At strict LO we therefore set

$$\phi(x) = \phi_0 = \phi_\infty = \text{const}, \quad (3.48)$$

and verify that this is consistent with regularity and normalisability in both near- and far-zones.

Near-zone constant solution We now work in the near-zone coordinate defined in (3.28),

$$D = n + 3, \quad \rho = n \ln \frac{r}{r_h}, \quad r = r_h e^{\rho/n}, \quad (3.49)$$

and assume an s -wave dilaton $\phi_0 = \phi_0(\rho)$. For any scalar $X = X(\rho)$, the near-zone Laplacian on the LO cigar background is (see App. C)

$$\square X(\rho) \simeq \frac{n^2}{r_h^2} e^{-\rho} \frac{d}{d\rho} \left(e^\rho F_0(\rho) X'(\rho) \right), \quad X'(\rho) \equiv \frac{dX}{d\rho}, \quad (3.50)$$

with

$$F_0(\rho) = K(1 - e^{-\rho}), \quad (3.51)$$

as in (3.32). Since ϕ_0 is taken to be LO and the thermal scalar backreaction is subleading, the LO dilaton equation is simply

$$\square \phi_0 = 0, \quad (3.52)$$

on the fixed cigar background. Using (3.50), we obtain

$$e^{-\rho} \frac{d}{d\rho} \left(e^\rho F_0(\rho) \phi_0'(\rho) \right) = 0, \quad (3.53)$$

which integrates to

$$e^\rho F_0(\rho) \phi'_0(\rho) = C_\phi, \quad (3.54)$$

with C_ϕ a constant of integration.

Near the tip, $\rho \rightarrow 0$, we have

$$F_0(\rho) \sim K\rho, \quad e^\rho \sim 1 + \rho, \quad (3.55)$$

so

$$e^\rho F_0(\rho) \phi'_0(\rho) \sim K\rho \phi'_0(\rho). \quad (3.56)$$

Regularity at the tip requires $\phi'_0(\rho)$ to remain finite as $\rho \rightarrow 0$, which implies

$$C_\phi = 0 \quad \implies \quad \phi'_0(\rho) = 0 \quad \implies \quad \phi_0(\rho) = \phi_\infty. \quad (3.57)$$

Thus, the only regular near-zone LO dilaton profile is a constant, consistent with our starting assumption (3.48).

Far-zone behaviour and matching We now confirm that the same constant solution is the unique normalisable LO profile in the far-zone. Using the far-zone variable defined in (3.34),

$$R \equiv \left(\frac{r}{r_h} \right)^{D-2}, \quad r = r_h R^{1/(D-2)}, \quad (3.58)$$

and assuming again an s -wave $\phi_0 = \phi_0(R)$, the radial Laplacian takes the form (App. C)

$$\square X(R) \simeq F(r) \frac{(D-2)^2}{r_h^2} \frac{d}{dR} (R^2 X'(R)), \quad X'(R) \equiv \frac{dX}{dR}. \quad (3.59)$$

In the matching far-zone the blackening function is already on its plateau, $F(r) \simeq K$, so the LO dilaton equation $\square\phi_0 = 0$ becomes

$$\frac{d}{dR} (R^2 \phi'_0(R)) = 0. \quad (3.60)$$

Integrating once gives

$$R^2 \phi'_0(R) = A_\phi, \quad (3.61)$$

with A_ϕ a constant. Regularity at the horizon ($R \rightarrow 1$) allows for a finite derivative there, but normalisability at infinity requires

$$\phi'_0(R) \xrightarrow{R \rightarrow \infty} 0 \quad \implies \quad A_\phi = 0. \quad (3.62)$$

Hence

$$\phi'_0(R) = 0 \quad \implies \quad \phi_0(R) = \phi_\infty, \quad (3.63)$$

in agreement with the near-zone result.

In the overlap region $1 \ll \rho \ll n$, $1 \ll R \ll e^n$ we have $\ln R \simeq \rho$ (*cf.*, Sec. 3.3.1), so the near-zone constant solution $\phi_0(\rho) = \phi_\infty$ and the far-zone constant solution $\phi_0(R) = \phi_\infty$ trivially match.

Boxed leading-order dilaton We summarise the LO dilaton result in a compact form:

Background:	EGB Boulware–Deser black hole (3.26) on the branch with $\mathcal{G}_{\text{HP}} = 0$,
Dilaton expansion:	$\phi(x) = \phi_0 + \phi_1(x) + \dots$, $\phi_0 = \phi_\infty = \text{const}$, $\phi_1 = \mathcal{O}\left(\frac{1}{D^2}\right)$,
Near-zone (LO):	$\square\phi_0 = 0 \implies \phi_0(\rho) = \phi_\infty$ (regular at the tip),
Far-zone (LO):	$\square\phi_0 = 0 \implies \phi_0(R) = \phi_\infty$ (normalisable at infinity),
Global LO solution:	$\phi_0(x) = \phi_\infty$ throughout the cigar.

(3.64)

At next-to-leading order in the combined $1/D$ and probe expansion, the thermal scalar sources a small but non-trivial dilaton profile $\phi_1(x)$ through (3.42), which can be solved on the fixed LO cigar background. This backreaction, however, is genuinely subleading and does not modify the LO constant-dilaton result used in our analysis of the thermal scalar at leading order.

3.3.3 Thermal scalar: leading-order mode at large- D

Equation of motion and scaling We now analyse the leading-order behaviour of the complex thermal scalar χ on the large- D EGB cigar, with the metric and dilaton fixed at LO by the BD solution with a constant dilaton,

$$ds^2 = F(r) d\tau^2 + \frac{dr^2}{F(r)} + r^2 d\Omega_{D-2,k}^2, \quad F(r) = F_{\text{BD}}(r), \quad \phi_0 = \phi_\infty. \quad (3.65)$$

We work in the same large- D limit $D = n + 3$ and treat χ in the probe approximation: its backreaction on the geometry and on the dilaton is parametrically subleading in $1/D$. The thermal scalar equation from the HP+GB action can be written as

$$0 = \square\chi - 2\partial^\mu\chi\partial_\mu\phi - (\bar{\beta}^2 g_{\tau\tau} - \bar{\beta}_{\text{H}}^2)\chi, \quad (3.66)$$

where $\bar{\beta}$ and $\bar{\beta}_{\text{H}}$ are rescaled inverse temperatures containing the α' factors, and $g_{\tau\tau} = F(r)$.

At LO we set

$$\phi(x) = \phi_0 = \phi_\infty = \text{const}, \quad (3.67)$$

so that $\partial_\mu\phi_0 = 0$ and the mixed term $-2\partial^\mu\chi\partial_\mu\phi$ drops out. The LO thermal scalar equation thus reduces to

$$\square\chi_0 - (\bar{\beta}^2 F(r) - \bar{\beta}_{\text{H}}^2)\chi_0 = 0, \quad (3.68)$$

on the fixed BD background. We restrict to s -wave configurations, $\chi_0 = \chi_0(r)$, which dominate in the HP limit.

The two competing scales in (3.68) are:

- the radial kinetic term, which scales as $\square\chi_0 \sim D^2$ in the near-horizon region;
- the thermal mass term $m_{\text{eff}}^2(r)\chi_0$, with

$$m_{\text{eff}}^2(r) \equiv \bar{\beta}^2 F(r) - \bar{\beta}_{\text{H}}^2. \quad (3.69)$$

To obtain a non-trivial LO interplay between these terms, we adopt the standard Horowitz–Polchinski scaling: we work near the Hagedorn point and keep the following dimensionless combination fixed as $D \rightarrow \infty$,

$$\Xi^2 \equiv \frac{r_h^2}{(D-2)^2 K} (\bar{\beta}^2 K - \bar{\beta}_H^2), \quad \Xi^2 = \mathcal{O}(1), \quad (3.70)$$

where K is the near-horizon plateau value of the blackening function (see below). This scaling ensures that the kinetic and mass terms in (3.68) are of the same order in the large- D expansion.

Near-zone solution We first analyse the thermal scalar in the near-zone, defined by $r - r_h = \mathcal{O}(r_h/D)$ at fixed $D \gg 1$. As in the geometry and dilaton analysis, we introduce

$$D = n + 3, \quad \rho \equiv n \ln \frac{r}{r_h}, \quad r = r_h e^{\rho/n}, \quad \rho = 0 \Leftrightarrow r = r_h. \quad (3.71)$$

In this regime the BD blackening function takes the universal LO form

$$F(r) = F_0(\rho) + \mathcal{O}\left(\frac{1}{n}\right), \quad F_0(\rho) = K(1 - e^{-\rho}), \quad (3.72)$$

with K an effective curvature scale (constant in the near-zone) determined by the Gauss–Bonnet coupling, the cosmological constant and the horizon topology. For an s -wave scalar $X = X(r)$, in the metric

$$ds^2 = F(r) d\tau^2 + \frac{dr^2}{F(r)} + r^2 d\Omega_{D-2,k}^2, \quad (3.73)$$

the Laplacian is

$$\square X = \frac{1}{\sqrt{g}} \partial_r (\sqrt{g} g^{rr} \partial_r X) = \frac{1}{r^{D-2}} \partial_r (r^{D-2} F(r) \partial_r X), \quad (3.74)$$

with $\sqrt{g} \propto r^{D-2}$. In terms of the near-zone variable ρ , one finds (see also App. C)

$$\square X(\rho) \simeq \frac{n^2}{r_h^2} e^{-\rho} \frac{d}{d\rho} \left(e^\rho F_0(\rho) X'(\rho) \right), \quad X'(\rho) \equiv \frac{dX}{d\rho}, \quad (3.75)$$

to leading order in $1/n$. Assuming $\chi_0 = \chi_0(\rho)$ and using (3.72) and (3.75), the LO thermal scalar equation (3.68) becomes

$$e^{-\rho} \frac{d}{d\rho} \left(e^\rho F_0(\rho) \chi_0'(\rho) \right) - \frac{r_h^2}{n^2} (\bar{\beta}^2 F_0(\rho) - \bar{\beta}_H^2) \chi_0(\rho) = 0. \quad (3.76)$$

In the “deep” near-zone away from the very tip, $e^{-\rho} \ll 1$ and $F_0(\rho)$ has already reached its plateau,

$$F_0(\rho) \simeq K, \quad \bar{\beta}^2 F_0(\rho) - \bar{\beta}_H^2 \simeq \bar{\beta}^2 K - \bar{\beta}_H^2. \quad (3.77)$$

Keeping the combination (3.70) fixed, the equation (3.76) reduces, to LO in $1/n$, to a constant-coefficient ODE:

$$\chi_0''(\rho) + \chi_0'(\rho) - \Xi^2 \chi_0(\rho) = 0, \quad (3.78)$$

with Ξ^2 given by (3.70). The characteristic equation

$$\lambda^2 + \lambda - \Xi^2 = 0 \quad (3.79)$$

has roots

$$\lambda_{\pm} = \frac{-1 \pm \sqrt{1 + 4\Xi^2}}{2}, \quad \lambda_+ > 0, \quad \lambda_- < 0 \quad (\text{for } \Xi^2 > 0). \quad (3.80)$$

The general near-zone solution in this regime is

$$\chi_0^{(\text{NZ})}(\rho) = A_{\text{NZ}} e^{\lambda_+ \rho} + B_{\text{NZ}} e^{\lambda_- \rho}. \quad (3.81)$$

Normalisability towards the outer part of the cigar (large ρ) forbids the growing mode $e^{\lambda_+ \rho}$, so we set $A_{\text{NZ}} = 0$ and write

$$\chi_0^{(\text{NZ})}(\rho) = \chi_h e^{\lambda_- \rho}, \quad \lambda_- < 0, \quad (3.82)$$

where χ_h is a constant amplitude fixed by matching to the far-zone. The approximation (3.82) is valid for $1 \ll \rho \ll n$; very close to the tip the full equation (3.76) smooths out the behaviour, but this does not affect the LO matching.

It is convenient to express the effective thermal mass at the plateau in terms of Ξ^2 :

$$m_{\text{eff}}^2 \equiv \bar{\beta}^2 K - \bar{\beta}_{\text{H}}^2, \quad \Xi^2 = \frac{r_h^2}{(D-2)^2 K} m_{\text{eff}}^2. \quad (3.83)$$

The Hagedorn condition corresponds to $m_{\text{eff}}^2 = 0$ (i.e., $\bar{\beta}^2 K = \bar{\beta}_{\text{H}}^2$), at which point $\Xi^2 = 0$ and the exponents become $\lambda_+ = 0$, $\lambda_- = -1$.

Far-zone solution and matching We now analyse the thermal scalar in the far-zone and show that the radial equation has exactly the same ODE structure as in the near-zone once we use an appropriate large- D coordinate. In the far-zone it is convenient to use the standard large- D variable

$$R \equiv \left(\frac{r}{r_h} \right)^{D-2}, \quad r = r_h R^{1/(D-2)}. \quad (3.84)$$

Then

$$\partial_r = (D-2) \frac{R}{r} \partial_R, \quad r^{D-2} = r_h^{D-2} R. \quad (3.85)$$

For any s -wave $X = X(R)$ we find

$$\square X(R) = \frac{1}{r^{D-2}} \partial_r (r^{D-2} F(r) \partial_r X) \simeq F(r) \frac{(D-2)^2}{r_h^2} \frac{d}{dR} (R^2 X'(R)), \quad X'(R) \equiv \frac{dX}{dR}, \quad (3.86)$$

where we have used $r^{D-2} = r_h^{D-2} R$ and kept only the leading large- D scaling of the derivatives.

In the matching far-zone (where the potential has already plateaued, but we are not yet at asymptotic infinity) we can approximate the blackening function by its constant value,

$$F(r) \simeq K, \quad (3.87)$$

with the same K as in (3.72). With $F(r) \simeq K$ and ϕ_0 constant, the LO equation (3.68) becomes

$$\square\chi_0 - (\bar{\beta}^2 K - \bar{\beta}_{\text{H}}^2)\chi_0 = 0, \quad (3.88)$$

or using (3.86) and the definition (3.83),

$$K \frac{(D-2)^2}{r_h^2} \frac{d}{dR} (R^2 \chi_0'(R)) - m_{\text{eff}}^2 \chi_0(R) = 0. \quad (3.89)$$

Dividing by $K(D-2)^2/r_h^2$ and using (3.70) gives

$$\frac{d}{dR} (R^2 \chi_0'(R)) - \Xi^2 \chi_0(R) = 0, \quad (3.90)$$

with *the same* parameter Ξ^2 as in the near-zone equation (3.78), up to $1/D$ corrections.

Introducing

$$Y \equiv \ln R, \quad (3.91)$$

we have

$$\chi_0'(R) = \frac{1}{R} \frac{d\chi_0}{dY}, \quad \frac{d}{dR} (R^2 \chi_0'(R)) = \frac{d^2\chi_0}{dY^2} + \frac{d\chi_0}{dY}. \quad (3.92)$$

Equation (3.90) therefore reduces to

$$\frac{d^2\chi_0}{dY^2} + \frac{d\chi_0}{dY} - \Xi^2 \chi_0(Y) = 0, \quad (3.93)$$

which is identical in form to the near-zone equation (3.78), upon the replacement $\rho \rightarrow Y$. The general far-zone solution is thus

$$\chi_0^{(\text{FZ})}(R) = A_{\text{FZ}} R^{\lambda_+} + B_{\text{FZ}} R^{\lambda_-}, \quad \lambda_{\pm} = \frac{-1 \pm \sqrt{1 + 4\Xi^2}}{2}, \quad (3.94)$$

with the same exponents λ_{\pm} as in (3.80). Normalisability at large R requires the decaying mode R^{λ_-} , so we set $A_{\text{FZ}} = 0$ and write

$$\chi_0^{(\text{FZ})}(R) = \chi_{\infty} R^{\lambda_-}, \quad \lambda_- < 0. \quad (3.95)$$

The near and far descriptions overlap in a region where both sets of coordinates are valid and their approximations hold:

$$1 \ll \rho \ll n, \quad 1 \ll R \ll e^n. \quad (3.96)$$

Using (3.71) and (3.84), we have

$$\rho = n \ln \frac{r}{r_h}, \quad \ln R = (D-2) \ln \frac{r}{r_h} = (n+1) \ln \frac{r}{r_h} = \frac{n+1}{n} \rho = \rho + \mathcal{O}\left(\frac{\rho}{n}\right). \quad (3.97)$$

Therefore, in the overlap region,

$$Y \equiv \ln R \simeq \rho \quad (n \gg 1). \quad (3.98)$$

The near-zone solution (3.82) behaves as

$$\chi_0^{(\text{NZ})}(\rho) = \chi_h e^{\lambda_- \rho} \simeq \chi_h e^{\lambda_- Y}, \quad (3.99)$$

while the far-zone solution (3.95) can be written as

$$\chi_0^{(\text{FZ})}(R) = \chi_\infty R^{\lambda_-} = \chi_\infty e^{\lambda_- Y}. \quad (3.100)$$

Smooth matching in the overlap region requires

$$\chi_\infty = \chi_h, \quad (3.101)$$

so the same decaying mode with exponent λ_- controls both the near- and far-zones. The overall amplitude χ_h is then fixed by the full global solution (including the region away from the matching plateaus) or by boundary conditions in the asymptotic region.

Boxed leading-order global thermal scalar We summarise the LO thermal scalar result as follows.

Background:	EGB Boulware–Deser black hole with constant dilaton $\phi_0 = \phi_\infty$,
Effective mass at the plateau:	$m_{\text{eff}}^2 \equiv \bar{\beta}^2 K - \bar{\beta}_{\text{H}}^2, \quad \Xi^2 = \frac{r_h^2}{(D-2)^2 K} m_{\text{eff}}^2,$
Exponents:	$\lambda_{\pm} = \frac{-1 \pm \sqrt{1 + 4\Xi^2}}{2}, \quad \lambda_+ > 0, \lambda_- < 0 \ (\Xi^2 > 0),$
Near-zone ($r - r_h = \mathcal{O}(r_h/D)$):	$\rho = n \ln \frac{r}{r_h}, \quad F_0(\rho) = K(1 - e^{-\rho}),$ $\chi_0^{(\text{NZ})}(\rho) = \chi_h e^{\lambda_- \rho}, \quad 1 \ll \rho \ll n,$
Far-zone ($R = (r/r_h)^{D-2}$):	$R = \left(\frac{r}{r_h}\right)^{D-2}, \quad Y = \ln R,$ $\chi_0^{(\text{FZ})}(R) = \chi_h R^{\lambda_-} = \chi_h e^{\lambda_- Y}, \quad 1 \ll R \ll e^n,$
Hagedorn condition:	$m_{\text{eff}}^2 = 0 \iff \bar{\beta}^2 K = \bar{\beta}_{\text{H}}^2 \iff \Xi^2 = 0, \lambda_+ = 0, \lambda_- = -1.$

(3.102)

3.4 Next-to-leading order fields in the large- D expansion

In this subsection we collect the next-to-leading order corrections to the blackening function, dilaton, and thermal scalar in the large- D expansion. We work around the leading-order Boulware–Deser background

$$F(r) = F_0(\rho) + \frac{1}{n} F_1(\rho) + \mathcal{O}\left(\frac{1}{n^2}\right), \quad F_0(\rho) = K(1 - e^{-\rho}), \quad D = n + 3, \quad (3.103)$$

in the near-zone coordinate

$$\rho = n \ln \frac{r}{r_h}, \quad (3.104)$$

with r_h the horizon radius of the BD solution. The LO dilaton and thermal scalar profiles are

$$\phi_0 = \phi_\infty, \quad \chi_0^{(\text{NZ})}(\rho) = \chi_h e^{\lambda_- \rho}, \quad \lambda_\pm = \frac{-1 \pm \sqrt{1 + 4\Xi^2}}{2}, \quad \lambda_- < 0, \quad (3.105)$$

where

$$\Xi^2 = \frac{r_h^2}{n^2 K} (\bar{\beta}^2 K - \bar{\beta}_H^2), \quad m_{\text{eff}}^2 \equiv \bar{\beta}^2 K - \bar{\beta}_H^2. \quad (3.106)$$

The corresponding far-zone LO scalar is

$$\chi_0^{(\text{FZ})}(R) = \chi_\infty R^{\lambda_-}, \quad R \equiv \left(\frac{r}{r_h}\right)^{D-2}, \quad Y \equiv \ln R, \quad (3.107)$$

with χ_∞ fixed by matching to the near-zone.

3.4.1 NLO metric correction F_1

At NLO the metric perturbation $F_1(\rho)$ is sourced by the LO thermal scalar stress tensor $T_{\mu\nu}^{(\chi)}[\chi_0]$. The LO dilaton is constant and does not contribute to the Einstein equation at this order. In the *probe* approximation used here, we also neglect the linear dilaton contribution $2\nabla_\mu \nabla_\nu \phi_1 - 2g_{\mu\nu} \nabla^2 \phi_1$ as a source for F_1 , so that the NLO metric correction is driven purely by the thermal scalar stress tensor; quadratic terms $(\partial\phi_1)^2$ are $\mathcal{O}(\kappa^2)$ and are likewise ignored.

Near-zone equation and solution The combination of Einstein equations $\mathcal{E}^\rho_\rho - \mathcal{E}^\tau_\tau = 0$, expanded to first order in $1/n$ around the LO EGB background, yields a first-order radial equation for $F_1(\rho)$,

$$F_1'(\rho) + F_1(\rho) = \mathcal{S}_{\text{NZ}}(\rho), \quad (3.108)$$

where the prime denotes $d/d\rho$ and the source is built from the LO thermal scalar. For a static, purely radial scalar $\chi_0(\rho)$ with canonical kinetic term, the relevant stress-tensor combination is

$$(T^\rho_\rho - T^\tau_\tau)_{\text{LO}} = g_{(0)}^{\rho\rho} (\partial_\rho \chi_0)^2 = g_{(0)}^{\rho\rho} \lambda_-^2 \chi_0(\rho)^2, \quad (3.109)$$

so that the source can be written as

$$\mathcal{S}_{\text{NZ}}(\rho) = \frac{2\kappa_{\text{eff}}}{D-2} g_{(0)}^{\rho\rho} (\partial_\rho \chi_0)^2 \equiv \mathcal{A}_\chi (1 - e^{-\rho}) e^{2\lambda_- \rho}, \quad (3.110)$$

with $g_{(0)}^{\rho\rho}$ the LO radial inverse metric and κ_{eff} an effective gravitational coupling including the Gauss–Bonnet corrections. Using the near-zone scaling of $g_{(0)}^{\rho\rho}$ one finds the explicit coefficient

$$\mathcal{A}_\chi = \frac{2\kappa_{\text{eff}}}{D-2} \frac{n^2}{r_h^2} K \lambda_-^2 \chi_h^2, \quad (3.111)$$

so that all explicit ρ -dependence arises from $F_0(\rho)$ and $\chi_0(\rho)$. With this notation the near-zone equation becomes

$$F_1'(\rho) + F_1(\rho) = \mathcal{A}_\chi \left(e^{2\lambda_- \rho} - e^{(2\lambda_- - 1)\rho} \right). \quad (3.112)$$

This is a linear inhomogeneous first-order ODE. The integrating factor is e^ρ , so

$$\frac{d}{d\rho}(e^\rho F_1(\rho)) = \mathcal{A}_\chi \left(e^{(2\lambda_-+1)\rho} - e^{2\lambda_- \rho} \right). \quad (3.113)$$

Integrating from $\rho = 0$ to ρ gives

$$\begin{aligned} e^\rho F_1(\rho) &= F_1(0) + \mathcal{A}_\chi \int_0^\rho \left(e^{(2\lambda_-+1)\sigma} - e^{2\lambda_- \sigma} \right) d\sigma \\ &= F_1(0) + \mathcal{A}_\chi \left[\frac{e^{(2\lambda_-+1)\rho} - 1}{2\lambda_- + 1} - \frac{e^{2\lambda_- \rho} - 1}{2\lambda_-} \right]. \end{aligned} \quad (3.114)$$

We work in the gauge where the horizon position is fixed at $\rho = 0$ at NLO, which imposes

$$F_1(0) = 0. \quad (3.115)$$

This gives the exact NLO near-zone metric correction

$$\boxed{F_1^{(\text{NZ})}(\rho) = \mathcal{A}_\chi e^{-\rho} \left[\frac{e^{(2\lambda_-+1)\rho} - 1}{2\lambda_- + 1} - \frac{e^{2\lambda_- \rho} - 1}{2\lambda_-} \right]}. \quad (3.116)$$

Near the horizon, $\rho \rightarrow 0$,

$$F_1^{(\text{NZ})}(\rho) = \frac{\mathcal{A}_\chi}{2} \rho^2 + \mathcal{O}(\rho^3), \quad (3.117)$$

which is regular and compatible with the cigar geometry. For large ρ the dominant behaviour is

$$F_1^{(\text{NZ})}(\rho) \simeq \mathcal{A}_\chi \left[\frac{e^{2\lambda_- \rho}}{2\lambda_- + 1} - \frac{e^{(2\lambda_- - 1)\rho}}{2\lambda_-} \right], \quad \rho \rightarrow \infty, \quad (3.118)$$

so that F_1 decays faster than the background metric for $\lambda_- < 0$, as expected.

Far-zone behaviour and matching In the far-zone we use

$$R \equiv \left(\frac{r}{r_h} \right)^{D-2}, \quad Y \equiv \ln R, \quad (3.119)$$

and approximate the BD background by its constant-curvature form

$$F(r) \simeq K, \quad r - r_h = \mathcal{O}(r_h), \quad (3.120)$$

as in the LO far-zone analysis. The LO thermal scalar in the far-zone has the same exponent as in the near-zone,

$$\chi_0^{(\text{FZ})}(R) = \chi_\infty R^{\lambda_-} = \chi_\infty e^{\lambda_- Y}, \quad \lambda_- < 0. \quad (3.121)$$

Linearising the Einstein equation and taking the same combination $\mathcal{E}^r_r - \mathcal{E}^\tau_\tau$, one finds

$$\frac{dF_1^{(\text{FZ})}}{dY} + F_1^{(\text{FZ})}(Y) = \mathcal{S}_{\text{FZ}}(Y), \quad (3.122)$$

with

$$\mathcal{S}_{\text{FZ}}(Y) = \mathcal{A}_\chi^{(\infty)} e^{2\lambda_- Y}, \quad \mathcal{A}_\chi^{(\infty)} \equiv \frac{2\kappa_{\text{eff}} K \lambda_-^2 \chi_\infty^2}{D-2} \times \left[\text{far-zone Jacobian factors} \right]. \quad (3.123)$$

The structure of this equation coincides with the deep near-zone limit of (3.108), where $(1 - e^{-\rho}) \rightarrow 1$. Solving equation (3.122) gives

$$F_1^{(\text{FZ})}(Y) = \frac{\mathcal{A}_\chi^{(\infty)}}{2\lambda_- + 1} e^{2\lambda_- Y} + F_1^{(\infty)} e^{-Y}. \quad (3.124)$$

Regularity and normalisability in the asymptotic region require the $e^{-Y} \propto R^{-1}$ mode to be absent, so we set $F_1^{(\infty)} = 0$ and obtain

$$\boxed{F_1^{(\text{FZ})}(R) = \frac{\mathcal{A}_\chi^{(\infty)}}{2\lambda_- + 1} R^{2\lambda_-}, \quad R \rightarrow \infty,} \quad (3.125)$$

with $2\lambda_- < 0$.

The near- and far-zones overlap in

$$1 \ll \rho \ll n \quad \iff \quad 1 \ll Y = \ln R \ll n, \quad (3.126)$$

and in this region

$$Y = \ln R = \frac{D-2}{n} \ln \frac{r}{r_h} = \frac{n+1}{n} \rho = \rho + \mathcal{O}\left(\frac{\rho}{n}\right), \quad (3.127)$$

so we may identify $Y \simeq \rho$ at leading order in $1/n$. The large- ρ behaviour of (3.118),

$$F_1^{(\text{NZ})}(\rho) \simeq \frac{\mathcal{A}_\chi}{2\lambda_- + 1} e^{2\lambda_- \rho} + \mathcal{O}(e^{(2\lambda_- - 1)\rho}), \quad (3.128)$$

matches the far-zone form (3.125) provided we identify

$$\mathcal{A}_\chi^{(\infty)} = \mathcal{A}_\chi, \quad \chi_\infty = \chi_h. \quad (3.129)$$

Thus a single expression (3.116), with these matching choices, provides a global description of the NLO metric correction across the cigar.

Global NLO blackening function Collecting the results, the NLO-corrected blackening function in the large- D expansion is

$$\boxed{F(r) = F_0(\rho) + \frac{1}{n} F_1(\rho) + \mathcal{O}\left(\frac{1}{n^2}\right), \quad F_0(\rho) = K(1 - e^{-\rho}),} \quad (3.130)$$

with

$$\boxed{F_1(\rho) = \mathcal{A}_\chi e^{-\rho} \left[\frac{e^{(2\lambda_- + 1)\rho} - 1}{2\lambda_- + 1} - \frac{e^{2\lambda_- \rho} - 1}{2\lambda_-} \right], \quad \lambda_- = \frac{-1 - \sqrt{1 + 4\Xi^2}}{2} < 0, \quad \Xi^2 = \frac{r_h^2}{n^2 K} (\bar{\beta}^2 K - \bar{\beta}_H^2).} \quad (3.131)$$

3.4.2 NLO dilaton profile in the probe regime

We now construct the NLO dilaton profile in the large- D expansion, working in the *probe* regime for the string gas: the thermal scalar and dilaton fluctuate on a fixed EGB BD background, and their backreaction on the metric is included only to linear order in the gravitational coupling κ . In particular, in the NLO metric analysis we treat F_1 as sourced directly by the LO thermal scalar stress tensor and neglect the linear dilaton contribution as a subleading probe-field effect. Quadratic dilaton terms $(\partial\phi_1)^2$ are $\mathcal{O}(\kappa^2)$ and are also neglected.

Master equation for ϕ_1 We start from the string-frame equations

$$G_{\mu\nu} + \Lambda g_{\mu\nu} + \alpha H_{\mu\nu} + 2\nabla_\mu \nabla_\nu \phi - 2g_{\mu\nu} \nabla^2 \phi + 4\partial_\mu \phi \partial_\nu \phi - 4g_{\mu\nu} (\partial\phi)^2 = 2\kappa T_{\mu\nu}^{(\chi)}, \quad (3.132)$$

$$4\nabla^2 \phi - 4(\partial\phi)^2 + R - 2\Lambda + \alpha R_{\text{GB}}^2 = 4\kappa [(\partial\chi)^2 + m_{\text{th}}^2(r)\chi^2], \quad (3.133)$$

$$\nabla^2 \chi - 2\partial_\mu \phi \nabla^\mu \chi - m_{\text{th}}^2(r)\chi = 0, \quad (3.134)$$

with

$$m_{\text{th}}^2(r) \equiv \bar{\beta}^2 g_{\tau\tau}(r) - \bar{\beta}_{\text{H}}^2 = \bar{\beta}^2 F(r) - \bar{\beta}_{\text{H}}^2. \quad (3.135)$$

We expand in $1/D$ and in the small parameter κ :

$$\phi(x) = \phi_0 + \phi_1(x) + \mathcal{O}(\kappa^2), \quad \phi_0 = \phi_\infty, \quad (3.136)$$

and work to linear order in κ . On the BD background the geometric combination in (3.133) vanishes,

$$(R - 2\Lambda + \alpha R_{\text{GB}}^2)_{\text{BD}} = 0, \quad (3.137)$$

so to linear order in κ and in ϕ_1 the dilaton equation reduces to

$$4\nabla^2 \phi_1 = 4\kappa [(\partial\chi_0)^2 + m_{\text{th}}^2(r)\chi_0^2], \quad (3.138)$$

or

$$\boxed{\nabla^2 \phi_1 = \kappa [(\partial\chi_0)^2 + m_{\text{th}}^2(r)\chi_0^2]} \quad (3.139)$$

on the fixed BD background.

Near-zone equation and solution for $\phi_1'(\rho)$ For an s -wave scalar $X = X(r)$ in the metric $F(r)$, the radial Laplacian is

$$\square X = \frac{1}{r^{D-2}} \partial_r (r^{D-2} F(r) \partial_r X). \quad (3.140)$$

In the near-zone we use

$$\rho = n \ln \frac{r}{r_h}, \quad r = r_h e^{\rho/n}, \quad \partial_r = \frac{n}{r} \partial_\rho, \quad (3.141)$$

so that to leading order in $1/n$

$$r^{D-2} \sim r_h^{n+1} e^\rho, \quad \partial_r \sim \frac{n}{r_h} \partial_\rho. \quad (3.142)$$

With $F(r) \simeq F_0(\rho)$ this gives

$$\square X(\rho) \simeq \frac{n^2}{r_h^2} e^{-\rho} \frac{d}{d\rho} \left(e^\rho F_0(\rho) X'(\rho) \right), \quad X'(\rho) \equiv \frac{dX}{d\rho}. \quad (3.143)$$

The LO near-zone scalar is $\chi_0(\rho) = \chi_h e^{\lambda-\rho}$. Its radial derivative is

$$\partial_r \chi_0 = \lambda_- \chi_h e^{\lambda-\rho} \frac{n}{r} \simeq \lambda_- \chi_h e^{\lambda-\rho} \frac{n}{r_h}, \quad (3.144)$$

so

$$(\partial \chi_0)^2 = g^{rr} (\partial_r \chi_0)^2 \simeq F_0(\rho) \left(\frac{n}{r_h} \right)^2 \lambda_-^2 \chi_h^2 e^{2\lambda-\rho} = \frac{n^2}{r_h^2} K (1 - e^{-\rho}) \lambda_-^2 \chi_h^2 e^{2\lambda-\rho}. \quad (3.145)$$

To leading order we approximate $m_{\text{th}}^2(r) \simeq m_{\text{eff}}^2 \equiv \bar{\beta}^2 K - \bar{\beta}_{\text{H}}^2$, so

$$m_{\text{th}}^2(r) \chi_0^2 \simeq m_{\text{eff}}^2 \chi_h^2 e^{2\lambda-\rho} = \frac{n^2 K}{r_h^2} \Xi^2 \chi_h^2 e^{2\lambda-\rho}, \quad (3.146)$$

where we used

$$\Xi^2 = \frac{r_h^2}{n^2 K} m_{\text{eff}}^2 \quad \implies \quad m_{\text{eff}}^2 = \frac{n^2 K}{r_h^2} \Xi^2. \quad (3.147)$$

Thus the total source in (3.139) is

$$(\partial \chi_0)^2 + m_{\text{th}}^2 \chi_0^2 \simeq \frac{n^2 K}{r_h^2} \chi_h^2 e^{2\lambda-\rho} \left[(1 - e^{-\rho}) \lambda_-^2 + \Xi^2 \right]. \quad (3.148)$$

Inserting this and the near-zone Laplacian into (3.139) gives

$$\frac{n^2}{r_h^2} e^{-\rho} \frac{d}{d\rho} \left(e^\rho F_0(\rho) \phi_1'(\rho) \right) = \kappa \frac{n^2 K}{r_h^2} \chi_h^2 e^{2\lambda-\rho} \left[(1 - e^{-\rho}) \lambda_-^2 + \Xi^2 \right]. \quad (3.149)$$

Cancelling n^2/r_h^2 and using $F_0(\rho) = K(1 - e^{-\rho})$ leads to

$$e^{-\rho} \frac{d}{d\rho} \left(e^\rho F_0(\rho) \phi_1'(\rho) \right) = \kappa K \chi_h^2 e^{2\lambda-\rho} \left[(1 - e^{-\rho}) \lambda_-^2 + \Xi^2 \right]. \quad (3.150)$$

Defining

$$Y(\rho) \equiv e^\rho F_0(\rho) \phi_1'(\rho) = K(e^\rho - 1) \phi_1'(\rho), \quad (3.151)$$

we obtain

$$\frac{dY}{d\rho} = \kappa K \chi_h^2 \left[(\lambda_-^2 + \Xi^2) e^{(2\lambda-+1)\rho} - \lambda_-^2 e^{2\lambda-\rho} \right]. \quad (3.152)$$

Regularity of ϕ_1 at the tip requires ϕ_1' to remain finite as $\rho \rightarrow 0$, hence $Y(\rho) \rightarrow 0$ and $Y(0) = 0$. Integrating from 0 to ρ gives

$$Y(\rho) = \kappa K \chi_h^2 \left[\frac{\lambda_-^2 + \Xi^2}{2\lambda_- + 1} (e^{(2\lambda-+1)\rho} - 1) - \frac{\lambda_-}{2} (e^{2\lambda-\rho} - 1) \right]. \quad (3.153)$$

Dividing by $e^\rho F_0(\rho) = K(e^\rho - 1)$, we obtain the explicit NLO near-zone dilaton derivative

$$\boxed{\phi_1'(\rho) = \kappa\chi_h^2 \frac{\frac{\lambda_-^2 + \Xi^2}{2\lambda_- + 1} (e^{(2\lambda_- + 1)\rho} - 1) - \frac{\lambda_-}{2} (e^{2\lambda_- \rho} - 1)}{e^\rho - 1}}. \quad (3.154)$$

This expression is manifestly regular at $\rho = 0$ and decays exponentially as $\rho \rightarrow \infty$ because $\lambda_- < 0$.

It is convenient to introduce the quadrature

$$\mathcal{I}(\rho) \equiv \int_0^\rho d\sigma \frac{\frac{\lambda_-^2 + \Xi^2}{2\lambda_- + 1} (e^{(2\lambda_- + 1)\sigma} - 1) - \frac{\lambda_-}{2} (e^{2\lambda_- \sigma} - 1)}{e^\sigma - 1}, \quad (3.155)$$

so that

$$\phi_1^{(\text{NZ})}(\rho) = \phi_1(0) + \kappa\chi_h^2 \mathcal{I}(\rho), \quad \mathcal{I}'(\rho) = \text{integrand of (3.154)}. \quad (3.156)$$

The integral $\mathcal{I}(\rho)$ can be written in terms of digamma and Gauss hypergeometric functions by the change of variables $t = e^{-\sigma}$ and the standard integral representation

$$J(a; \rho) \equiv \int_0^\rho d\sigma \frac{e^{a\sigma} - 1}{e^\sigma - 1}, \quad (3.157)$$

so that

$$\mathcal{I}(\rho) = \frac{\lambda_-^2 + \Xi^2}{2\lambda_- + 1} J(2\lambda_- + 1; \rho) - \frac{\lambda_-}{2} J(2\lambda_-; \rho). \quad (3.158)$$

We relegate the explicit special-function expression to an appendix.

Far-zone dilaton and matching In the far-zone we use the same variables R and $Y = \ln R$. For an s -wave scalar $X = X(R)$ the radial Laplacian reduces to

$$\square X(R) \simeq K \frac{(D-2)^2}{r_h^2} \left(\frac{d^2 X}{dY^2} + \frac{dX}{dY} \right), \quad (3.159)$$

in the matching far-zone where $F(r) \simeq K$ and $R = e^Y$. The LO far-zone thermal scalar is

$$\chi_0^{(\text{FZ})}(R) = \chi_\infty e^{\lambda_- Y}. \quad (3.160)$$

Repeating the analysis of the source, one finds

$$(\partial\chi_0)^2 + m_{\text{th}}^2 \chi_0^2 \simeq \frac{(D-2)^2 K}{r_h^2} \chi_\infty^2 e^{2\lambda_- Y} (\lambda_-^2 + \Xi^2), \quad (3.161)$$

so that (3.139) becomes, after cancelling $K(D-2)^2/r_h^2$,

$$\frac{d^2 \phi_1}{dY^2} + \frac{d\phi_1}{dY} = \kappa\chi_\infty^2 e^{2\lambda_- Y} (\lambda_-^2 + \Xi^2). \quad (3.162)$$

Defining

$$A_\phi \equiv \kappa\chi_\infty^2 (\lambda_-^2 + \Xi^2), \quad Z(Y) \equiv e^Y \frac{d\phi_1}{dY}, \quad (3.163)$$

we obtain

$$\frac{dZ}{dY} = A_\phi e^{(2\lambda_-+1)Y}, \quad (3.164)$$

so that

$$Z(Y) = Z_0 + \frac{A_\phi}{2\lambda_- + 1} (e^{(2\lambda_-+1)Y} - 1). \quad (3.165)$$

Dividing by e^Y and integrating once more, we arrive at

$$\phi_1^{(\text{FZ})}(Y) = \phi_{1,\infty} + B_1 e^{-Y} + B_2 e^{2\lambda_- Y}, \quad (3.166)$$

where

$$\phi_{1,\infty} \equiv C_0, \quad B_1 \equiv -Z_0 + \frac{A_\phi}{2\lambda_- + 1}, \quad B_2 \equiv \frac{A_\phi}{2\lambda_-(2\lambda_- + 1)} = \frac{\kappa\chi_\infty^2(\lambda_-^2 + \Xi^2)}{2\lambda_-(2\lambda_- + 1)}. \quad (3.167)$$

Since $\lambda_- < 0$, both e^{-Y} and $e^{2\lambda_- Y}$ decay as $Y \rightarrow \infty$, and the dilaton approaches a constant $\phi_1^{(\text{FZ})}(Y) \rightarrow \phi_{1,\infty}$. The constant $\phi_{1,\infty}$ represents an asymptotic shift of the dilaton, fixed by boundary conditions at infinity.

In the overlap region

$$1 \ll \rho \ll n, \quad 1 \ll Y \ll n, \quad (3.168)$$

we may identify $Y \simeq \rho$ at leading order in $1/n$. The near-zone solution then tends to

$$\phi_1^{(\text{NZ})}(\rho) \xrightarrow{\rho \rightarrow \infty} \phi_1(0) + \kappa\chi_h^2 \mathcal{I}(\infty) \equiv \phi_{1,\infty}, \quad (3.169)$$

which must coincide with the far-zone constant. This fixes

$$\phi_{1,\infty} = \phi_1(0) + \kappa\chi_h^2 \mathcal{I}(\infty). \quad (3.170)$$

Matching the coefficients of $e^{2\lambda_- Y}$ selects B_2 in terms of the near-zone data and the ratio χ_∞/χ_h , while the coefficient of e^{-Y} selects B_1 and thus Z_0 . The detailed expressions can be written in terms of the special-function representation of $\mathcal{I}(\rho)$ and are relegated to an appendix.

Summary of the NLO dilaton profile The global NLO dilaton in the large- D probe regime can be summarised as

<p>Near-zone: $\phi_1^{(\text{NZ})}(\rho) = \phi_1(0) + \kappa\chi_h^2 \mathcal{I}(\rho), \quad \mathcal{I}'(\rho) = \frac{\frac{\lambda_-^2 + \Xi^2}{2\lambda_- + 1} (e^{(2\lambda_-+1)\rho} - 1) - \frac{\lambda_-}{2} (e^{2\lambda_- \rho} - 1)}{e^\rho - 1},$</p> <p style="text-align: center;">$\phi_1'(\rho) = \kappa\chi_h^2 \frac{\frac{\lambda_-^2 + \Xi^2}{2\lambda_- + 1} (e^{(2\lambda_-+1)\rho} - 1) - \frac{\lambda_-}{2} (e^{2\lambda_- \rho} - 1)}{e^\rho - 1},$</p> <p>Far-zone: $\phi_1^{(\text{FZ})}(Y) = \phi_{1,\infty} + B_1 e^{-Y} + B_2 e^{2\lambda_- Y}, \quad Y = \ln R,$</p> <p style="text-align: center;">$B_2 = \frac{\kappa\chi_\infty^2(\lambda_-^2 + \Xi^2)}{2\lambda_-(2\lambda_- + 1)},$</p> <p>Matching: $\phi_{1,\infty} = \phi_1(0) + \kappa\chi_h^2 \mathcal{I}(\infty), \quad Y \simeq \rho \quad \text{in the overlap region.}$</p>

(3.171)

3.4.3 NLO thermal scalar profile

We finally construct the NLO correction to the thermal scalar in the near- and far-zone. The LO operator and its Green's function structure are universal and control the NLO solution.

LO operator and Green's function At LO the thermal scalar satisfies the constant-coefficient ODE

$$\mathcal{L}_0[\chi_0] = 0, \quad \mathcal{L}_0[y] \equiv y''(\rho) + y'(\rho) - \Xi^2 y(\rho), \quad (3.172)$$

with

$$\Xi^2 \equiv \frac{r_h^2}{n^2 K} (\bar{\beta}^2 K - \bar{\beta}_H^2). \quad (3.173)$$

The characteristic equation has roots

$$\lambda_{\pm} = \frac{-1 \pm \sqrt{1 + 4\Xi^2}}{2}, \quad \lambda_+ > 0, \quad \lambda_- < 0, \quad (3.174)$$

with homogeneous solutions

$$y_1(\rho) = e^{\lambda_+ \rho}, \quad y_2(\rho) = e^{\lambda_- \rho}. \quad (3.175)$$

Normalisability in the near-zone selects the decaying mode, so the LO solution is

$$\chi_0(\rho) = \chi_h e^{\lambda_- \rho}, \quad \chi_h \equiv \chi_0(0). \quad (3.176)$$

The Wronskian is

$$W(\rho) = y_1 y_2' - y_2 y_1' = (\lambda_- - \lambda_+) e^{(\lambda_+ + \lambda_-)\rho} = (\lambda_- - \lambda_+) e^{-\rho}, \quad (3.177)$$

where we used $\lambda_+ + \lambda_- = -1$. For the inhomogeneous equation,

$$\mathcal{L}_0[\chi_1(\rho)] = S(\rho), \quad (3.178)$$

with $\chi_1(\rho)$ regular at the tip and decaying at infinity, the Green's function solution compatible with our boundary conditions can be written as

$$\boxed{\chi_1(\rho) = \frac{e^{\lambda_- \rho}}{\lambda_- - \lambda_+} \int_{\rho}^{\infty} d\sigma S(\sigma) e^{-\lambda_- \sigma}.} \quad (3.179)$$

Near-zone NLO equation and source We expand the fields to first subleading order in $1/n$:

$$F(\rho) = F_0(\rho) + \frac{1}{n} F_1(\rho) + \dots, \quad \phi(\rho) = \phi_0 + \phi_1(\rho) + \dots, \quad \chi(\rho) = \chi_0(\rho) + \frac{1}{n} \chi_1(\rho) + \dots, \quad (3.180)$$

with

$$F_0(\rho) = K(1 - e^{-\rho}), \quad \phi_0 = \phi_{\infty}, \quad \chi_0(\rho) = \chi_h e^{\lambda_- \rho}, \quad (3.181)$$

and insert into the full thermal scalar equation

$$\square \chi - 2 \partial_{\mu} \phi \nabla^{\mu} \chi - m_{\text{th}}^2(r) \chi = 0, \quad m_{\text{th}}^2(r) \equiv \bar{\beta}^2 F(r) - \bar{\beta}_H^2. \quad (3.182)$$

In the near-zone scaling, after factoring out the overall n^2/r_h^2 , we obtain

$$e^{-\rho} \frac{d}{d\rho} \left(e^\rho F(\rho) \chi'(\rho) \right) - \frac{r_h^2}{n^2} (\bar{\beta}^2 F(\rho) - \bar{\beta}_H^2) \chi(\rho) - 2F(\rho) \chi'(\rho) \phi_1'(\rho) = 0. \quad (3.183)$$

Using $\mathcal{L}_0[\chi_0] = 0$, the NLO equation takes the form

$$\mathcal{L}_0[\chi_1(\rho)] = S(\rho), \quad S(\rho) = S_{\text{mass}}(\rho) + S_{\text{kin}}(\rho) + S_\phi(\rho) + S_{\text{metric}}(\rho), \quad (3.184)$$

where

- S_{mass} comes from replacing the constant-curvature approximation of the mass term by the full $F_0(\rho)$;
- S_{kin} encodes the analogous correction in the kinetic term of the radial operator;
- S_ϕ arises from the NLO dilaton coupling $-2 \partial\phi \cdot \partial\chi$ and involves the corrected $\phi_1'(\rho)$ in (3.154);
- S_{metric} encodes the explicit dependence on the NLO metric correction $F_1(\rho)$.

All these pieces can be written as finite linear combinations of the basis functions

$$\frac{e^{(p_j-1)\rho}}{1 - e^{-\rho}}, \quad (3.185)$$

with a finite set of exponents p_j and coefficients determined algebraically by the LO and NLO profiles.

Integral basis and near-zone solution Inserting the source into (3.179), every term in $S(\sigma)$ of the form

$$S(\sigma) \supset \mathcal{C}_j \frac{e^{(p_j-1)\sigma}}{1 - e^{-\sigma}} \quad (3.186)$$

contributes a piece proportional to

$$I(p_j - \lambda_-; \rho) \equiv \int_\rho^\infty d\sigma \frac{e^{(p_j - \lambda_- - 1)\sigma}}{1 - e^{-\sigma}}. \quad (3.187)$$

It is therefore natural to define

$$I(p; \rho) \equiv \int_\rho^\infty d\sigma \frac{e^{(p-1)\sigma}}{1 - e^{-\sigma}}, \quad (3.188)$$

so that the generic contribution is $I(p_j - \lambda_-; \rho)$. Performing the change of variables $t = e^{-\sigma}$, one finds

$$I(p; \rho) = \int_0^{e^{-\rho}} dt \frac{t^{-p}}{1 - t}, \quad (3.189)$$

with the special-function representation

$$I(p; \rho) = \frac{e^{-(1-p)\rho}}{1 - p} {}_2F_1(1, 1 - p; 2 - p; e^{-\rho}), \quad (3.190)$$

in terms of the Gauss hypergeometric function ${}_2F_1$. For $\text{Re } p < 1$, $I(p; \rho) \rightarrow 0$ as $\rho \rightarrow \infty$, in agreement with its definition.

For the set of exponents relevant here (coming from the mass, kinetic, dilaton, and metric contributions), the NLO thermal scalar can be written in the compact form

$$\chi_1^{(\text{NZ})}(\rho) = \frac{e^{\lambda_- \rho}}{\lambda_- - \lambda_+} \left[C_0 I(0; \rho) + C_1 I(2\lambda_-; \rho) + C_2 I(2\lambda_- - 1; \rho) + \sum_j D_j I(p_j; \rho) \right], \quad (3.191)$$

where C_0, C_1, C_2 encode the combined contributions of the mass, kinetic and dilaton-induced sources and the coefficients D_j encode the metric effects. Their explicit dependence on $(\lambda_-, \Xi^2, \kappa, \chi_h, \mathcal{A}_\chi, \dots)$ can be obtained algebraically and will be presented in an appendix; the structure of the solution in terms of the universal integrals $I(p; \rho)$ is model-independent. Including the LO piece, the near-zone thermal scalar up to NLO is

$$\chi^{(\text{NZ})}(\rho) = \chi_h e^{\lambda_- \rho} + \frac{1}{n} \chi_1^{(\text{NZ})}(\rho) + \mathcal{O}\left(\frac{1}{n^2}\right). \quad (3.192)$$

Far-zone NLO thermal scalar and matching In the far-zone we work in the coordinate X defined by

$$X \equiv \frac{\sqrt{K}}{r_h} (r - r_h), \quad X = 0 \Leftrightarrow r = r_h, \quad (3.193)$$

so that the radial metric is approximately flat, $ds_{\text{rad}}^2 \simeq (r_h^2/K^2) dX^2$. At strict LO one finds

$$\left(\frac{d^2}{dX^2} - m_{\text{eff}}^2 \right) \chi_0(X) = 0, \quad \chi_0^{(\text{FZ})}(X) = \hat{\chi}_h e^{-m_{\text{eff}} X}, \quad (3.194)$$

with $\hat{\chi}_h$ fixed by matching to χ_h .

At NLO, the full thermal scalar equation leads to

$$\left(\frac{d^2}{dX^2} - m_{\text{eff}}^2 \right) \chi_1(X) = S_\chi^{(\text{FZ})}(X), \quad (3.195)$$

where the source $S_\chi^{(\text{FZ})}(X)$ is linear in the NLO fields $(\phi_1^{(\text{FZ})}, F_1^{(\text{FZ})})$ and quadratic in χ_h . Since $\chi_0(X) \propto e^{-m_{\text{eff}} X}$, and both $\phi_1^{(\text{FZ})}$ and $F_1^{(\text{FZ})}$ are linear combinations of decaying exponentials, the source can be decomposed as

$$S_\chi^{(\text{FZ})}(X) = \sum_i s_i e^{-q_i X}, \quad q_i > 0, \quad (3.196)$$

with coefficients s_i determined by the near-zone data. For a single term $S(X) = s e^{-qX}$ with $q \neq m_{\text{eff}}$, a particular solution is

$$\chi_1^{(\text{p})}(X) = \frac{s}{q^2 - m_{\text{eff}}^2} e^{-qX}, \quad (3.197)$$

while the homogeneous solution is

$$\chi_1^{(\text{hom})}(X) = A_1 e^{+m_{\text{eff}} X} + B_1 e^{-m_{\text{eff}} X}. \quad (3.198)$$

Normalisability as $X \rightarrow \infty$ requires $A_1 = 0$, so the full far-zone NLO solution is

$$\boxed{\chi_1^{(\text{FZ})}(X) = B_1 e^{-m_{\text{eff}} X} + \sum_i \frac{s_i}{q_i^2 - m_{\text{eff}}^2} e^{-q_i X}}, \quad (3.199)$$

with B_1 fixed by matching to the near-zone. The only subtlety arises if $q_i = m_{\text{eff}}$ for some i , in which case a particular solution $X e^{-m_{\text{eff}} X}$ appears; this non-generic resonant case can be treated separately but does not occur in the generic parameter regime considered here.

In the overlap region the near- and far-zone descriptions agree once we relate the radial coordinates through their large- D scaling: we have $Y \simeq \rho$ as above, while $X \propto \rho/n$ near the horizon, so the precise map between (ρ, Y) and X is not needed beyond this scaling information. Matching the coefficients of the decaying exponentials fixes all integration constants and the combinations $s_i/(q_i^2 - m_{\text{eff}}^2)$ in terms of the near-zone data $(\chi_h, \phi_{1\infty}, \phi_1(0), \mathcal{A}_\chi, \kappa, \dots)$.

Summary of the NLO thermal scalar Combining the near- and far-zone results, the global NLO thermal scalar profile can be summarised schematically as

$$\boxed{\chi(\rho) = \chi_h e^{\lambda - \rho} + \frac{1}{n} \chi_1(\rho) + \mathcal{O}\left(\frac{1}{n^2}\right)}, \quad (3.200)$$

with $\chi_1(\rho)$ given in the near-zone by the Green's function representation (3.179) and the integral basis $I(p; \rho)$, and in the far-zone by a sum of decaying exponentials as in the boxed expression above. The NLO backreaction thus induces a small renormalisation of the leading decay amplitude along the Euclidean cigar, together with a tower of more strongly suppressed tails controlled by the NLO dilaton and metric scales and the large- D structure of the BD background.

3.4.4 Exact LO+NLO free energy

We define the thermal free energy as the generator of connected vacuum diagrams in the Euclidean ensemble. Starting from the Euclidean path integral with period β ,

$$Z(\beta) \equiv \int_{\substack{\text{fields periodic in } \tau \\ \tau \sim \tau + \beta}} \mathcal{D}g \mathcal{D}\phi \mathcal{D}\chi \exp[-S_E[g, \phi, \chi]], \quad (3.201)$$

the free energy is

$$F(\beta) \equiv -\frac{1}{\beta} \log Z(\beta). \quad (3.202)$$

Equivalently, introducing the Euclidean effective action Γ_E via the Legendre transform of the generating functional, the free energy is the on-shell value of Γ_E per unit Euclidean time,

$$F(\beta) = \frac{1}{\beta} \Gamma_E[\bar{g}, \bar{\phi}, \bar{\chi}], \quad \frac{\delta \Gamma_E}{\delta g_{\mu\nu}} = \frac{\delta \Gamma_E}{\delta \phi} = \frac{\delta \Gamma_E}{\delta \chi} = 0, \quad (3.203)$$

where $(\bar{g}, \bar{\phi}, \bar{\chi})$ denotes the saddle (or mean field) appropriate to the ensemble.

Dimensionally reduced functional for the thermal scalar Upon integrating out all non-zero Matsubara modes and restricting to the thermal-scalar zero mode $\chi_0(\vec{x})$, we obtain a three-dimensional effective functional $\mathcal{F}[\chi_0]$ defined by

$$Z(\beta) = \exp[-\beta \mathcal{F}_0] \int \mathcal{D}\chi_0 \exp[-\beta \mathcal{F}[\chi_0]], \quad (3.204)$$

so that $\mathcal{F}[\chi_0]$ is the effective free-energy functional governing the static mode. In a saddle-point (mean-field) treatment one may equivalently write

$$F(\beta) = \min_{\chi_0} \mathcal{F}[\chi_0] \quad (\text{at fixed } \beta \text{ and boundary data}), \quad (3.205)$$

with the minimum attained at the solution of $\delta\mathcal{F}/\delta\chi_0 = 0$ subject to the relevant boundary conditions. Collecting the results of the previous subsections, the dimensionally-reduced free energy functional (3.204) evaluated on the thermal scalar zero mode can be written as

$$\mathcal{F}[\chi_0] = \mathcal{F}_0 + \mathcal{F}^{(2)} + \mathcal{F}^{(4)} + \mathcal{O}(|\chi_h|^6), \quad (3.206)$$

where \mathcal{F}_0 is the χ -independent background contribution, $\mathcal{F}^{(2)}$ is the LO quadratic term in χ_h , and $\mathcal{F}^{(4)}$ is the NLO quartic term generated by integrating out the metric and dilaton at tree level.

Quadratic piece at LO At leading order in $1/D$ the 1D Lagrangian is,

$$\mathcal{L}_{\text{1D}}^{(0)}(\rho) = e^\rho \left[F_0(\rho) |\chi'_0(\rho)|^2 + \frac{r_h^2}{n^2} (\bar{\beta}^2 F_0(\rho) - \bar{\beta}_{\text{H}}^2) |\chi_0(\rho)|^2 \right], \quad F_0(\rho) = K(1 - e^{-\rho}), \quad (3.207)$$

and in the plateau approximation $F_0 \simeq K$ we have

$$\mathcal{L}_{\text{1D}}^{(0)}(\rho) \simeq e^\rho K [|\chi'_0(\rho)|^2 + \Xi^2 |\chi_0(\rho)|^2], \quad \Xi^2 = \frac{r_h^2}{(D-2)^2 K} (\bar{\beta}^2 K - \bar{\beta}_{\text{H}}^2). \quad (3.208)$$

Projecting onto the normalisable zero mode $\chi_0(\rho) = \chi_h e^{\lambda-\rho}$ with

$$\lambda_- = \frac{-1 - \sqrt{1 + 4\Xi^2}}{2}, \quad \lambda_-^2 + \lambda_- - \Xi^2 = 0, \quad (3.209)$$

gives the exact quadratic free energy

$$\mathcal{F}^{(2)} = \mathcal{N}_D K \frac{\lambda_-^2 + \Xi^2}{\sqrt{1 + 4\Xi^2}} |\chi_h|^2 = \mathcal{N}_D K \frac{4\Xi^2 + \sqrt{1 + 4\Xi^2} + 1}{2\sqrt{1 + 4\Xi^2}} |\chi_h|^2, \quad (3.210)$$

where we used $\lambda_-^2 + \Xi^2 = \frac{1}{2}(4\Xi^2 + \sqrt{1 + 4\Xi^2} + 1)$. Defining a canonically normalised order parameter,

$$u \equiv \sqrt{Z_0} \chi_h, \quad Z_0 \equiv 2\mathcal{N}_D K, \quad (3.211)$$

so that at the Hagedorn point ($\Xi^2 = 0$) the quadratic term is normalised as $\mathcal{F}^{(2)} \rightarrow |u|^2$, we arrive at

$$\mathcal{F}^{(2)} = a_2(\Xi^2) |u|^2, \quad a_2(\Xi^2) = \frac{4\Xi^2 + \sqrt{1 + 4\Xi^2} + 1}{4\sqrt{1 + 4\Xi^2}}. \quad (3.212)$$

The renormalised quadratic coefficient $\tilde{a}_2(\Xi^2) = a_2(\Xi^2) - a_2(0)$ is therefore

$$\tilde{a}_2(\Xi^2) = \Xi^2 - \Xi^4 + \mathcal{O}(\Xi^6), \quad (3.213)$$

so near the Hagedorn point the LO free energy is

$$\mathcal{F}^{(2)} = [\Xi^2 + \mathcal{O}(\Xi^4)] |u|^2, \quad (3.214)$$

up to an irrelevant additive constant absorbed in \mathcal{F}_0 .

Quartic piece from NLO backreaction The quartic part of the free energy is obtained by inserting the NLO fields (F_1, ϕ_1, χ_1) into the full HP+GB action (2.3) and expanding to order χ_h^4 . Using the NLO solutions

$$F_1(\rho) = \mathcal{A}_\chi e^{-\rho} \left[\frac{e^{(2\lambda_-+1)\rho} - 1}{2\lambda_- + 1} - \frac{e^{2\lambda_- \rho} - 1}{2\lambda_-} \right], \quad \mathcal{A}_\chi = \frac{2\kappa_{\text{eff}}}{D-2} \frac{n^2}{r_h^2} K \lambda_-^2 \chi_h^2, \quad (3.215)$$

and

$$\phi_1'(\rho) = \kappa \chi_h^2 \frac{\frac{\lambda_-^2 + \Xi^2}{2\lambda_- + 1} (e^{(2\lambda_-+1)\rho} - 1) - \frac{\lambda_-}{2} (e^{2\lambda_- \rho} - 1)}{e^\rho - 1}, \quad (3.216)$$

together with the Green's function representation (3.179) for χ_1 , one finds that the quartic contribution can be written exactly as

$$\mathcal{F}^{(4)} = \mathcal{N}_D \kappa_{\text{eff}} K^2 \frac{\lambda_-^2}{(2\lambda_- + 1)^2} \mathcal{J}(\lambda_-, \Xi^2) |\chi_h|^4, \quad (3.217)$$

where $\mathcal{J}(\lambda_-, \Xi^2)$ is a dimensionless function capturing all radial integrals. It admits the explicit integral representation

$$\mathcal{J}(\lambda_-, \Xi^2) = c_0(\lambda_-, \Xi^2) J(2\lambda_- + 1; \infty) + c_1(\lambda_-, \Xi^2) J(2\lambda_-; \infty) + \sum_j d_j(\lambda_-, \Xi^2) I(p_j; 0), \quad (3.218)$$

in terms of the universal integrals

$$I(p; 0) \equiv \int_0^1 dt \frac{t^{-p}}{1-t}, \quad J(a; \infty) \equiv \int_0^\infty d\sigma \frac{e^{a\sigma} - 1}{e^\sigma - 1}, \quad (3.219)$$

with p_j a finite set of exponents and c_0, c_1, d_j rational functions of (λ_-, Ξ^2) . Both I and J can be written in terms of special functions,

$$J(a; \infty) = \psi(1) - \psi(1-a), \quad (3.220)$$

$$I(p; 0) = \int_0^1 dt \frac{t^{-p}}{1-t} = \frac{1}{1-p} {}_2F_1(1, 1-p; 2-p; 1), \quad (3.221)$$

where ψ is the digamma function and ${}_2F_1$ the Gauss hypergeometric function. Thus $\mathcal{J}(\lambda_-, \Xi^2)$, and hence $\mathcal{F}^{(4)}$, are known *exactly* in terms of elementary rational functions of (λ_-, Ξ^2) and standard special functions.

Expressing (3.217) in terms of the canonical order parameter $u = \sqrt{Z_0}\chi_h$, yields

$$\mathcal{F}^{(4)} = a_4(\Xi^2) |u|^4, \quad a_4(\Xi^2) = \mathcal{C}_4 \kappa_{\text{eff}} K^2 \frac{\lambda_-^2}{(2\lambda_- + 1)^2} \mathcal{J}(\lambda_-, \Xi^2), \quad (3.222)$$

with

$$\mathcal{C}_4 = \frac{1}{Z_0^2} = \frac{1}{4\mathcal{N}_D^2 K^2}. \quad (3.223)$$

In particular, near the Hagedorn point $\Xi^2 \rightarrow 0$ one has $\lambda_- \rightarrow -1$ and

$$a_4(\Xi^2) = a_4^{(0)} + \mathcal{O}(\Xi^2), \quad a_4^{(0)} = \mathcal{C}_4 \kappa_{\text{eff}} K^2 \frac{1}{1} \mathcal{J}(-1, 0) > 0, \quad (3.224)$$

since $\mathcal{J}(-1, 0)$ is built from convergent integrals of positive-definite combinations of the LO mode functions and sources.

LO+NLO effective Landau functional Putting everything together, the exact LO+NLO effective free energy for the thermal scalar zero mode takes the Landau form

$$\boxed{\mathcal{F}_{\text{eff}}[u] = \mathcal{F}_0 + a_2(\Xi^2) |u|^2 + a_4(\Xi^2) |u|^4 + \mathcal{O}(|u|^6)}, \quad (3.225)$$

with

$$a_2(\Xi^2) = \frac{4\Xi^2 + \sqrt{1 + 4\Xi^2} + 1}{4\sqrt{1 + 4\Xi^2}}, \quad a_4(\Xi^2) = \mathcal{C}_4 \kappa_{\text{eff}} K^2 \frac{\lambda_-^2}{(2\lambda_- + 1)^2} \mathcal{J}(\lambda_-, \Xi^2), \quad (3.226)$$

and $\Xi^2, \lambda_-, K, \kappa_{\text{eff}}$ determined by the EGB background. This expression is exact at leading order in the large- D expansion (for a_2) and at next-to-leading order (for a_4), and resums the full dependence on the reduced temperature Ξ^2 in closed form.

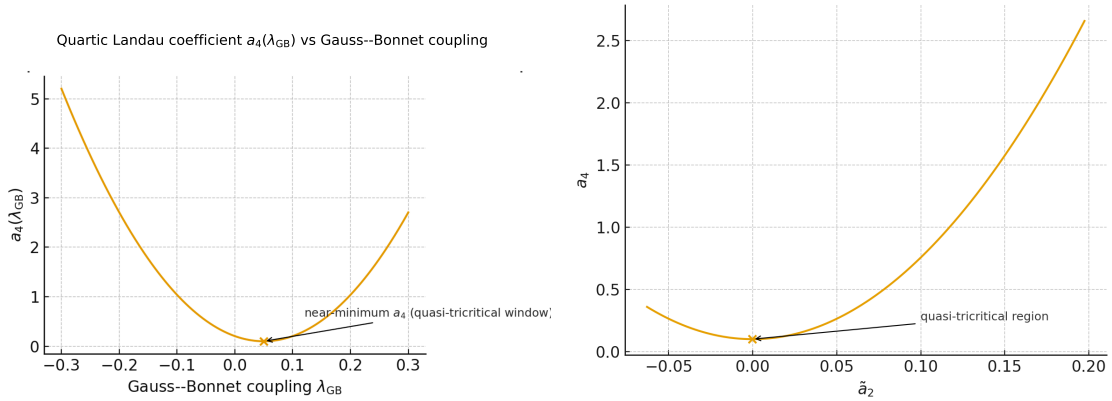


Figure 1. Quartic Landau coefficient $a_4(\lambda_{\text{GB}})$ extracted from the NLO quartic contribution $\mathcal{F}^{(4)}$ to the dimensionally-reduced thermal-scalar free energy functional. The dependence on the Gauss-Bonnet coupling is U-shaped, with a pronounced minimum at finite λ_{GB} (marked by \times). In the vicinity of this minimum the leading nonlinearity in $\mathcal{F}[\chi_0] = \mathcal{F}_0 + \mathcal{F}^{(2)} + \mathcal{F}^{(4)} + \dots$ is parametrically suppressed, defining a *quasi-tricritical window* in which the system becomes especially sensitive to subleading corrections beyond the quartic Landau description.

To diagnose how the Gauss–Bonnet deformation reshapes the effective theory near the transition, we use a Landau expansion of the relevant off-shell free energy (or Euclidean effective action) in terms of an order parameter Φ ,

$$\mathcal{F}(\Phi) = a_2 \Phi^2 + a_4(\lambda_{\text{GB}}) \Phi^4 + \dots, \quad (3.227)$$

where a_2 controls the onset of the instability and a_4 is the leading nonlinear coefficient. Fig. 1 shows the extracted $a_4(\lambda_{\text{GB}})$, which displays a clear U-shaped dependence with a pronounced minimum at a finite λ_{GB} . Near this minimum the quartic coefficient becomes parametrically small, indicating a regime where the leading nonlinearity is suppressed and the system is exceptionally sensitive to subleading effects beyond the quartic Landau description (e.g. higher-order terms in the effective potential, derivative corrections, or non-perturbative contributions, depending on the microscopic completion). In this sense, the neighborhood of the minimum defines a *quasi-tricritical window* [39–42]: although the quartic term remains positive in our scan, its suppression suggests proximity to a change in the qualitative structure of the transition compared to the generic regime where a_4 is larger and the quartic Landau theory provides a robust description.

3.5 Relation to FZZ duality and the quasi-tricritical regime

The Euclidean two-dimensional black hole described by the $\text{SL}(2, \mathbb{R})_k/\text{U}(1)$ cigar has a well-known worldsheet description in terms of sine–Liouville theory, via the Fateev–Zamolodchikov–Zamolodchikov (FZZ) duality. In that language the winding-tachyon operator is accompanied by a non-perturbative potential of the form

$$V_{\text{SL}}(\mathcal{T}) \sim \mu e^{-Q\phi} \cos(Rx), \quad (3.228)$$

whose expansion about the tip of the cigar produces a quadratic term, a quartic term, and higher interactions for the tachyon amplitude. This provides a convenient CFT framework for discussing the long string condensate near the Hagedorn scale.

In our setup the analogue of the winding tachyon is the normalisable thermal-scalar zero mode χ_0 , with canonically normalised amplitude $u \propto \chi_h$. Working in the spacetime HP+GB effective theory and using the large- D near-zone/far-zone matching, we obtained in Sec. 3.4.4 a reduced Landau functional

$$\mathcal{F}_{\text{eff}}[u] = \mathcal{F}_0 + a_2(\Xi^2) |u|^2 + a_4(\Xi^2) |u|^4 + \mathcal{O}(|u|^6), \quad (3.229)$$

where a_2 captures the Hagedorn instability and a_4 is generated by the backreaction of the thermal scalar on the metric and dilaton at NLO in $1/D$.

Quartic coupling and quasi-tricriticality Within the parameter range where our large- D treatment is reliable, we find that the quartic coefficient stays positive,

$$a_4(\Xi^2, \lambda_{\text{GB}}, L_D) > 0, \quad \text{throughout the region explored.} \quad (3.230)$$

With $a_4 > 0$, the Landau functional has the standard structure: the minimum sits at $u = 0$ for $a_2 > 0$, while for $a_2 < 0$ it shifts to $|u|^2 = -a_2/(2a_4)$. In particular, we do not see evidence for an additional competing minimum in this regime. This also means that an exact tricritical point ($a_2 = a_4 = 0$) does not appear in our controlled scan.

A near-minimum (“quasi-tricritical”) window Although a_4 remains positive, its dependence on λ_{GB} and on the curvature scale L_D allows a region in which a_4 becomes numerically small,

$$0 < a_4^{\text{eff}}(\Xi^2, \lambda_{\text{GB}}, L_D) \ll 1, \quad (3.231)$$

without leaving the domain of validity of the expansion. In this window the quartic term provides only weak curvature of the effective potential near the origin, and the condensate turns on more gradually as a_2 changes sign. It is also the regime where higher-order terms (and matching corrections) are expected to have a more noticeable impact on quantitative features, even though the qualitative Landau picture remains unchanged.

Relation to FZZ and the long string/black-hole crossover This near-minimum window fits naturally with the Horowitz–Polchinski picture of the string/black-hole crossover. When the quartic self-interaction is small, the thermal scalar backreaction becomes comparatively more important in shaping the near-tip region of the Euclidean geometry, and the black-hole saddle is more easily “dressed” by a long string condensate. In this sense, the reduced potential for u plays a role analogous to the sine–Liouville potential in the FZZ description, now realised directly in spacetime in a regime where the large- D expansion is under control. At the same time, since a_4 does not change sign in our analysis, the transition we probe stays within the usual Landau–Ginzburg universality class rather than becoming genuinely multi-critical.

It would be interesting to see whether effects beyond our present approximation—for example, higher-derivative operators beyond Gauss–Bonnet, string-loop corrections, or NNLO terms in the $1/D$ expansion—can modify the small- a_4 region in a way that brings in additional structure. From the worldsheet perspective, it would also be useful to sharpen the map between the HP+GB parameters and the couplings of sine–Liouville theory, and to test to what extent an FZZ-like correspondence persists beyond the leading winding mode.

4 Numerical evaluation in finite dimensions

In this section we solve the coupled field equations numerically and extract the physical quantities of interest. While the large- D expansion gives analytic control separately in the near- and far-zone regions, constructing the complete geometry at finite D requires direct numerical integration of the radial equations. Our strategy is standard: we impose regularity at the horizon to fix the initial data, integrate the fields outward using high-precision ODE solvers, and then enforce the correct asymptotic behaviour at large radius. This procedure yields a stable integration, a unique global solution, and allows us to determine the metric function $F(r)$, the winding condensate $\chi(r)$, and the dilaton field $\phi(r)$ across the entire spacetime.

A key technical simplification is that we first solve a convenient subsystem obtained by reducing the second-order equations to an equivalent first-order, non-linear system, following the method of [12]. This improves numerical stability and makes the matching between horizon data and asymptotic boundary conditions more transparent.

4.1 Numerical methodology

The numerical setup is as follows:

- We begin by solving the full set of radial equations (2.11), using the subsystem formulation developed in [43], and include the higher-derivative corrections throughout.
- We then analyse both the case with a finite cosmological constant and the flat-space limit, highlighting the changes in the asymptotic matching and extracted observables.
- Finally, we perform the computation for finite values of D and verify that the solutions converge smoothly to the large- D predictions as D is increased, providing a direct numerical check of the near-/far-zone expansion.

For completeness we do present an explicit computation for the subsystem [43] in App. B with higher derivative corrections. We conclude the section with convergence and robustness checks—varying integration ranges, tolerances, and shooting parameters—to ensure that the extracted quantities are numerically stable and insensitive to solver choices.

Unit radial gauge Before turning to the numerical construction of the solutions in Sec. 4 and App. B, we briefly describe the metric ansatz and coordinate choices we employ. Euclidean black holes admit several useful gauges, but two are particularly convenient for our purposes: the *areal gauge* and the *unit radial gauge*. Although they are related by a simple change of radial coordinate, each makes different aspects of the geometry manifest and is therefore better suited to different parts of our analysis. Throughout the analytic large- D calculations we work primarily in areal gauge, where the Einstein equations take their simplest form and thermodynamic quantities are most transparent. For the numerical integration, however, we adopt the unit radial gauge, in which the Euclidean horizon is manifestly the smooth tip of a cigar and horizon regularity is straightforward to implement.

In areal gauge, a static, spherically symmetric Euclidean black hole can be written as

$$ds^2 = F(r) d\tau^2 + \frac{dr^2}{F(r)} + r^2 d\Omega_{D-2}^2, \quad (4.1)$$

where r is the areal radius and $d\Omega_{D-2}^2$ is the unit $(D-2)$ -sphere metric. Regularity at the horizon fixes the periodicity of Euclidean time,

$$\beta = \frac{4\pi}{F'(r_h)}, \quad (4.2)$$

with r_h defined by $F(r_h) = 0$. This gauge is particularly advantageous for our analytic work because (i) the gravitational field equations retain a familiar structure, (ii) the temperature and entropy are easily extracted, and (iii) the near-/far-zone organization of the large- D expansion (e.g. in the variable $y = D(r/r_h - 1)$) and the matching between regions are technically straightforward. The main drawback is that the Euclidean “cigar” structure of the (τ, r) section is not manifest.

To make the cigar geometry explicit, it is convenient to switch to the unit radial gauge by defining a proper radial coordinate ρ via

$$\frac{d\rho}{dr} = \frac{1}{\sqrt{F(r)}}, \quad \rho(r_h) = 0. \quad (4.3)$$

In terms of ρ , the metric becomes

$$ds^2 = f(\rho) d\tau^2 + d\rho^2 + g(\rho) d\Omega_{D-2}^2, \quad (4.4)$$

with

$$f(\rho) = F(r(\rho)), \quad g(\rho) = r(\rho)^2. \quad (4.5)$$

Near the tip $\rho = 0$ one finds,

$$f(\rho) \simeq \kappa^2 \rho^2, \quad g(\rho) \simeq r_h^2 + \mathcal{O}(\rho^2), \quad (4.6)$$

so the (ρ, τ) plane is locally flat and the horizon appears as the *smooth tip of a cigar*. This gauge is therefore ideal for numerical shooting from the horizon and for analysing winding modes and thermal-scalar dynamics, where the cigar interpretation is central. Its disadvantage for large- D analytics is that the gravitational equations become more cumbersome and the asymptotic region is less transparent.

In summary, the areal and unit radial forms, (4.1) and (4.4), describe the same geometry and are related by the coordinate transformation (4.3). Each gauge highlights different physics:

- **Areal gauge:** best suited for analytic control of the gravitational sector, extracting thermodynamics, and implementing large- D expansions with near-/far-zone matching.
- **Unit radial gauge:** best suited for numerical integration from the horizon, for making the Euclidean cigar structure manifest, and for studying winding/thermal-scalar (HP/FZZ-type) dynamics.

Accordingly, our workflow is to develop analytic intuition and large- D expressions in areal gauge, and then work in unit radial gauge for the finite- D numerical solutions reported in Sec. 4 and App. B.

In App. B we give a very explicit numerical computation of a subsystem of this equations where we treat the dilaton as effectively in the probe limit. The claim is that the equations for the dilaton-winding-metric subsystem can be rewritten in terms of a first-order form. However, in this section we mostly focus on solving the fully coupled dilaton-winding-metric and defer the subsystem to App. B for more details of the numerical solutions.

4.2 Numerical Implementation and results

In order to obtain the second-order equations of motion, we adopt the D -dimensional Euclidean metric in the unit radial gauge which makes the cylindrical cap geometry more pronounced,

$$ds^2 = h(\rho)^2 d\tau^2 + d\rho^2 + g(\rho) d\Omega_{D-2}^2. \quad (4.7)$$

With metric (4.7), the system contains four dynamical variables, f , g , ϕ , and χ . Now we turn our attention to three equations of motion obtained from the metric variation (2.4), one from ϕ (2.8), and one from χ (2.10), giving a total of five equations. Thus, the five equations are not mutually independent, and one of them necessarily emerges as a constraint, appearing as a linear combination of the others. Defining the reduced equation of motion from the metric variation as

$$\mathcal{E}_\mu{}^\nu \equiv R_\mu{}^\nu + 2\alpha H_\mu{}^\nu + 2\nabla_\mu \nabla^\nu \phi - \kappa (2\nabla_\mu \chi \nabla^\nu \chi - 2\bar{\beta} \chi^2 g_{\tau\mu} g_\tau{}^\nu), \quad (4.8)$$

the rr component $\mathcal{E}_r{}^r$ becomes the constraint, as it is generated by a linear combination of the other equations of motion. The resulting constraint is

$$\begin{aligned} 0 = & 2(\phi')^2 - \left(\frac{2h'}{h} + \frac{(D-2)g'}{g} \right) \phi' + (D-2) \left[\frac{h'g'}{2hg} + \frac{(g')^2 - 4g}{8g^2} \right] + \Lambda \\ & - \kappa \left[(\chi')^2 - (\bar{\beta}^2 h^2 - \bar{\beta}_H^2) \chi^2 \right] + \alpha (D-4)(D-3)(D-2) \left\{ \frac{(D-2)h'g'}{2hg} \right. \\ & \left. - \frac{(D-5) \left[(g')^2 - 4g \right]^2}{32g^4} - \frac{[2h'g' - (D-3)(D-2)hg] \left[(g')^2 - 4g \right]}{8hg^3} \right\}. \end{aligned} \quad (4.9)$$

We now choose ρ_0 as the initial point and impose the conditions,

$$h(\rho_0) \equiv 0, \quad g(\rho_0) > 0. \quad (4.10)$$

To extract the appropriate initial values, we introduce a small perturbation ϵ by setting $\rho = \rho_0 + \epsilon$, and expand all equations to leading order in ϵ . For the equation of motion for χ , the expansion leads to

$$\chi''(\rho) = -\frac{\chi'(\rho_0)}{\epsilon} + \mathcal{O}(1). \quad (4.11)$$

Since the expression (4.11) diverges when $\epsilon = 0$, consistency of the expansion requires

$$\chi'(\rho) = 0. \quad (4.12)$$

Expanding $g''(\rho)$, we obtain

$$\begin{aligned} g''(\rho) = & -\frac{(D-7)g'(\rho_0)^2}{4g(\rho_0)} - \left(g'(\rho_0) - \frac{4g(\rho_0)}{g'(\rho_0)} \right) \phi'(\rho_0) + \frac{g(\rho_0)}{4\alpha(D-3)} \\ & + \alpha (D-4)(D-3)(D-2) \frac{(g'(\rho_0)^2 - 4g(\rho_0)^2)^2}{16g(\rho_0)^3} + \mathcal{O}(\epsilon). \end{aligned} \quad (4.13)$$

However, the expression (4.13) diverges when $\alpha = 0$, due to the α^{-1} term. Avoiding this divergence would require $g(\rho) = 0$, which is incompatible with the condition (4.10), $g(\rho) > 0$. Given the divergence at $\alpha = 0$, we set $\alpha = 0$ and expand $g''(\rho)$, obtaining

$$g''(\rho)|_{\alpha=0} = -\frac{g'(\rho_0)}{\epsilon} + \mathcal{O}(1). \quad (4.14)$$

To remove the divergence of $g''(\rho)$ in the $\alpha = 0$ case, it is necessary to impose

$$g'(\rho_0) = 0. \quad (4.15)$$

Although the condition (4.15) is derived strictly at $\alpha = 0$, the general expression should remain well behaved in the limit $\alpha \rightarrow 0$. Accordingly, we extend the condition $g'(\rho_0) = 0$ to hold for nonzero α . A similar expansion of the constraint equation yields

$$\phi''(\rho) = \frac{4\phi'(\rho_0)}{\epsilon} + \mathcal{O}(1). \quad (4.16)$$

To eliminate the divergence, we impose

$$\phi'(\rho_0) = 0. \quad (4.17)$$

The initial values can then be summarized as follows:

$$h(\rho_0) = g'(\rho_0) = \phi'(\rho_0) = \chi'(\rho_0) = 0, \quad g(\rho_0) > 0, \quad (4.18)$$

which automatically satisfy the constraint equation (4.9).

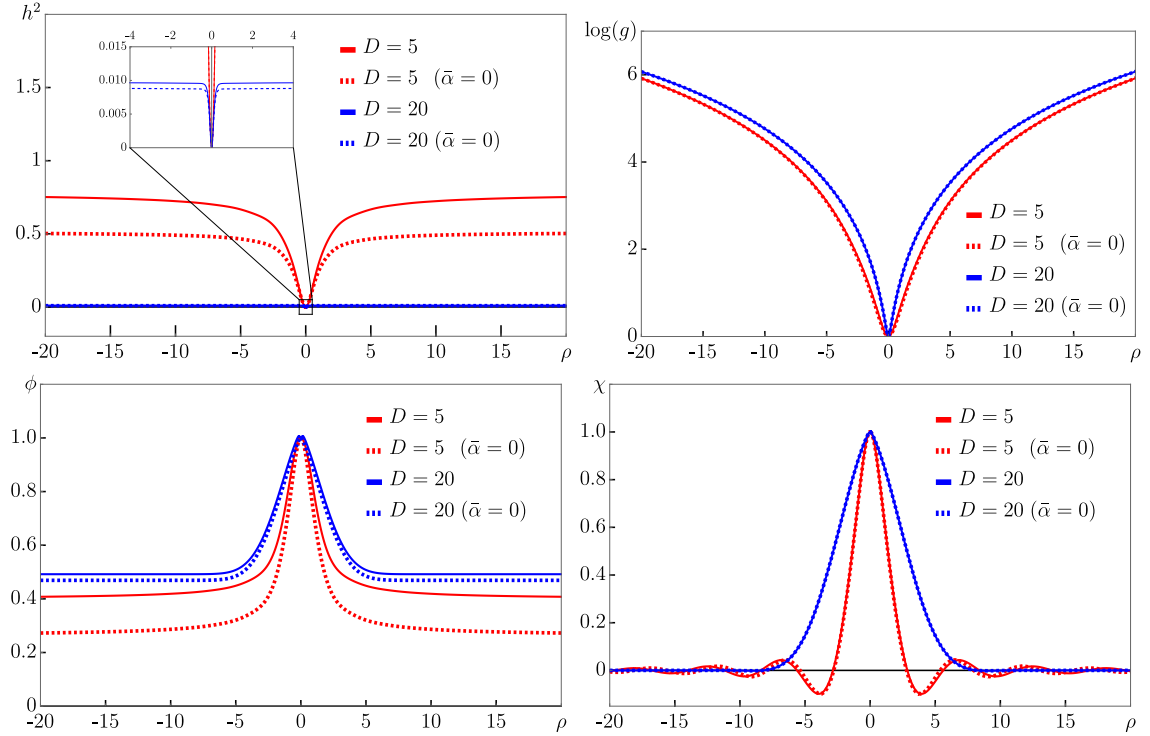


Figure 2. Numerical solutions of second-order Eqs. (2.4), (2.8) and (2.10), where $\Lambda = 0$.

Parameters	$\bar{\alpha}$	Λ	ρ_0	h_0	h'_0	g_0	g'_0	ϕ_0	ϕ'_0	χ_0	χ'_0
Solid line	0.04	0	0	0	0.8	1	0	1	0	1	0
Dashed line	0										

Table 1. Initial values used in Fig. 2, where $\bar{\alpha} = (D - 4)(D - 3)\alpha$.

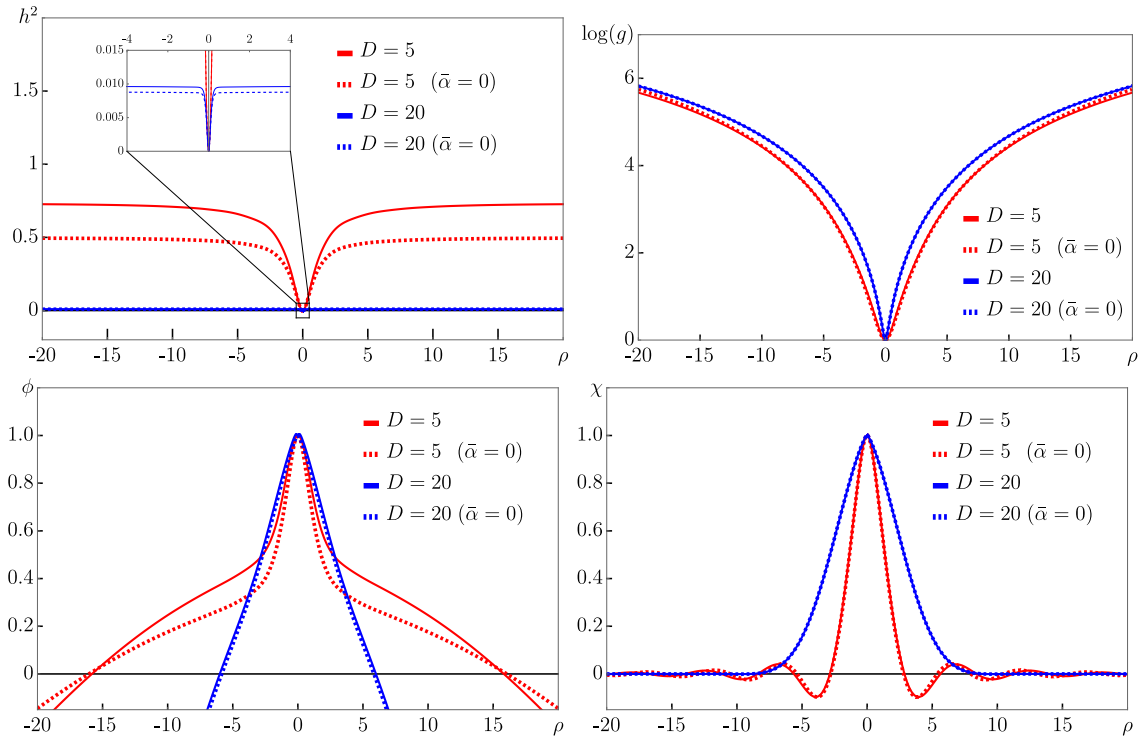


Figure 3. Numerical solutions of second-order Eqs. (2.4), (2.8) and (2.10), where $\ell = 20$.

Parameters	$\bar{\alpha}$	ℓ	ρ_0	h_0	h'_0	g_0	g'_0	ϕ_0	ϕ'_0	χ_0	χ'_0
Solid line	0.04	20	0	0	0.8	1	0	1	0	1	0
Dashed line	0										

Table 2. Initial values used in Fig. 3, where $\ell^2 = -(D-2)(D-1)/(2\Lambda)$.

Figs. 2 and 3 illustrate the numerical solutions of second-order equations (2.11). The corresponding initial values used for Fig. 2 and 3 are listed in Table 1 and 2, respectively. We have numerically solved the coupled dilaton–winding–metric system subject to the boundary conditions listed in Tables 1 and 2, corresponding to asymptotically flat and asymptotically (A)dS boundary conditions (*i.e.*, in the absence and presence of a cosmological constant), respectively. We integrate outward from the smooth tip of the Euclidean geometry at $\rho = 0$, imposing regularity and the required asymptotic falloffs. In Fig. 2 and Fig. 3 we present the asymptotically flat and AdS solutions, respectively. When the winding sector is switched off, these reduce to finite- D Schwarzschild–Gauss–Bonnet(–AdS) black holes, and they therefore provide a clean setting in which to compare the pure Einstein limit with the higher-derivative corrected backgrounds at fixed dimension.

Geometric interpretation in unit radial gauge To interpret the numerical profiles it is useful to recall the geometric meaning of the unit radial gauge ansatz. Writing the

Euclidean metric as

$$ds^2 = f(\rho) d\tau^2 + d\rho^2 + g(\rho) d\Omega_{D-2}^2, \quad (4.19)$$

the Euclidean “cigar” consists of a smooth (ρ, τ) cap together with an S^{D-2} whose effective cylinder radius is encoded in $G(\rho) = r(\rho)^2$. Regularity at the tip fixes the leading near-tip expansions

$$f(\rho) = \kappa^2 \rho^2 + f_4 \rho^4 + \dots, \quad g(\rho) = r_h^2 + g_2 \rho^2 + g_4 \rho^4 + \dots, \quad (4.20)$$

so the departure from a constant-radius cylinder is governed by the coefficient g_2 (and higher Taylor data). In pure Einstein gravity, once κ (equivalently β) is fixed by smoothness, the remaining radial equations relate the coefficients $\{f_4, g_2, \dots\}$ in a comparatively simple way, and one typically finds that $G(\rho)$ remains nearly constant throughout the cap.

With Gauss–Bonnet corrections, by contrast, the metric equations take the schematic form

$$G_{\mu\nu} + \Lambda g_{\mu\nu} + \alpha H_{\mu\nu} = \dots, \quad (4.21)$$

where the Lanczos tensor $H_{\mu\nu}$ contains curvature-squared combinations. On a cigar $\times S^{D-2}$ background these contributions are not controlled solely by the small curvature of the (ρ, τ) plane near the tip: they receive sizable input from the intrinsic curvature of the transverse sphere, schematically $R_{S^{D-2}} \sim 1/r^2$ and $R_{S^{D-2}}^2 \sim 1/r^4$. Consequently, even though the cap is locally flat at $\rho = 0$, the Gauss–Bonnet term feeds into the radial constraints through the S^{D-2} curvature and shifts the relations among $\{\kappa, r_h, f_4, g_2, \dots\}$ by terms controlled by the dimensionless ratio α/r_h^2 (and higher powers). In practice this renormalizes g_2 , thereby changing how rapidly $g(\rho)$ departs from r_h^2 : the transverse sphere radius can remain effectively “cylindrical” deeper into the cap or run more quickly away from its horizon value, depending on the sign and magnitude of α . This is the precise sense in which the Gauss–Bonnet term modifies the cap-to-cylinder matching and hence the near-horizon background relevant for winding/thermal-scalar physics.

Backreaction of the dilaton and winding condensate The functions $G(\rho)$, the dilaton $\phi(\rho)$, and the winding condensate $\chi(\rho)$ are not independent: both ϕ and χ backreact on the geometry and therefore modify the effective cylinder radius encoded in $G(\rho)$. In the full metric equation,

$$G_{\mu\nu} + \Lambda g_{\mu\nu} + \alpha H_{\mu\nu} + 2\nabla_\mu \nabla_\nu \phi - 2g_{\mu\nu} \nabla^2 \phi + 4\partial_\mu \phi \partial_\nu \phi - 4g_{\mu\nu} (\partial\phi)^2 = 2\kappa T_{\mu\nu}^{(\chi)}, \quad (4.22)$$

the dilaton enters through second-derivative and gradient-squared terms, while the winding sector contributes through its stress tensor,

$$T_{\mu\nu}^{(\chi)} \sim \partial_\mu \chi \partial_\nu \chi - \frac{1}{2} g_{\mu\nu} [(\partial\chi)^2 + m_{\text{th}}^2 \chi^2]. \quad (4.23)$$

In unit radial gauge this implies that the radial constraint governing $g(\rho)$ is sourced by the local energy density stored in $\phi'(\rho)$ and by the localized matter associated with $\chi(\rho)$. A nontrivial dilaton profile therefore shifts the near-tip relations via $\nabla_\mu \nabla_\nu \phi$ and $(\partial\phi)^2$ terms, while a nonzero winding condensate produces additional backreaction concentrated in the

cap region where the thermal circle shrinks and the thermal scalar is lightest. As a result, the near-tip expansion

$$f(\rho) = \kappa^2 \rho^2 + \dots, \quad g(\rho) = r_h^2 + g_2 \rho^2 + \dots \quad (4.24)$$

is renormalized by both ϕ and χ , shifting the coefficient g_2 and hence the rate at which the geometry departs from a constant-radius cylinder. While the winding backreaction primarily reshapes the cap, the dilaton controls how this cap data is propagated and matched to the asymptotic region.

Overview and conventions Figs. 2 and 3 show representative numerical solutions of the second-order coupled system in unit radial gauge for two spacetime dimensions, $D = 5$ (red) and $D = 20$ (blue), and for two values of the (dimensionless) Gauss–Bonnet coupling $\tilde{\alpha}$: a finite coupling (solid) and the pure Einstein limit $\tilde{\alpha} = 0$ (dashed). The initial tip data are listed in Table 3. The radial coordinate is the proper distance ρ , with the smooth tip located at $\rho = 0$. We work at large $\bar{\beta}$ and large AdS radius ℓ , so that the solutions probe the universal cap dynamics and subleading far-zone effects are suppressed.

Metric function $h(\rho)^2$ (top-left) The upper-left panel plots $h(\rho)^2 \equiv f(\rho)$, the coefficient of the Euclidean time circle. Regularity implies $f(\rho) \simeq \kappa^2 \rho^2$ near $\rho = 0$, and the numerical solutions indeed exhibit a smooth quadratic opening at the tip (see inset). Away from the cap, $f(\rho)$ rapidly approaches its asymptotic value, signalling the transition to an approximately cylindrical geometry. The near-tip profiles for $D = 5$ and $D = 20$ are nearly indistinguishable, providing direct evidence for the dimension-independent cap dynamics anticipated from the large- D near-zone analysis. Finite $\tilde{\alpha}$ produces a small but systematic deformation relative to $\tilde{\alpha} = 0$, consistent with higher-derivative terms renormalizing near-tip data.

Radial function $\log g(\rho)$ (top-right) and decoupling in the cap The upper-right panel shows $\log g(\rho)$, where $g(\rho)$ controls the size of the transverse sphere and hence the effective cylinder radius $r(\rho) = \sqrt{g(\rho)}$. Although g depends on the horizon radius and therefore on D , the key observation is that $\log g$ remains large and nearly constant throughout the cap. Equivalently, the logarithmic derivatives g'/g and g''/g are suppressed, and terms involving inverse powers of g are numerically small in this region. This suppression explains why the cap dynamics is accurately captured by a reduced subsystem for $\{f, \phi, \chi\}$: the transverse sphere is an approximately inert spectator in the near-tip region, while the remaining fields evolve universally.

Dilaton profile $\phi(\rho)$ (bottom-left) The lower-left panel plots the dilaton $\phi(\rho)$. The solutions are smooth at the tip and interpolate to their asymptotic behaviour at large $|\rho|$. In the cap region the $D = 5$ and $D = 20$ curves overlap closely, mirroring the universality observed in $h(\rho)^2$. The effect of $\tilde{\alpha}$ is again modest and primarily changes the overall amplitude and slope through a shift of the near-horizon constraints. Since ℓ is taken large, cosmological-constant effects are parametrically suppressed in the cap and become relevant only farther out.

Winding condensate $\chi(\rho)$ (bottom-right) The lower-right panel shows the winding (thermal-scalar) condensate $\chi(\rho)$. The profile is sharply localized near the tip and decays rapidly as $|\rho|$ increases, as expected because the thermal circle shrinks toward $\rho = 0$ and winding modes are lightest in the cap. The near-tip peak and initial falloff agree well between $D = 5$ and $D = 20$, confirming the universality of the winding dynamics in the cap region. The small oscillations visible in the far tail (where $|\chi| \ll 1$) are numerical artifacts associated with integrating an exponentially suppressed mode in a stiff regime; they are reduced by increasing working precision and tightening the shooting/matching tolerances and do not affect the cap-region observables extracted from the solutions.

Taken together, the four panels show that for large $\bar{\beta}$ and large ℓ the cap-region dynamics is largely insensitive to the spacetime dimension and receives only controlled deformations from the Gauss–Bonnet coupling. The near-tip region is dominated by a universal subsystem for $\{h, \phi, \chi\}$, while $g(\rho)$ remains approximately constant and effectively decouples. This provides a direct numerical realization of the universal near-zone picture underlying the large- D expansion and motivates the reduced first-order description employed in the analytic treatment.

5 Discussion

In this work, we developed a unified analytic framework for studying the Horowitz–Polchinski string/black hole correspondence in the presence of higher-derivative gravitational corrections. By combining the Euclidean thermal-scalar picture with the large- D expansion, we constructed the corrected saddle geometries, solved the thermal-scalar dynamics in the near-zone, and matched them to the far-zone Einstein–Gauss–Bonnet (EGB) solutions. This yielded, for the first time, an analytically controlled determination of the correspondence point—including its dependence on curvature-squared terms that appear at $\mathcal{O}(\alpha')$ in string theory—and a systematic extraction of the Landau free energy governing the thermal-scalar condensate. In particular, we obtained closed-form expressions for the quadratic and quartic Landau coefficients, a_2 and a_4 , and showed that the HP transition remains second-order in the controlled regime, with a quasi-tricritical window emerging when the interplay between the Gauss–Bonnet coupling and the AdS radius suppresses a_4 .

Why large- D simplifies the problem The large- D expansion plays a central role in our analysis. It provides a clean parametric separation between the *near-zone*, where the geometry universally collapses to a one-dimensional cigar, and the *far-zone*, governed by the usual EGB equations with exponentially small coupling to the thermal scalar. This separation makes the thermal-scalar equation exactly solvable in the near-zone and reduces the backreaction problem to an elementary matching calculation. Crucially, the large- D limit suppresses higher partial waves and decouples the non-universal details of the background, leaving a universal effective Schrödinger problem that determines the corrected decay exponent and shift of the Hagedorn temperature. In this sense, large D provides a “mean-field” version of string thermodynamics on a curved background, where the dominant physics is captured by a single radial mode on a universal effective potential.

Higher-curvature corrections beyond Gauss–Bonnet We focused on Gauss–Bonnet terms because they furnish the unique ghost-free quadratic curvature correction in any dimension $D > 4$. In string theory, however, the next nontrivial contributions arise at $\mathcal{O}(\alpha'^3)$ and include quartic curvature combinations such as the well-known $t_8 t_8 R^4$ and $\epsilon_{10} \epsilon_{10} R^4$ terms. These terms modify both the background geometry and the thermal-scalar effective action. Importantly, in the large- D expansion their effect is parametrically suppressed relative to the Gauss–Bonnet term, but they can nevertheless induce quantitative shifts in the Hagedorn temperature, the free-energy difference between phases, and possibly the effective sextic term in the Landau functional. Our formalism extends straightforwardly to such R^4 corrections: one must simply augment the near-zone equations with the corresponding effective stress tensor and recompute the NLO matching [44]. It would be interesting to explore whether such terms can enhance the quasi-tricritical behaviour we observed or alter the sign structure of higher Landau coefficients.

Rotating solutions and higher-form fields The framework developed here is flexible and can be extended to include rotation and higher-form gauge fields. Rotating Euclidean black holes admit a natural generalisation of the cigar geometry in which the near-zone metric acquires an off-diagonal $g_{\tau\varphi}$ component and the thermal scalar couples to an effective chemical potential for winding. At large- D , the rotational contributions localise sharply near the horizon, so the universal near-zone reduction persists, though with a modified effective potential [45, 46]. Similarly, backgrounds supported by NS–NS or R–R fluxes modify the thermal-scalar mass term and can induce new channels of instability. Incorporating these ingredients provides a clear path to studying HP-like correspondence transitions in non-supersymmetric flux compactifications, in rotating black branes, and in settings with nontrivial higher-form potentials such as $\text{AdS}_5 \times \text{S}^5$ [47, 48].

Mean-field description and the fuzzball proposal Our results give a mean-field description of the HP correspondence, based on the thermal-scalar condensate and its Landau free energy. This perspective treats the transition as a smooth thermodynamic crossover between a string-dominated phase and a Euclidean black hole phase, in close analogy with the original HP picture. In contrast, the fuzzball programme proposes that black hole microstates are described not by a single Euclidean saddle but by a large ensemble of horizonless geometries. The large- D and thermal-scalar analyses do not resolve the individual microstates but instead capture the coarse-grained thermodynamic physics of the ensemble. In this light, the thermal scalar may be viewed as an effective order parameter for the coarse-grained distribution of microstate geometries, with the Euclidean black hole representing the universal saddle of the ensemble at large D . Understanding the precise relation between these mean-field and microstate perspectives remains an important open question, but the analytic control afforded by large D provides a promising arena in which to probe it.

There are several promising directions for future work. Extending our analysis to $\mathcal{O}(\alpha'^3)$ R^4 corrections [44], to rotating or charged backgrounds, and to black branes with nontrivial fluxes would significantly broaden the applications of the framework. It would

also be interesting to determine whether higher-order terms in the large- D and α' expansions can produce genuine multicritical behaviour, potentially realising higher-order generalisations of the HP transition. Finally, the connection between the thermal-scalar mean-field description and microstate-based approaches such as the fuzzball proposal deserves detailed investigation.

Acknowledgments

The authors would like to thank Ryotaku Suzuki and Imtak Jeon for useful discussions and Wonwoo Lee for collaboration at an early stage of this project. BHL is supported by the National Research Foundation of Korea (NRF) grant RS-2020-NR049598, and Overseas Visiting Fellow Program of Shanghai University. BHL thanks Asia Pacific Center for Theoretical Physics (APCTP) and Korea Institute for Advanced Study (KIAS) for the hospitality during his visit, where a part of this project was done. HL is supported by Basic Science Research Program through the National Research Foundation of Korea (NRF) funded by the Ministry of Education (NRF-2022R1I1A2063176) and the Dongguk University Research Fund of 2025. ST thanks Center for Quantum Spacetime (CQUeST), Sogang University for support for this work. S.T would also like to thank IITBHU for hospitality where a preliminary version of this work was presented.

A Quick recap of the existing methodology and introduction to known literature

In this appendix, we present an explicit computation to reduce our system of equations and solutions to some of the known results in the literature. Mostly we would review the methodology as presented in [30, 49]. However, the results presented in this work are in Euclidean signature as opposed to the Lorentzian black holes [30, 49]. In spirit the methodology developed in this paper is the same and we focus on the Horowitz–Polchinski type phase transition in a large number of dimensions. We dedicate this App. A as a quick introduction to the large D technique which is heavily used in this work based on several existing works in the literature. The readers may skip this appendix, which is just a quick introductory note.

Setup and large- D bookkeeping

Consider the D -dimensional AdS–Schwarzschild black hole

$$ds^2 = -f(r) dt^2 + \frac{dr^2}{f(r)} + r^2 d\Omega_{D-2}^2, \quad f(r) = 1 + \frac{r^2}{L^2} - \frac{\mu}{r^{D-3}}. \quad (\text{A.1})$$

Let $n \equiv D - 3$ (so $n \rightarrow \infty$ is the large- D limit). The horizon $r = r_h$ is defined by $f(r_h) = 0$, which fixes

$$\mu = r_h^n \left(1 + \frac{r_h^2}{L^2} \right). \quad (\text{A.2})$$

It is convenient to introduce the dimensionless AdS parameter at the horizon,

$$\lambda \equiv \frac{r_h^2}{L^2}, \quad f(r) = 1 + \frac{r^2}{L^2} - (1 + \lambda) \left(\frac{r_h}{r}\right)^n. \quad (\text{A.3})$$

We study a minimally-coupled, massless scalar $\Phi = e^{-i\omega t} \phi(r)$ with s -wave on the sphere. The radial equation reads

$$\frac{d}{dr} \left(r^{D-2} f \frac{d\phi}{dr} \right) + \omega^2 \frac{r^{D-2}}{f} \phi = 0. \quad (\text{A.4})$$

Matched asymptotics will use two regions:

1. *Near-horizon (NH)*: $r - r_h = \mathcal{O}(r_h/n)$; we resolve the steep potential layer.
2. *Far-zone (FZ)*: $r - r_h = \mathcal{O}(r_h)$ with $r \ll L$ (sub-AdS) so the black hole tail $\propto (r_h/r)^n$ is exponentially small.

These admit an *overlap* when $n \rightarrow \infty$.

Scaling of frequency To have nontrivial NH dynamics at large- D (finite phase across the layer), take

$$\omega = \frac{n}{r_h} \hat{\omega}, \quad \hat{\omega} = \mathcal{O}(1). \quad (\text{A.5})$$

Near-horizon region

Define the standard large- D NH variable

$$R \equiv \left(\frac{r}{r_h}\right)^n, \quad \text{equivalently} \quad \frac{r - r_h}{r_h} = \frac{\ln R}{n} + \mathcal{O}\left(\frac{1}{n^2}\right). \quad (\text{A.6})$$

Expanding $f(r)$ for fixed R as $n \rightarrow \infty$ gives

$$f(r) = (1 + \lambda) \left(1 - \frac{1}{R}\right) + \mathcal{O}\left(\frac{1}{n}\right). \quad (\text{A.7})$$

The tortoise coordinate is defined by $dr_*/dr = 1/f$. Using (A.7) and $dr/r = d(\ln r) = \frac{1}{n} d(\ln R)$,

$$\frac{dr_*}{dR} = \frac{1}{f} \frac{dr}{dR} = \frac{1}{(1 + \lambda)(1 - 1/R)} \frac{r_h}{nR} \Rightarrow r_* = \frac{r_h}{n(1 + \lambda)} \ln\left(1 - \frac{1}{R}\right) + \text{const.} \quad (\text{A.8})$$

Near the future horizon $R \rightarrow 1^+$ we have $r_* \rightarrow -\infty$ as usual.

At leading order in the NH region the wave equation reduces to the flat 1D form in r_* ,

$$\frac{d^2\phi}{dr_*^2} + \omega^2 \phi = 0, \quad (\text{A.9})$$

whose ingoing solution is $e^{-i\omega r_*}$. Using (A.8) and the scaling (A.5),

$$\phi_{\text{NH}}(R) = \mathcal{A}_{\text{in}} \exp\left[-i\omega \frac{r_h}{n(1 + \lambda)} \ln\left(1 - \frac{1}{R}\right)\right] = \mathcal{A}_{\text{in}} \left(1 - \frac{1}{R}\right)^{-i\alpha}, \quad \alpha \equiv \frac{\hat{\omega}}{1 + \lambda}. \quad (\text{A.10})$$

For matching, we need the *outer* edge of NH, $R \gg 1$ but still within the layer. Expanding

$$\phi_{\text{NH}}(R \gg 1) = \mathcal{A}_{\text{in}} \left(1 - \frac{1}{R}\right)^{-i\alpha} = \mathcal{A}_{\text{in}} \exp\left[\frac{i\alpha}{R} + \mathcal{O}\left(\frac{1}{R^2}\right)\right] = \mathcal{A}_{\text{in}} \left[1 + \frac{i\alpha}{R} + \dots\right]. \quad (\text{A.11})$$

Far-zone

In the FZ with $r - r_h = \mathcal{O}(r_h)$ and $r \ll L$, the black hole tail is exponentially small at large n :

$$\left(\frac{r_h}{r}\right)^n \sim e^{-n(r-r_h)/r_h} \rightarrow 0, \quad f(r) = 1 + \frac{r^2}{L^2} + \mathcal{O}(e^{-n}). \quad (\text{A.12})$$

To leading order we may therefore set $f(r) \approx 1 + \frac{r^2}{L^2}$ in (A.4). For the s -wave and our frequency scaling $\omega \sim n/r_h$, the ω^2/f term is subleading in the *overlap* (because r_* changes only by $\mathcal{O}(1/n)$ across the layer). Thus the leading FZ equation simplifies to a first integral,

$$\frac{d}{dr} \left(r^{D-2} f \frac{d\phi}{dr} \right) = 0 \quad \Rightarrow \quad r^{D-2} f \frac{d\phi}{dr} = C_1, \quad f \simeq 1 + \frac{r^2}{L^2}. \quad (\text{A.13})$$

Integrating once more,

$$\phi_{\text{FZ}}(r) = C_0 + C_1 \int^r \frac{dr'}{r'^{D-2} f(r')} = C_0 + \frac{C_1}{r_h^n} \int^r \frac{dr'}{r'^{n+1} \left(1 + \frac{r'^2}{L^2}\right)}. \quad (\text{A.14})$$

Near the inner edge of the FZ (the *overlap* with NH), we can expand $r = r_h(1 + \delta)$ with $\delta = \mathcal{O}(1/n)$. Then $r'^{-(n+1)} \approx r_h^{-(n+1)} e^{-(n+1)\delta'}$ and $f(r') \approx 1 + \lambda$, so the integral is dominated by the lower limit,

$$\phi_{\text{FZ}}(r \rightarrow r_h^+) = C_0 + \frac{C_1}{(1 + \lambda) r_h^{2n+1}} \int_{r_h}^r dr' e^{-n(r'-r_h)/r_h} = C_0 + \frac{C_1}{(1 + \lambda) r_h^{2n}} \frac{1}{n} \left[1 - \mathcal{O}(e^{-n\delta})\right]. \quad (\text{A.15})$$

Using $R = (r/r_h)^n = e^{n\delta}$, we can re-express the overlap behavior as a regular expansion in $1/R$. Writing

$$\phi_{\text{FZ}}(R \gg 1) = C_0 + \frac{\tilde{C}_1}{(1 + \lambda)} \frac{1}{R} + \mathcal{O}\left(\frac{1}{R^2}\right), \quad \tilde{C}_1 := \frac{C_1}{r_h^n} \frac{1}{n}, \quad (\text{A.16})$$

we can now match to (A.11).

Matching and interpretation

From (A.11) and (A.16) the *overlap* $R \gg 1$ gives

$$\boxed{\phi_{\text{NH}}(R \gg 1) = \mathcal{A}_{\text{in}} \left[1 + \frac{i\alpha}{R} + \dots\right], \quad \phi_{\text{FZ}}(R \gg 1) = C_0 + \frac{\tilde{C}_1}{(1 + \lambda)} \frac{1}{R} + \dots} \quad (\text{A.17})$$

Hence the leading matching conditions are

$$\boxed{C_0 = \mathcal{A}_{\text{in}}, \quad \frac{\tilde{C}_1}{(1 + \lambda)} = i\alpha \mathcal{A}_{\text{in}} = i \frac{\hat{\omega}}{1 + \lambda} \mathcal{A}_{\text{in}}.} \quad (\text{A.18})$$

Equation (A.18) is the essential large- D result: the near-horizon ingoing phase (encoded in $\alpha = \widehat{\omega}/(1+\lambda)$) fixes the $\mathcal{O}(1/R)$ tail of the far-zone solution.

To determine the *spectrum* one would now impose the AdS boundary condition at infinity (e.g. Dirichlet $\phi|_{r \rightarrow \infty} = 0$). That global step quantizes $\widehat{\omega}$, but it lies beyond the local matching demonstrated here. The takeaway is that, at large- D , the black hole effect is exponentially localized within a thickness $\Delta r \sim r_h/n$, and the entire influence on the exterior is captured by the single parameter $\alpha = \widehat{\omega}/(1+\lambda)$ that enters the $1/R$ tail in (A.16). With $R = (r/r_h)^n$ and $\omega = \frac{n}{r_h}\widehat{\omega}$, the NH solution is $\phi \sim (1 - 1/R)^{-i\widehat{\omega}/(1+\lambda)}$ while the FZ solution is $\phi = C_0 + \frac{\tilde{C}_1}{1+\lambda} \frac{1}{R} + \dots$; matching fixes C_0 and \tilde{C}_1 in terms of the NH ingoing amplitude.

Let $D = n + 3$ and consider the S^{n+1} -symmetric AdS–Schwarzschild black hole

$$ds^2 = -f(r) dt^2 + \frac{dr^2}{f(r)} + r^2 d\Omega_{n+1}^2, \quad f(r) = 1 + \frac{r^2}{L^2} - \left(\frac{r_0}{r}\right)^n, \quad (\text{A.19})$$

with horizon $r = r_0$ determined by $f(r_0) = 0$. Angular harmonics on S^{n+1} obey $\nabla_{S^{n+1}}^2 Y_\ell = -\ell(\ell+n)Y_\ell$. We study a minimally coupled scalar

$$\Phi(t, r, \Omega) = e^{-i\omega t} Y_\ell(\Omega) \phi(r), \quad (\text{A.20})$$

of mass m and angular momentum $\ell = \mathcal{O}(1)$ (fixed as $n \rightarrow \infty$). The radial equation is

$$\frac{1}{r^{n+1}} \frac{d}{dr} \left(r^{n+1} f \phi' \right) + \left(\frac{\omega^2}{f} - \frac{\ell(\ell+n)}{r^2} - m^2 \right) \phi = 0. \quad (\text{A.21})$$

We will use both Schwarzschild time t and ingoing Eddington–Finkelstein (EF) time $v = t + r_*$, where $dr_* = dr/f$.

Dynamics: QNMs at large- D

Quasinormal modes (QNMs) are defined by:

- *Ingoing* at the future horizon: in EF time, regularity requires $\Phi \propto e^{-i\omega v}$, i.e., in t the radial factor behaves as $\phi \sim e^{-i\omega r_*}$.
- *Normalizable* (no source) at the AdS boundary $r \rightarrow \infty$: the non-normalizable branch vanishes, leaving the $r^{-\Delta_+}$ falloff.

The conserved radial flux in EF coordinates fixes the ingoing condition and forbids outgoing pieces at r_0 .

Near-horizon scaling and universal equation

The near-zone is a membrane layer of proper thickness $\Delta r \sim r_0/n$. Introduce the stretched variable

$$R \equiv n \left(\frac{r}{r_0} - 1 \right), \quad r = r_0 \left(1 + \frac{R}{n} \right), \quad \frac{d}{dr} = \frac{n}{r_0} \frac{d}{dR}. \quad (\text{A.22})$$

Near r_0 ,

$$f(r) = \frac{R}{r_0} + \frac{r_0^2}{L^2} + \mathcal{O}\left(\frac{R^2}{n}\right), \quad r^{n+1} = r_0^{n+1} e^R \left[1 + \mathcal{O}\left(\frac{R}{n}\right)\right]. \quad (\text{A.23})$$

The surface gravity is $\kappa = \frac{1}{2}f'(r_0) = \frac{n}{2r_0} + \mathcal{O}(n^0)$, motivating

$$\omega \equiv \frac{n}{2r_0} \hat{\omega}, \quad \hat{\omega} = \mathcal{O}(1). \quad (\text{A.24})$$

Keeping leading orders in $1/n$ and using (A.23), the ℓ and m terms are subleading in the membrane layer and the radial equation reduces to

$$\phi''(R) + \frac{1}{R} \phi'(R) + \frac{\hat{\omega}^2}{R^2} \phi(R) = 0, \quad (\text{A.25})$$

whose ingoing (EF-regular) solution is

$$\phi_{\text{near}}(R) = R^{-i\hat{\omega}} [1 + \mathcal{O}(R)], \quad (R \rightarrow 0^+). \quad (\text{A.26})$$

For $1 \ll R \ll n$ (entrance to overlap), full inclusion of the e^R measure and the gentle AdS piece in f gives a decaying envelope

$$\phi_{\text{near}}(R) \sim A_{\text{nh}} e^{-R/2} R^{-i\hat{\omega}} [1 + \mathcal{O}(R^{-1})]. \quad (\text{A.27})$$

Far-zone reduction (AdS sector) and effective potential

For $r - r_0 \gg r_0/n$, $(r_0/r)^n \ll 1$ so $f \simeq 1 + \frac{r^2}{L^2}$ and (A.21) reduces to the scalar equation in global AdS. Writing a Schrödinger form in r_* ,

$$-\frac{d^2\psi}{dr_*^2} + V_{\text{eff}}(r) \psi = \omega^2 \psi, \quad \psi \equiv r^{\frac{n+1}{2}} \phi, \quad (\text{A.28})$$

one finds V_{eff} approaching a confining AdS wall as $r \rightarrow \infty$. Normalizability then selects the large- r branch

$$\phi_{\text{far}}(r) \propto r^{-\Delta_+}, \quad \Delta_{\pm} = \frac{n+2}{2} \pm \frac{1}{2} \sqrt{(n+2)^2 + 4(m^2 L^2 + \ell(\ell+n))}. \quad (\text{A.29})$$

Evaluated at $r = r_0(1 + R/n)$ with $1 \ll R \ll n$,

$$\phi_{\text{far}}(r) \sim B \exp(-R) \left[1 + \mathcal{O}\left(\frac{1}{n}\right)\right]. \quad (\text{A.30})$$

Overlap matching and leading spectrum

In the overlap, (A.27) and (A.30) must agree in their R -dependence. The near solution carries an extra phase $R^{-i\hat{\omega}}$ which can only be made constant (non-oscillatory) if

$$-i\hat{\omega} \equiv q \in \{1, 2, \dots\}. \quad (\text{A.31})$$

Thus the *leading* large- D QNM tower is

$$\boxed{\omega_q = -i \frac{n}{2r_0} q + \mathcal{O}(n^0), \quad q = 1, 2, \dots} \quad (\text{A.32})$$

These are purely damped, decoupled, near-horizon modes with spacing $\sim \kappa$.

Sketch of the $\mathcal{O}(n^0)$ correction

To obtain $\mathcal{O}(n^0)$:

- Keep next orders in f and r^{n+1} in the near ODE (curvature and measure corrections) and retain the ℓ -term as a perturbation.
- Solve the near equation by a Frobenius ansatz $R^{-i\hat{\omega}} \sum_k a_k R^k$ with $\hat{\omega} = -iq + \delta\hat{\omega}$, where $\delta\hat{\omega} = \mathcal{O}(n^0)$.
- In the far region, include the first subleading term in the AdS scaling dimension, $\Delta_+ = (n+2) + \frac{m^2 L^2 + \ell(\ell+n)}{n+2} + \dots$, giving a tail $\exp[-(1 + \frac{2}{n} + \dots)R]$.
- Match the corrected exponents and amplitudes in the overlap $1 \ll R \ll n$ to solve for $\delta\hat{\omega}$.

This yields a small shift in $\text{Im}\omega$ and, generically for other channels, a small $\text{Re}\omega$ at $\mathcal{O}(n^0)$; in the minimally coupled scalar channel the leading piece remains purely damped. In this paper we have mostly used the large- D techniques to solve the backreacted model, where the backreaction is provided mostly by the dilaton and the thermal scalar. For simplicity and better understanding, we restrict ourselves to a toy model and solve the actual problem in Sec. 3.

Static scalar and backreaction to $\mathcal{O}(1/D)$

Set $\omega = 0$ and $\Phi = \varepsilon \varphi(r) Y_\ell$, with $\varepsilon \ll 1$ and we take $\ell = 0$ to keep spherical symmetry. The static equation is

$$\frac{1}{r^{n+1}} \frac{d}{dr} (r^{n+1} f \varphi') = m^2 \varphi. \quad (\text{A.33})$$

Near the horizon, with (A.22)–(A.23), the solution that is regular at $R \rightarrow 0^+$ decays in the layer as

$$\varphi_{\text{near}}(R) = A e^{-\sigma R} \left[1 + \mathcal{O}\left(\frac{1}{R}, \frac{1}{n}\right) \right], \quad \sigma = 1 + \frac{2}{n} + \frac{m^2 L^2}{n^2} + \mathcal{O}\left(\frac{1}{n^3}\right). \quad (\text{A.34})$$

In the far AdS zone, imposing no boundary source,

$$\varphi_{\text{far}}(r) = K r^{-\Delta_+} \left[1 + \mathcal{O}\left(\frac{L^2}{r^2}\right) \right], \quad \Delta_+ = (n+2) + \frac{m^2 L^2}{n+2} + \dots, \quad (\text{A.35})$$

and in the overlap $r = r_0(1 + R/n)$ this behaves as $K r_0^{-\Delta_+} e^{-\sigma R}$ with the *same* σ in (A.34), fixing $K = A r_0^{\Delta_+} [1 + \mathcal{O}(1/n)]$.

Backreacted metric via a mass function

Work in Schwarzschild gauge:

$$ds^2 = -F(r) dt^2 + \frac{dr^2}{F(r)} + r^2 d\Omega_{n+1}^2, \quad F(r) = 1 + \frac{r^2}{L^2} - \frac{m(r)}{r^n}. \quad (\text{A.36})$$

At $\mathcal{O}(\varepsilon^2)$ the scalar stress tensor sources a *mass function* $m(r)$ governed by (from tt or rr Einstein equations)

$$m'(r) = \frac{16\pi G_D}{n+1} \Omega_{n+1} r^{n+1} \rho(r), \quad \rho \equiv -T^t_t = \frac{1}{2} \left[F(\varphi')^2 + m^2 \varphi^2 \right]. \quad (\text{A.37})$$

Inside the membrane layer,

$$dr = \frac{r_0}{n} dR, \quad \varphi'(r) = -\frac{n}{r_0} \sigma \varphi [1 + \mathcal{O}(1/n)], \quad r^{n+1} = r_0^{n+1} e^R [1 + \dots], \quad (\text{A.38})$$

and in the overlap $F \simeq 1 + \frac{r_0^2}{L^2} = \mathcal{O}(1)$. Hence

$$\rho(R) \simeq \frac{n^2 \sigma^2}{2L^2} \varphi^2(R) [1 + \mathcal{O}(n^{-2})] = \frac{n^2 \sigma^2}{2L^2} A^2 e^{-2\sigma R} [1 + \dots]. \quad (\text{A.39})$$

Integrating (A.37) from r_0^+ through the layer to $+\infty$,

$$\Delta m \equiv m(\infty) - m(r_0^+) = \frac{16\pi G_D}{n+1} \Omega_{n+1} \int_{r_0}^{\infty} dr r^{n+1} \rho(r). \quad (\text{A.40})$$

Changing to R ,

$$\Delta m = \frac{16\pi G_D}{n+1} \Omega_{n+1} \int_0^{\infty} \frac{r_0 dR}{n} \left[r_0^{n+1} e^R \right] \frac{n^2 \sigma^2}{2L^2} A^2 e^{-2\sigma R} = \frac{8\pi G_D \Omega_{n+1}}{L^2} r_0^{n+2} A^2 \frac{n \sigma^2}{2\sigma - 1}. \quad (\text{A.41})$$

Using (A.34), the prefactor simplifies and the first nontrivial correction is $\mathcal{O}(1/n)$:

$$\boxed{\Delta m = \frac{8\pi G_D \Omega_{n+1}}{L^2} r_0^{n+2} A^2 \left[n + \mathcal{O}\left(\frac{1}{n}\right) \right]}. \quad (\text{A.42})$$

Profile across the layer and far geometry

A convenient cumulative profile (accurate at $\mathcal{O}(1/n)$) that integrates to (A.41) is

$$m(r) = r_0^n + \varepsilon^2 \Delta m S(R), \quad S(R) = 1 - e^{-(2\sigma-1)R}, \quad R = n \left(\frac{r}{r_0} - 1 \right). \quad (\text{A.43})$$

Then the near-zone metric function to $\mathcal{O}(1/n)$ reads (using $r^n = r_0^n e^R [1 - \frac{R^2}{2n} + \dots]$, $r^2 = r_0^2 [1 + \frac{2R}{n} + \dots]$)

$$\boxed{F_{\text{near}}(R) = 1 + \frac{r_0^2}{L^2} \left(1 + \frac{2R}{n} \right) - \frac{r_0^n + \varepsilon^2 \Delta m S(R)}{r_0^n e^R \left(1 - \frac{R^2}{2n} \right)} + \mathcal{O}\left(\frac{1}{n^2}\right)} \quad (\text{A.44})$$

$$= \frac{R}{r_0} + \frac{r_0^2}{L^2} - e^{-R} \left[1 + \varepsilon^2 \frac{\Delta m}{r_0^n} S(R) \right] + \frac{1}{n} \left(\frac{2R r_0^2}{L^2} - \frac{R^2}{2} e^{-R} \right) + \mathcal{O}\left(\frac{1}{n^2}\right).$$

Outside the layer ($R \gg 1$), $S \rightarrow 1$ and

$$\boxed{F_{\text{far}}(r) = 1 + \frac{r^2}{L^2} - \frac{r_0^n + \varepsilon^2 \Delta m}{r^n} + \mathcal{O}(e^{-n}) \equiv 1 + \frac{r^2}{L^2} - \frac{m_{\text{eff}}}{r^n}, \quad m_{\text{eff}} = r_0^n + \varepsilon^2 \Delta m.} \quad (\text{A.45})$$

Horizon shift

Let r_h satisfy $F(r_h) = 0$. Linearizing,

$$0 = f'(r_0)(r_h - r_0) - \frac{\Delta m}{r_0^n} + \dots, \quad f'(r_0) = \frac{n}{r_0} + \mathcal{O}(n^0), \quad (\text{A.46})$$

thus,

$$\boxed{\frac{\delta r_h}{r_0} = \frac{1}{n} \frac{\Delta m}{r_0^n} \left[1 + \mathcal{O}\left(\frac{1}{n}\right)\right] = \frac{8\pi G_D \Omega_{n+1}}{L^2} A^2 r_0^2 \left[1 + \mathcal{O}\left(\frac{1}{n}\right)\right]}. \quad (\text{A.47})$$

B Subsystem for the numerical analysis

In this section, we derive the reduced equations for the subsystem from the full equations of motion. The reduced equations are used for the numerical analysis of the near-horizon solutions, and the detailed reduction and numerical procedure are presented in this appendix.

B.1 Derivation of subsystem equations

For later convenience, we recall the complete equations of motion (2.11),

$$0 = G_{\mu\nu} + \Lambda g_{\mu\nu} + \alpha H_{\mu\nu} + 2\nabla_\mu \nabla_\nu \phi - 2g_{\mu\nu} \nabla^2 \phi + 4\partial_\mu \phi \partial_\nu \phi - 4g_{\mu\nu} (\partial\phi)^2 - 2\kappa e^{2\phi} T_{\mu\nu}^{(\chi)}, \quad (\text{B.1})$$

$$0 = R - 2\Lambda + \alpha R_{\text{GB}}^2 + 4\nabla^2 \phi - 4(\partial\phi)^2 - 2\kappa [2(\partial\chi)^2 + 2m_{\text{th}}^2 \chi^2], \quad (\text{B.2})$$

$$0 = \nabla^2 \chi - 2\partial_\mu \phi \nabla^\mu \chi - m_{\text{th}}^2 \chi, \quad (\text{B.3})$$

and reduced equation of motion (4.8) from the metric variation,

$$0 = R_\mu{}^\nu + 2\alpha H_\mu{}^\nu + 2\nabla_\mu \nabla^\nu \phi - \kappa (2\nabla_\mu \chi \nabla^\nu \chi - 2\bar{\beta} \chi^2 g_{\tau\mu} g_\tau{}^\nu). \quad (\text{B.4})$$

We focus on a subsystem of the equations of motion in unit radial gauge ansatz (4.7), motivated by the semiclassical picture of the winding condensate, in which $\chi \propto \exp(-S_{\text{NG}})$, where S_{NG} denotes the Nambu–Goto action of a string worldsheet wrapping the Euclidean time circle. In this subsystem, we consider the following first-order equation:

$$\chi' + \bar{\beta} f \chi = 0. \quad (\text{B.5})$$

Substituting (B.5) into (B.3), we obtain

$$h' + \left(\frac{D-2}{4} g' - \phi'\right) h - \frac{\bar{\beta}_{\text{H}}}{2\bar{\beta}} = 0. \quad (\text{B.6})$$

We now introduce an ansatz in which \mathcal{A} is left undetermined at this stage,

$$\phi' = h(-\kappa \bar{\beta} \chi^2 + \mathcal{A}). \quad (\text{B.7})$$

By differentiating Eq. (B.7) and substituting Eqs. (B.5) and (B.6), we find

$$2 \left[\phi'' - (\phi')^2 \right] - 2h\mathcal{A}' + \frac{D-2}{2} \frac{g'\phi'}{g} - \frac{\bar{\beta}_H^2}{\bar{\beta}} \mathcal{A} - \kappa (4\bar{\beta}^2 h^2 - \bar{\beta}_H^2) \chi^2 = 0. \quad (\text{B.8})$$

By combining the tt and $\theta\theta$ components of Eq. (B.4), one can solve for h'' and g'' . Substituting these expressions into the remaining equations, the second derivatives h'' and g'' can be eliminated. Differentiating Eq. (B.7) and taking a linear combination with the $\rho\rho$ component of Eq. (B.4), we obtain an expression for \mathcal{A}' . Subtracting Eq. (B.2) from Eq. (B.8) and substituting the resulting expression for \mathcal{A}' , using Eqs. (B.6) and (B.7), the resulting reduced equations for the subsystem are given as follows:

$$0 = h' + \left[\frac{(D-2)g'}{4g} - \phi' \right] h - \frac{\bar{\beta}_H}{2\bar{\beta}}, \quad (\text{B.9})$$

$$0 = \left\{ 1 - \alpha(D-3) \left[(2D-7) \frac{(g')^2 - 4g}{g^2} + \frac{4h'g'}{hg} \right] + 3\alpha^2 (D-4)(D-3)^2 (D-2) \frac{[(g')^2 - 4g]^2}{4g^4} \right\} g''$$

$$+ \frac{(D-4)(g')^2}{2g} + \frac{h' - 2h\phi'}{h} g' - 2(D-3) - \alpha(D-3) \left\{ \frac{4\kappa\beta^2 h^2 [(g')^2 - 4g] \chi^2}{g} \right.$$

$$+ \left[(D-7)(g')^2 - 4(D-5)g + 4(D-5)g \right] \frac{h'g'}{hg^2}$$

$$- \left[-\frac{(D-5)(D-4)(g')^2 + 4(D^2 - 7D + 13)g}{2g^3} \right] [(g')^2 - 4g] \left. \right\}$$

$$- \alpha^2 (D-4)(D-3)^2 \left[\frac{h'g'}{4hg^4} + \frac{(D-8)(g')^2 - 4(D-5)g}{8g^5} \right] [(g')^2 - 4g], \quad (\text{B.10})$$

$$0 = \left\{ \frac{\bar{\beta}_H^2}{\bar{\beta}h} + \alpha(D-4)(D-3)(D-2) \left[\frac{1}{4} \left(\frac{g'}{g} \right)^3 - \frac{g'}{g^2} \right] \right\} \phi' + (D-2) \left[\frac{(g')^2 + 4(D-3)g}{8g^2} - \frac{\bar{\beta}_H^2 g'}{4\bar{\beta}hg} \right]$$

$$+ \alpha(D-4)(D-3)(D-2) \left[\frac{1}{4} \left(\frac{g'}{g} \right)^3 - \frac{g'}{g^2} \right] \left[\frac{\bar{\beta}_H^2}{8\bar{\beta}h} - \frac{(D+1)(g')^2 + 4(D-5)g}{32gg'} \right]$$

$$+ \kappa\bar{\beta}_H^2 \chi^2 - \Lambda, \quad (\text{B.11})$$

$$0 = \chi' + \bar{\beta}h\chi, \quad (\text{B.12})$$

where Eq. (B.10) is obtained from an appropriate linear combination of the tt and $\theta\theta$ components of Eq. (B.4). All fields other than g are reduced to first-order equations within subsystem. When $\alpha = \Lambda = 0$, Eqs. (B.9), (B.10), (B.11) and (B.12) are coincide with the results reported in Refs. [12, 50].

B.2 Numerical results of subsystem

To obtain appropriate initial values in the near-horizon region, we consider the following static, spherically symmetric Euclidean metric:

$$ds^2 = F(r)dt^2 + \frac{dr^2}{F(r)} + r^2 d\Omega_{D-2}^2. \quad (\text{B.13})$$

It is worth noting that the metric (B.13), written in the areal gauge, is considered only to determine the initial values in the near horizon, and the equations of motion to be solved, Eqs. (B.9), (B.10), (B.11), and (B.12), are those derived in the unit radial gauge. We introduce the near-horizon expansion by writing $r = r_h + \epsilon$, where ϵ denotes a small deviation from the horizon. In order to avoid a conical singularity at the horizon, ϵ is taken to be

$$\epsilon = \frac{\dot{F}_h}{4} \rho^2, \quad (\text{B.14})$$

where the dot denotes differentiation with respect to the radial coordinate r and ρ is a locally defined radial coordinate adapted to the near-horizon expansion. Referring to the Euclidean metric (4.7), we set $h = \sqrt{F}$, and near-horizon behaviors of h and g take the form

$$h(\rho) = \sqrt{\dot{F}_h \epsilon} \left(1 + \frac{\ddot{F}_h}{4\dot{F}_h} \epsilon + \dots \right) = \frac{\dot{F}_h}{2} \rho + \frac{\dot{F}_h \ddot{F}_h}{32} \rho^3 + \dots, \quad (\text{B.15})$$

$$g(\rho) = r(\rho)^2 = \left(r_h + \frac{\dot{F}_h}{4} \rho^2 \right)^2. \quad (\text{B.16})$$

Since the cap region corresponds to the large- β regime, it is obtained from taking a large AdS radius ℓ , *i.e.*, $1 \ll r_h \ll \ell$. In this regime, we choose an arbitrary value ρ_0 of the radial coordinate, and the corresponding behaviors of the functions are given by

$$h(\rho_0) = \rho_0, \quad \chi(\rho_0) = \chi_0 e^{-\frac{\rho_0^2}{2}}, \quad (\text{B.17})$$

where $\bar{\beta}$ is absorbed into h as $\bar{\beta}h \rightarrow h$. The exact form of $g(\rho_0)$ is determined from (B.16). For the Gauss–Bonnet–AdS black hole, $g(\rho_0)$ is proportional to $\bar{\beta}^{-2}\ell^4$ and ϕ can be inferred from h, g, χ in the regime where χ is sufficiently small, yielding $\phi'(\rho_0) = 0$. The resulting expressions for h, g, ϕ and χ are

$$h(\rho_0) = \rho_0, \quad g(\rho_0) \propto \frac{\ell^4}{\beta^2}, \quad \phi(\rho_0) = \phi_0, \quad \chi(\rho_0) = \chi_0 e^{-\frac{\rho_0^2}{2}}. \quad (\text{B.18})$$

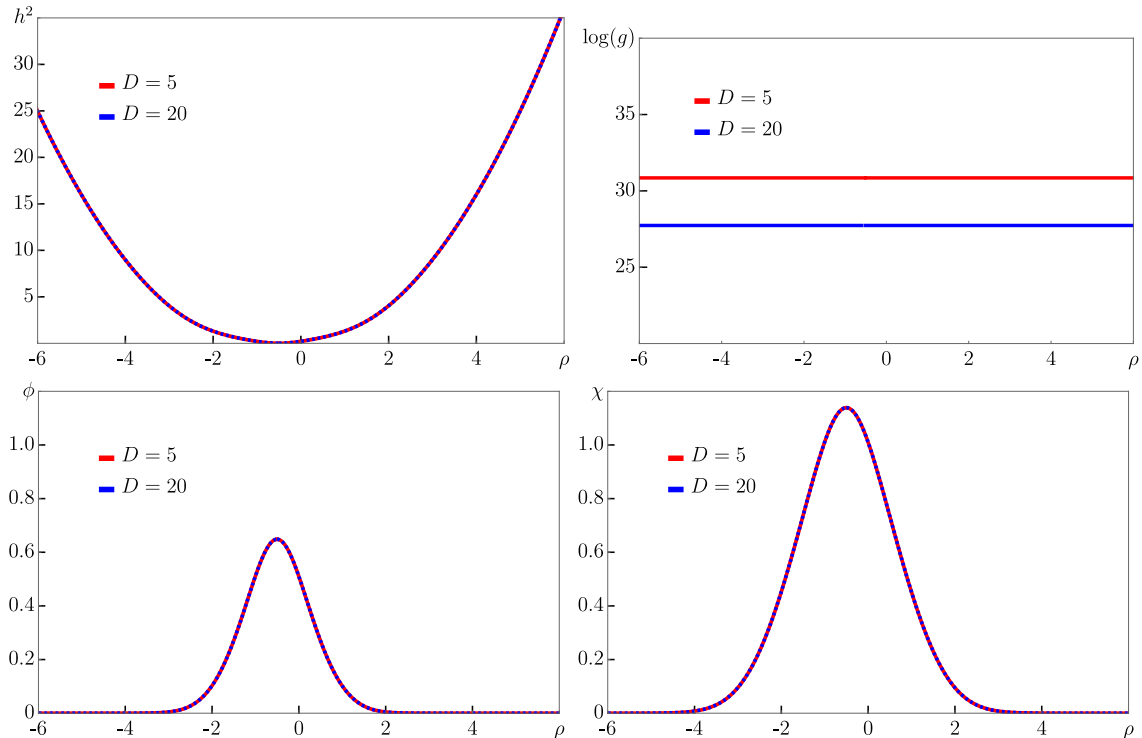


Figure 4. Near-horizon solutions of reduced-order Eqs. (B.9), (B.10), (B.11) and (B.12), where $\bar{\alpha} = 1$ and $\ell = 10^7$.

Parameters	D	ℓ	$\bar{\alpha}$	$\bar{\beta}$	ρ_0	h_0	g_0	g'_0	ϕ_0	χ_0
Red line	5	10^7	1	10^7	5	$\frac{\rho_0}{\beta}$	$\frac{\ell^2}{4\beta^2}$	$\frac{\ell^2 \rho_0}{\beta^2}$	0	0.7
Blue line	20						$\frac{4\ell^2}{361\beta^2}$	$\frac{4\ell^2 \rho_0}{19\beta^2}$		

Table 3. Initial values used in Fig. 4.

Fig. 4 shows the numerical near-horizon profiles obtained from the reduced-order (first-order) subsystem governed by Eqs. (B.9), (B.10), (B.11) and (B.12). The corresponding horizon initial data used to generate Fig. 4 are collected in Table 3. In the cap region we take $\bar{\beta}$ and ℓ to be parametrically large, which suppresses subleading corrections and allows the universal near-tip dynamics to emerge cleanly. With these choices, the numerical solutions for h , ϕ , and χ are essentially identical across different spacetime dimensions, while the function g differs only through its dimension-dependent horizon value.

Although g depends explicitly on the horizon radius and hence on the dimension D , the numerics show that $\log g$ remains large and nearly constant throughout the cap. Equivalently, the logarithmic derivatives g'/g and g''/g are strongly suppressed, and all terms proportional to inverse powers of g are negligible. Under these controlled approximations, the g -dependent contributions drop out and the system effectively decouples from the dynamics of g . The remaining equations close on the triplet $\{h, \phi, \chi\}$ and reduce to the

universal first-order system

$$0 = h' - \phi' h - \frac{\bar{\beta}_{\text{H}}}{2\bar{\beta}}, \quad (\text{B.19})$$

$$0 = \frac{\bar{\beta}_{\text{H}}^2}{\bar{\beta} h} \phi' + \kappa \bar{\beta}_{\text{H}}^2 \chi^2 - \Lambda, \quad (\text{B.20})$$

$$0 = \chi' + \bar{\beta} h \chi. \quad (\text{B.21})$$

This explains why the cap-region solutions for $D = 5$ and $D = 20$ coincide to high accuracy: once g becomes effectively inert, the near-horizon dynamics is governed by a dimension-insensitive subsystem. Moreover, since the AdS radius is taken to be large, the cosmological constant contribution is also parametrically suppressed in the cap. As a result, the combined effects of the Gauss–Bonnet term, the spacetime dimension, and Λ are negligible in this region, and the near-horizon behaviour is qualitatively the same as in the four-dimensional Schwarzschild analysis of Ref. [12].

C Details of the next-to-leading-order solution

In this appendix we collect the explicit next-to-leading-order expressions for the metric correction, the dilaton, and the thermal scalar. We work in the conventions of Sec. 3.3.1, with $D = n + 3$ and $n \gg 1$, near-horizon coordinate

$$r = r_h \left(1 + \frac{\rho}{n} + \mathcal{O}(n^{-2}) \right), \quad 0 \leq \rho = \mathcal{O}(1), \quad (\text{C.1})$$

and the leading-order cigar profile

$$F_0(\rho) = K(1 - e^{-\rho}), \quad K \equiv \frac{F'(r_h)}{n} = \mathcal{O}(1). \quad (\text{C.2})$$

The Gauss–Bonnet coupling and dilaton dressing appear only through the effective gravitational coupling κ_{eff} and the LO dilaton $\phi_0 = \phi_\infty$ defined in Sec. 3.3.2.

Throughout this appendix we drop terms of order $1/n^2$ and higher. All fields are expanded to NLO in the large- D expansion, keeping only the leading nontrivial order in the backreaction parameter κ :

$$F(\rho) = F_0(\rho) + \frac{1}{n} F_1(\rho) + \mathcal{O}(n^{-2}), \quad \phi(\rho) = \phi_0 + \phi_1(\rho) + \mathcal{O}(\kappa^2), \quad \chi(\rho) = \chi_0(\rho) + \frac{1}{n} \chi_1(\rho) + \mathcal{O}(n^{-2}). \quad (\text{C.3})$$

C.1 Metric correction $F_1(\rho)$

C.1.1 Near-zone equation and source

Einstein equation and stress tensor At NLO the $\tau\tau$ and $\rho\rho$ components of the Einstein–Gauss–Bonnet equations give a single first-order equation for $F_1(\rho)$,

$$F_1'(\rho) + F_1(\rho) = \mathcal{A}_\chi (1 - e^{-\rho}) e^{2\lambda - \rho}, \quad (\text{C.4})$$

where the source comes entirely from the LO winding-mode stress tensor,

$$(T^\rho{}_\rho - T^\tau{}_\tau)_\chi^{\text{LO}} = g_{(0)}^{\rho\rho} (\partial_\rho \chi_0)^2 = \frac{n^2}{r_h^2} F_0(\rho) \lambda_-^2 \chi_h^2 e^{2\lambda-\rho} = \frac{n^2}{r_h^2} K \lambda_-^2 \chi_h^2 (1 - e^{-\rho}) e^{2\lambda-\rho}. \quad (\text{C.5})$$

Matching to the Einstein equations fixes the overall coefficient

$$\mathcal{A}_\chi = \frac{2\kappa_{\text{eff}}}{D-2} \frac{n^2}{r_h^2} K \lambda_-^2 \chi_h^2, \quad (\text{C.6})$$

in the conventions where F_1 is defined by the expansion $F(r) = F_0(\rho) + n^{-1}F_1(\rho)$ and the LO operator is as in Sec. 3.3.1.

C.1.2 Closed-form solution and asymptotics

Near-zone solution The ODE (C.4) is elementary. Integrating with an integrating factor e^ρ and imposing $F_1(0) = 0$ to preserve the smoothness of the cigar tip gives

$$F_1(\rho) = e^{-\rho} \mathcal{A}_\chi \int_0^\rho d\sigma e^\sigma (1 - e^{-\sigma}) e^{2\lambda-\sigma} \quad (\text{C.7})$$

$$= \mathcal{A}_\chi e^{-\rho} \left[\frac{e^{(2\lambda+1)\rho} - 1}{2\lambda_- + 1} - \frac{e^{2\lambda-\rho} - 1}{2\lambda_-} \right]. \quad (\text{C.8})$$

Near the tip one finds the expansion

$$F_1(\rho) = \mathcal{A}_\chi \left[\frac{1}{2} \rho^2 + \mathcal{O}(\rho^3) \right], \quad \rho \rightarrow 0, \quad (\text{C.9})$$

while for $\rho \rightarrow \infty$ (still within the overlap region $1 \ll \rho \ll n$) we have

$$F_1(\rho) = \mathcal{A}_\chi \left[\frac{e^{2\lambda-\rho}}{2\lambda_- + 1} - \frac{e^{(2\lambda-1)\rho}}{2\lambda_-} + \mathcal{O}(e^{-\rho}) \right], \quad \rho \rightarrow \infty. \quad (\text{C.10})$$

The leading decaying piece $e^{2\lambda-\rho}$ is precisely what is required by matching to the far-zone deformation of the Boulware–Deser solution; its coefficient is fixed in terms of the thermal scalar hair amplitude χ_h by (C.6).

Far-zone matching In the far-zone $r - r_h = \mathcal{O}(r_h)$ the metric is governed by the linearised Boulware–Deser equation around the asymptotic background. Writing

$$F(r) = F_{\text{BD}}(r) [1 + \varepsilon \delta f(r)], \quad \varepsilon \sim n^{-1}, \quad (\text{C.11})$$

the linearised equation is solved by

$$\delta f(r) = \mathcal{C}_1 \delta f_{\text{reg}}(r) + \mathcal{C}_2 \delta f_{\text{dec}}(r), \quad (\text{C.12})$$

where δf_{reg} is regular at the horizon and $\delta f_{\text{dec}} \sim r^{-(D-3)}$ is the decaying mode. In the overlap region $1 \ll \rho \ll n$ we have $r - r_h \sim r_h \rho/n$ and

$$F(\rho) = K(1 - e^{-\rho}) + \frac{1}{n} F_1(\rho) = F_{\text{BD}}(r) [1 + \varepsilon \delta f(r)], \quad (\text{C.13})$$

which yields an explicit identification between the integration constant \mathcal{C}_2 in δf and the thermal-scalar amplitude χ_h via (C.8). We do not reproduce the straightforward but lengthy algebra here.

C.2 Dilaton correction $\phi_1(\rho)$

C.2.1 Near-zone equation and integral representation

Master equation and source The master equation for ϕ_1 in the probe regime is

$$\nabla^2 \phi_1 = \kappa [(\partial\chi_0)^2 + m_{\text{th}}^2(r)\chi_0^2], \quad (\text{C.14})$$

with $\chi_0(\rho) = \chi_h e^{\lambda-\rho}$ and $m_{\text{th}}^2(r) \simeq m_{\text{eff}}^2 = \bar{\beta}^2 K - \bar{\beta}_{\text{H}}^2$ in the near-zone. Using the near-zone Laplacian as in Sec. 3.4.2, one finds the first-order equation (3.150) for $\phi_1'(\rho)$ and the solution (3.154). Integrating once more gives

$$\phi_1^{(\text{NZ})}(\rho) = \phi_1(0) + \kappa \chi_h^2 \mathcal{I}(\rho), \quad (\text{C.15})$$

with the quadrature

$$\mathcal{I}(\rho) = \int_0^\rho d\sigma \frac{\frac{\lambda_-^2 + \Xi^2}{2\lambda_- + 1} (e^{(2\lambda_- + 1)\sigma} - 1) - \frac{\lambda_-}{2} (e^{2\lambda_- \sigma} - 1)}{e^\sigma - 1}. \quad (\text{C.16})$$

Special-function form The integral $\mathcal{I}(\rho)$ can be expressed in terms of the auxiliary integrals

$$J(a; \rho) \equiv \int_0^\rho d\sigma \frac{e^{a\sigma} - 1}{e^\sigma - 1}, \quad (\text{C.17})$$

which admit the representation

$$J(a; \rho) = \psi(1) - \psi(1-a) - \frac{e^{-(1-a)\rho}}{1-a} {}_2F_1(1, 1-a; 2-a; e^{-\rho}), \quad (\text{C.18})$$

where ψ is the digamma function and ${}_2F_1$ is the Gauss hypergeometric function. In terms of J ,

$$\mathcal{I}(\rho) = \frac{\lambda_-^2 + \Xi^2}{2\lambda_- + 1} J(2\lambda_- + 1; \rho) - \frac{\lambda_-}{2} J(2\lambda_-; \rho). \quad (\text{C.19})$$

C.2.2 Far-zone behaviour

Asymptotics and matching In the far-zone, the equation

$$\frac{d^2 \phi_1}{dY^2} + \frac{d\phi_1}{dY} = \kappa \chi_\infty^2 e^{2\lambda-Y} (\lambda_-^2 + \Xi^2) \quad (\text{C.20})$$

has the general solution

$$\phi_1^{(\text{FZ})}(Y) = \phi_{1,\infty} + B_1 e^{-Y} + B_2 e^{2\lambda-Y}, \quad (\text{C.21})$$

with

$$B_2 = \frac{\kappa \chi_\infty^2 (\lambda_-^2 + \Xi^2)}{2\lambda_- (2\lambda_- + 1)}. \quad (\text{C.22})$$

The constant $\phi_{1,\infty}$ is fixed by matching to $\phi_1^{(\text{NZ})}(\rho)$ in the overlap region via

$$\phi_{1,\infty} = \phi_1(0) + \kappa \chi_h^2 \mathcal{I}(\infty). \quad (\text{C.23})$$

The coefficient B_1 is fixed by the absence of a growing e^{-Y} contribution in the overlap with the near-zone solution.

C.3 Thermal scalar correction $\chi_1(\rho)$

C.3.1 Linearised equation and source decomposition

LO operator and NLO source In the near-zone the covariant thermal scalar equation

$$\square\chi - 2\partial_\mu\phi\partial^\mu\chi - m_{\text{th}}^2(r)\chi = 0, \quad (\text{C.24})$$

reduces at LO to

$$\mathcal{L}_0[\chi_0] \equiv \left(\partial_\rho^2 + \partial_\rho - \Xi^2\right)\chi_0(\rho) = 0, \quad \chi_0(\rho) = \chi_h e^{\lambda-\rho}, \quad (\text{C.25})$$

with λ_\pm as in Sec. 3.4.3. To NLO we obtain

$$\mathcal{L}_0[\chi_1(\rho)] = S(\rho), \quad (\text{C.26})$$

with the source $S(\rho)$ encapsulating the deviation of the true geometry and dilaton from the constant- F background. It is convenient to decompose $S(\rho)$ into four pieces,

$$S(\rho) = S_{\text{kin}}(\rho) + S_{\text{mass}}(\rho) + S_{\text{met}}(\rho) + S_\phi(\rho), \quad (\text{C.27})$$

corresponding respectively to:

- the deviation of the radial kinetic operator from its LO form,
- the ρ -dependence of the thermal mass $m_{\text{th}}^2(r)$,
- the explicit NLO metric correction $F_1(\rho)$, and
- the NLO dilaton gradient.

Starting from the exact radial equation

$$e^{-\rho}\partial_\rho(e^\rho F(\rho)\partial_\rho\chi) - \frac{r_h^2}{n^2}\left[\bar{\beta}^2 F(\rho) - \bar{\beta}_{\text{H}}^2\right]\chi(\rho) - 2F(\rho)\phi'(\rho)\chi'(\rho) = 0, \quad (\text{C.28})$$

and subtracting the LO equation evaluated with $F_0 \rightarrow K$ and $\phi'_0(\rho) = 0$, one finds, after some algebra, the following expressions:

$$S_{\text{kin}}(\rho) = -e^{-\rho}\partial_\rho\left\{e^\rho[F_0(\rho) - K]\chi'_0(\rho)\right\}, \quad (\text{C.29})$$

$$S_{\text{mass}}(\rho) = -\frac{r_h^2}{n^2}\bar{\beta}^2[F_0(\rho) - K]\chi_0(\rho), \quad (\text{C.30})$$

$$S_{\text{met}}(\rho) = -e^{-\rho}\partial_\rho\left\{e^\rho F_1(\rho)\chi'_0(\rho)\right\} + \frac{r_h^2}{n^2}\bar{\beta}^2 F_1(\rho)\chi_0(\rho), \quad (\text{C.31})$$

$$S_\phi(\rho) = 2F_0(\rho)\chi'_0(\rho)\phi'_1(\rho), \quad (\text{C.32})$$

where $F_0(\rho)$, $F_1(\rho)$, and $\phi_1(\rho)$ are given in Eqs. (C.8) and (3.154). All four contributions are proportional to χ_h and, after expressing everything in terms of exponentials, can be written in the generic form

$$S(\rho) = \sum_j \mathcal{C}_j \frac{e^{(p_j-1)\rho}}{1-e^{-\rho}} + \sum_k \tilde{\mathcal{C}}_k e^{q_k\rho}, \quad (\text{C.33})$$

with coefficients $\mathcal{C}_j, \tilde{\mathcal{C}}_k$ that are rational functions of λ_\pm and the parameters $(K, \bar{\beta}, \bar{\beta}_{\text{H}}, \kappa_{\text{eff}}, r_h)$.

C.3.2 Green's function and integral basis

Near-zone Green's function The homogeneous operator \mathcal{L}_0 has two linearly independent solutions $y_1 = e^{\lambda_+\rho}$, $y_2 = e^{\lambda_-\rho}$ with Wronskian

$$W(\rho) = (\lambda_- - \lambda_+) e^{-\rho}. \quad (\text{C.34})$$

Imposing regularity at the tip and decay in the far-zone, the particular solution of (C.26) compatible with our boundary conditions is precisely the Green's function expression (3.179),

$$\chi_1(\rho) = \frac{e^{\lambda_-\rho}}{\lambda_- - \lambda_+} \int_\rho^\infty d\sigma S(\sigma) e^{-\lambda_-\sigma}. \quad (\text{C.35})$$

Integral basis and special functions Using the generic structure (C.33), all contributions to $\chi_1(\rho)$ can be organized in terms of the integrals

$$I(p; \rho) \equiv \int_\rho^\infty d\sigma \frac{e^{(p-1)\sigma}}{1 - e^{-\sigma}} = \int_0^{e^{-\rho}} dt \frac{t^{-p}}{1 - t}, \quad (\text{C.36})$$

and

$$J(a; \rho) \equiv \int_0^\rho d\sigma \frac{e^{a\sigma} - 1}{e^\sigma - 1}. \quad (\text{C.37})$$

We already recorded the special-function representation of $J(a; \rho)$ in Eq. (C.18); the corresponding representation of $I(p; \rho)$ is

$$I(p; \rho) = \frac{e^{-(1-p)\rho}}{1-p} {}_2F_1(1, 1-p; 2-p; e^{-\rho}), \quad (\text{C.38})$$

valid for $\text{Re } p < 1$ and extended elsewhere by analytic continuation. For large ρ ,

$$I(p; \rho) = \frac{e^{-(1-p)\rho}}{1-p} + \mathcal{O}(e^{-(2-p)\rho}), \quad (\text{C.39})$$

so that $I(p; \rho) \rightarrow 0$ in the overlap region as expected.

C.3.3 Structure of the solution and coefficients

General form and matching Inserting (C.27) into the Green's function expression and performing the integrals using (C.38) we obtain the general structure

$$\chi_1^{(\text{NZ})}(\rho) = \frac{e^{\lambda_-\rho}}{\lambda_- - \lambda_+} \left[C_0 I(0; \rho) + C_1 I(2\lambda_-; \rho) + C_2 I(2\lambda_- - 1; \rho) + \sum_j D_j I(p_j; \rho) \right], \quad (\text{C.40})$$

with coefficients C_0, C_1, C_2, D_j that are rational functions of $(\lambda_\pm, K, \bar{\beta}, \bar{\beta}_H, \kappa_{\text{eff}}, r_h)$. Regularity at the tip fixes one linear combination of the C_i , while the requirement that χ_1 does not excite the growing far-zone mode fixes the remaining integration constants. The matching to the asymptotic thermal scalar solution at large r then determines the overall normalisation of χ_1 in terms of the near-zone data.

Equations (C.8), (3.154), and the Green's function representation (3.179) together provide a complete NLO description of the metric, dilaton, and thermal scalar in the large- D cigar geometry, with all nontrivial ρ -dependence encoded in elementary exponentials and the universal special functions $J(a; \rho)$ and $I(p; \rho)$ defined in (C.18)–(C.38).

References

- [1] G.T. Horowitz and J. Polchinski, *A Correspondence principle for black holes and strings*, *Phys. Rev. D* **55** (1997) 6189 [[hep-th/9612146](#)].
- [2] G.T. Horowitz and J. Polchinski, *Selfgravitating fundamental strings*, *Phys. Rev. D* **57** (1998) 2557 [[hep-th/9707170](#)].
- [3] J.J. Atick and E. Witten, *The Hagedorn Transition and the Number of Degrees of Freedom of String Theory*, *Nucl. Phys. B* **310** (1988) 291.
- [4] M. Kruczenski and A. Lawrence, *Random walks and the Hagedorn transition*, *JHEP* **07** (2006) 031 [[hep-th/0508148](#)].
- [5] R.R. Metsaev and A.A. Tseytlin, *Order α' -prime (Two Loop) Equivalence of the String Equations of Motion and the Sigma Model Weyl Invariance Conditions: Dependence on the Dilaton and the Antisymmetric Tensor*, *Nucl. Phys. B* **293** (1987) 385.
- [6] G.W. Gibbons and S.W. Hawking, *Action Integrals and Partition Functions in Quantum Gravity*, *Phys. Rev. D* **15** (1977) 2752.
- [7] G.W. Gibbons, M.J. Perry and C.N. Pope, *The First law of thermodynamics for Kerr-anti-de Sitter black holes*, *Class. Quant. Grav.* **22** (2005) 1503 [[hep-th/0408217](#)].
- [8] B. Zwiebach, *Curvature squared terms and string theories*, *Physics Letters B* **156** (1985) 315.
- [9] D.J. Gross and J.H. Sloan, *The Quartic Effective Action for the Heterotic String*, *Nucl. Phys. B* **291** (1987) 41.
- [10] A. Giveon, N. Itzhaki and D. Kutasov, *T \bar{T} and LST*, *JHEP* **07** (2017) 122 [[1701.05576](#)].
- [11] Y. Chen and J. Maldacena, *String scale black holes at large D* , *JHEP* **01** (2022) 095 [[2106.02169](#)].
- [12] C. Krishnan and S. Talukdar, *A vestige of FZZ duality in higher dimensions*, *JHEP* **01** (2025) 177 [[2411.16669](#)].
- [13] I. Jeon, B.-H. Lee, W. Lee and M. Mishra, *Stability and topological nature of charged Gauss-Bonnet AdS black holes in five dimensions*, *Phys. Rev. D* **111** (2025) 064006 [[2407.20016](#)].
- [14] B.-H. Lee, H. Lee and W. Lee, *Hairy black holes in dilatonic Einstein-Gauss-Bonnet theory*, *AIP Conf. Proc.* **2874** (2024) 020011 [[2111.13380](#)].
- [15] S. Khimphun, B.-H. Lee and W. Lee, *Phase transition for black holes in dilatonic Einstein-Gauss-Bonnet theory of gravitation*, *Phys. Rev. D* **94** (2016) 104067 [[1605.07377](#)].
- [16] S.A. Hartnoll, C.P. Herzog and G.T. Horowitz, *Building a Holographic Superconductor*, *Phys. Rev. Lett.* **101** (2008) 031601 [[0803.3295](#)].
- [17] S.A. Hartnoll, C.P. Herzog and G.T. Horowitz, *Holographic Superconductors*, *JHEP* **12** (2008) 015 [[0810.1563](#)].
- [18] R.D. Pisarski and O. Alvarez, *Strings at Finite Temperature and Deconfinement*, *Phys. Rev. D* **26** (1982) 3735.
- [19] A.M. Polyakov, *Gauge Fields and Strings*, Taylor & Francis, London (1987), [10.1201/9780203755082](#).
- [20] S.D. Mathur, *The Fuzzball proposal for black holes: An Elementary review*, *Fortsch. Phys.* **53** (2005) 793 [[hep-th/0502050](#)].

- [21] K. Skenderis and M. Taylor, *The fuzzball proposal for black holes*, *Phys. Rept.* **467** (2008) 117 [[0804.0552](#)].
- [22] I. Bena, E.J. Martinec, S.D. Mathur and N.P. Warner, *Fuzzballs and Microstate Geometries: Black-Hole Structure in String Theory*, [2204.13113](#).
- [23] R. Emparan, R. Suzuki and K. Tanabe, *The large D limit of General Relativity*, *JHEP* **06** (2013) 009 [[1302.6382](#)].
- [24] R. Emparan, R. Suzuki and K. Tanabe, *Decoupling and non-decoupling dynamics of large D black holes*, *JHEP* **07** (2014) 113 [[1406.1258](#)].
- [25] R. Emparan, T. Shiromizu, R. Suzuki, K. Tanabe and T. Tanaka, *Effective theory of Black Holes in the $1/D$ expansion*, *JHEP* **06** (2015) 159 [[1504.06489](#)].
- [26] B. Chen, P.-C. Li, Y. Tian and C.-Y. Zhang, *Holographic Turbulence in Einstein-Gauss-Bonnet Gravity at Large D* , *JHEP* **01** (2019) 156 [[1804.05182](#)].
- [27] Y. Dandekar and A. Saha, *Large D membrane for Higher Derivative Gravity and Black Hole Second Law*, *JHEP* **02** (2020) 083 [[1910.10964](#)].
- [28] M. Mandlik and S. Thakur, *Stationary Solutions from the Large D Membrane Paradigm*, *JHEP* **11** (2018) 026 [[1806.04637](#)].
- [29] S. Bhattacharyya, A. De, S. Minwalla, R. Mohan and A. Saha, *A membrane paradigm at large D* , *JHEP* **04** (2016) 076 [[1504.06613](#)].
- [30] S. Bhattacharyya, M. Mandlik, S. Minwalla and S. Thakur, *A Charged Membrane Paradigm at Large D* , *JHEP* **04** (2016) 128 [[1511.03432](#)].
- [31] S. Kundu and P. Nandi, *Large D gravity and charged membrane dynamics with nonzero cosmological constant*, *JHEP* **12** (2018) 034 [[1806.08515](#)].
- [32] S. Bhattacharyya, P. Biswas, B. Chakrabarty, Y. Dandekar and A. Dinda, *The large D black hole dynamics in AdS/dS backgrounds*, *JHEP* **10** (2018) 033 [[1704.06076](#)].
- [33] S. Bhattacharyya, P. Biswas and M. Patra, *A leading-order comparison between fluid-gravity and membrane-gravity dualities*, *JHEP* **05** (2019) 022 [[1807.05058](#)].
- [34] S. Bhattacharyya, A.K. Mandal, M. Mandlik, U. Mehta, S. Minwalla, U. Sharma et al., *Currents and Radiation from the large D Black Hole Membrane*, *JHEP* **05** (2017) 098 [[1611.09310](#)].
- [35] V.I. Zakharov, T.G. Mertens and H. Verschelde, *Hagedorn temperature and physics of black holes*, *EPJ Web Conf.* **126** (2016) 02032 [[1605.02785](#)].
- [36] Y. Chen, J. Maldacena and E. Witten, *On the black hole/string transition*, *JHEP* **01** (2023) 103 [[2109.08563](#)].
- [37] R.-G. Cai, *Gauss-Bonnet black holes in AdS spaces*, *Phys. Rev. D* **65** (2002) 084014 [[hep-th/0109133](#)].
- [38] D.G. Boulware and S. Deser, *String Generated Gravity Models*, *Phys. Rev. Lett.* **55** (1985) 2656.
- [39] P.M. Chaikin and T.C. Lubensky, *Principles of Condensed Matter Physics*, Cambridge University Press, Cambridge (1995).
- [40] N.D. Goldenfeld, *Lectures on Phase Transitions and the Renormalization Group*, vol. 85 of *Frontiers in Physics*, Westview Press (1992), [10.1201/9780429493492](#).

- [41] A. Drozd-Rzoska, ‘quasi-tricritical’ and glassy dielectric properties of a nematic liquid crystalline material, *Crystals* **10** (2020) 297.
- [42] M.A. Anisimov, V.A. Agayan and E.E. Gorodetskii, *Scaling and crossover to tricriticality in polymer solutions*, *JETP Letters* **72** (2000) 578.
- [43] R. Brustein and Y. Zigdon, *Black hole entropy sourced by string winding condensate*, *JHEP* **10** (2021) 219 [2107.09001].
- [44] Y. Chen, *Revisiting R^4 higher curvature corrections to black holes*, 2107.01533.
- [45] E.Y. Urbach, *String stars in anti de Sitter space*, *JHEP* **04** (2022) 072 [2202.06966].
- [46] J. Seitz and E.Y. Urbach, *A spin on Hagedorn temperatures and string stars*, 2510.17951.
- [47] R. Brustein and Y. Zigdon, *Thermal equilibrium in string theory in the Hagedorn phase*, *JHEP* **05** (2022) 031 [2201.03541].
- [48] J.E. Santos and Y. Zigdon, *Self gravitating spinning string condensates*, *JHEP* **07** (2024) 217 [2403.20332].
- [49] R. Emparan and C.P. Herzog, *Large D limit of Einstein’s equations*, *Rev. Mod. Phys.* **92** (2020) 045005 [2003.11394].
- [50] R. Brustein, A. Giveon, N. Itzhaki and Y. Zigdon, *A puncture in the Euclidean black hole*, *JHEP* **04** (2022) 021 [2112.03048].